



NASA CR-159,280

NASA Contractor Report 159280

NASA-CR-159280
19800019962

Investigation of the Feasibility of CARS Measurements in Scramjet Combustion

J.A. Shirley, R.J. Hall and A.C. Eckbreth

United Technologies Research Center
East Hartford, CT 06108

Contract NASA1-15491
July 1980

LIBRARY COPY

AUG 8 1980

LANGLEY RESEARCH CENTER
LIBRARY, NASA
HAMPTON, VIRGINIA



National Aeronautics and
Space Administration

Langley Research Center
Hampton, Virginia 23665



NF01089

INVESTIGATION OF THE FEASIBILITY OF CARS MEASUREMENTS IN SCRAMJET COMBUSTION

John A. Shirley, Alan C. Eckbreth and Robert J. Hall
United Technologies Research Center

SUMMARY

Results are presented of analytical and experimental investigations performed under Contract NAS1-15491, sponsored by the NASA Langley Research Center to determine the feasibility of using coherent anti-Stokes Raman spectroscopy (CARS) to measure temperature and species concentrations in supersonic combustion experiments. It is concluded that temperature and concentration measurements of major molecular species in H_2 -air combustion can be made with CARS. Calculations predict and experiments verify that accurate and spatially precise measurements can be made; however, tradeoffs in spatial or temporal resolution will be required at the lowest species density conditions. For example, with H_2 at atmosphere and 2500 °K, a measurement accuracy of 1% can be achieved at 0.2 cm spatial resolution with state-of-the-art lasers. At 0.1 atmosphere pressure, similar accuracy can be achieved only at 2 cm resolution. CARS spectra of H_2O , O_2 and H_2 have been measured in laboratory flames. Computer code calculated spectra agree very well with the measured spectra. Temperature and concentration measurements of O_2 and H_2 have been made in a H_2 -air diffusion flame. CARS temperature measurements in both species generally agreed to within 5 percent with radiation corrected thermocouple measurements. Measured H_2 CARS signal magnitudes are in good agreement with the analytical predictions. The use of reference cells to eliminate the effects of small optical misalignments was investigated. The feasibility of measuring O_2 concentrations from the interference between the nonresonant background susceptibility and resonant O_2 susceptibility at low concentrations has been demonstrated experimentally. The post flame nonresonant background susceptibility of H_2 -air and CH_4 -air flames has been measured. A preliminary measurement of the nonresonant susceptibility of water vapor has been made. Calculations indicate that the nonresonant susceptibility of the combustion gas mixture can vary by about 40 percent due to composition changes (neglecting the effect of temperature) through the flame.

A conceptual design for the LaRC scramjet combustion facility has been formulated. Specifications of key components have been prescribed and auxiliary apparatus for measurements have been identified.

N80-28463 #

INTRODUCTION

Laser light scattering and wave mixing spectroscopic techniques are being increasingly applied to diagnosis of the hostile, yet easily perturbed, environments typical of combustion. Laser spectroscopic diagnostics should facilitate greatly improved understanding of a variety of combustion processes which, in turn, should lead to enhanced efficiencies and lower pollutant formation in propulsion, energy, and waste disposal systems.

Experimental diagnostics of supersonic combustion phenomena are important toward gaining the understanding necessary to improve and control these processes for propulsion applications. Physical probes for combustion processes are not only confronted with survival considerations, but are of questionable utility since their presence may seriously perturb the phenomena under study. This is particularly true of supersonic combustion where probes may choke the flow, behave as flameholders, or otherwise cause the medium to behave differently. Optical techniques are ideally suited to diagnosing such phenomena. A variety of laser spectroscopic techniques exist which permit the remote, "point" probing of hostile environments. Coherent anti-Stokes Raman Spectroscopy (CARS) appears as the most attractive candidate for the remote, point probing of temperature and species number densities in the NASA Langley scramjet combustion facility, based upon its signal strength and "laser-like" signal character. Before the CARS technique can be actually implemented in such a practical application, however, a number of measurement system approaches need to be addressed.

The objective of this investigation is to evaluate analytically and experimentally the feasibility and definition of a CARS system for the measurement of temperature and O_2 , H_2 , and H_2O densities in the LaRC scramjet facility. The investigation is divided into three tasks. In the first task, various approaches to CARS diagnosis of temperature and primary species density are analytically evaluated based on scramjet operating parameters supplied by NASA. The second task is to make CARS temperature and concentration measurements of H_2 , O_2 , and H_2O in laboratory hydrogen/air flames. The third task is the formulation of a conceptual design of a CARS system to be installed in the LaRC scramjet test facility.

The following section opens with a brief description of the principles of coherent anti-Stokes Raman spectroscopy. A review of scramjet operating parameters is given, and the application of CARS and its potential interferences and limitations for these measurements are discussed. The three tasks are discussed sequentially in the remainder of this section. In the last section, conclusions are given concerning the feasibility of measuring scramjet temperature and species concentrations. The investigation of the use of reference cells to provide a calibration for concentration measurements is set forth in Appendix A.

FEASIBILITY OF CARS SCRAMJET MEASUREMENTS

This section opens with a brief review of the principles of coherent anti-Stokes Raman spectroscopy. The fundamental expressions relating CARS signal strengths to the incident laser powers, gas concentration, temperature, and molecular parameters are presented. The NASA LARC Scramjet facility is described, and an example CARS signal calculation is worked out. Potential interferences and limitations are discussed as regards the NASA application. In the remainder of this section, the three Tasks of this investigation are discussed. These are: (1) identification of preferred approaches to the CARS diagnosis of temperature and density, (2) experimental examination of the selected diagnostic approaches applied to laboratory H_2 flames, and (3) formulation of a conceptual design of a CARS system for the scramjet facility.

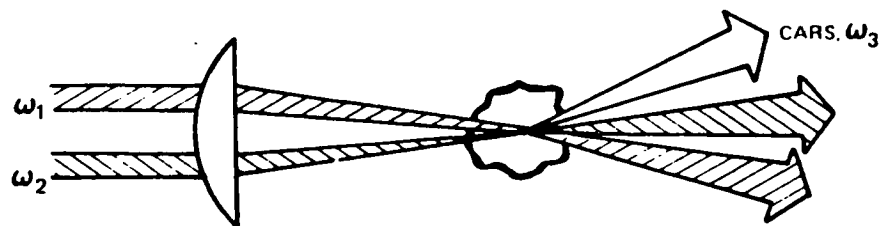
Principle of the CARS Technique

CARS techniques have recently come to prominence for combustion diagnostics based upon the investigations of Taran and his coworkers (Refs. 1-5) at ONERA in France. The effect was originally discovered in the early sixties by Maker and Terhune (Ref. 6) and essentially remained in the province of nonlinear optics investigations until Taran's application of it for gas phase diagnostics. In the United States, Harvey, Byer and their coworkers (Refs. 7-10) have conducted numerous investigations into the technique. Barrett has demonstrated both cw CARS generation (Ref. 11) and pure rotational CARS (Ref. 12). Broadband CARS generation in a single pulse has also been obtained (Ref. 13). Publications describing investigations into the technique are appearing at an ever increasing rate, and several good reviews have recently appeared (Refs. 14-17). The technique has also been described as degenerate four wave mixing or three wave mixing, but use of the acronym CARS seems to be gaining broad acceptance.

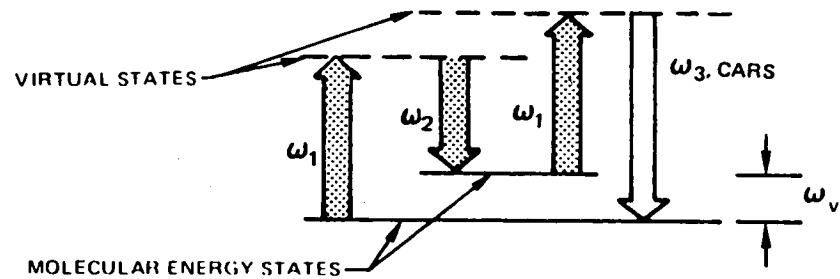
CARS is probably best understood by reference to Fig. 1. The explanations outlined in Refs. 1 and 8 will be followed. Incident pump photons at frequency ω_1 interact with photons at ω_2 (often termed the Stokes beam) through the third order nonlinear susceptibility $\chi^{(3)}_{ijkl}(-\omega_3, \omega_1, \omega_1, -\omega_2)$ to generate a polarization component which produces radiation at the frequency $\omega_3 = 2\omega_1 - \omega_2$. Note that the CARS signal is in a spectral region largely free of fluorescent interferences, i.e., anti-Stokes region. When the frequency difference $\omega_1 - \omega_2$ is close to the vibrational frequency of a Raman active resonance, the magnitude of the signal generated becomes very large as will be seen. Assuming a fixed narrowband pump frequency, ω_1 , the CARS spectrum at ω_3 can be mapped out piecewise by scanning a variable frequency, narrowband laser source at ω_2 . Or, as depicted in Fig. 1, if a broadband source at ω_2 is employed, the entire CARS spectrum can be generated simultaneously permitting fast time-

CARS — COHERENT ANTI-STOKES RAMAN SPECTROSCOPY

● APPROACH



● ENERGY LEVEL DIAGRAM



● SPECTRUM

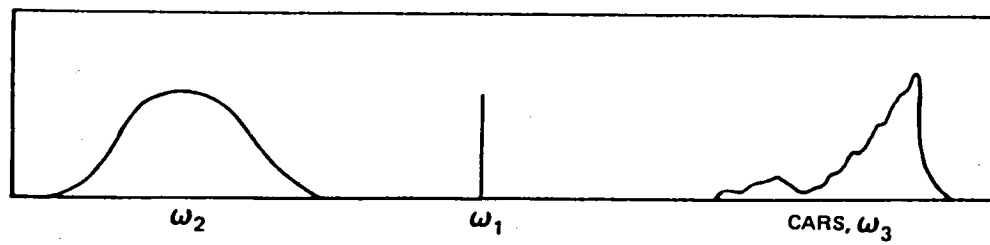


FIG. 1

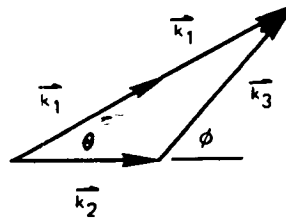
resolved measurements of fluctuating phenomena. In fact, for turbulent combustion diagnosis, the CARS spectrum must be captured in a single pulse due to the highly nonlinear dependence of CARS on temperature and density. Scanning the CARS spectrum or Stokes dye laser over a period of time would result in an accumulation of terms involving self- and cross-correlations between the density and temperature fluctuations. This obviously would render the spectrum ambiguous from a data reduction standpoint.

To produce CARS, the incident pump and Stokes laser beams must be aligned in a precise manner so that the CARS generation process is properly phased. The general phase-matching diagram for three wave mixing is shown in Fig. 2a and requires that $2\vec{k}_1 = \vec{k}_2 + \vec{k}_3$. \vec{k}_i is the wave vector at frequency ω_i with absolute magnitude equal to $\omega_i n_i / c$, where c is the speed of light and n_i , the refractive index at frequency ω_i . Since gases are virtually dispersionless, i.e., the refractive index is nearly invariant with frequency, the photon energy conservation condition $\omega_3 = 2\omega_1 - \omega_2$ indicates that phase matching occurs when the input beams are aligned parallel to each other, Fig. 2b. Collinear phase matching, however, possess a problem in regard to spatial resolution. Since the CARS signal is coherent and undergoes an integrative growth process, the spatial resolution cannot be well defined by imaging techniques such as those successfully employed in spontaneous Raman approaches to yield fine resolution. Because CARS signal generation scales as the intensity product $I_1^2 I_2$ (where I_i is the intensity at frequency ω_i), the incident laser beams are generally tightly focused for diagnostic purposes when collinear phase-matching is used. Although most of the signal generation occurs in the region about the focus, the spatial resolution can be poor for large focal lengths or for laser beam divergence angles in excess of the diffraction limit. In the presence of density gradients, the resolution further degrades since CARS scales linearly or as the square of the gas density. For probing of hot flames or other gases, significant contributions to the total CARS signal may originate from cooler, higher density regions adjacent to the flame. CARS signal contributions may also derive from the various elements in the optical train, e.g., lenses, when collinear approaches are being used. Clearly, it would be desirable to avoid beam overlap and potential three wave mixing in all regions except the desired measurement location.

In an effort to avoid collinearity, one could attempt to introduce the ω_1 and ω_2 beams at a slight angle to one another since a small amount of phase mismatch is tolerable. As phase mismatch is deliberately introduced in this manner, the CARS signal generating efficiency will drop. At $\Delta k \approx 3$ where Δk is the magnitude of the phase mismatch, i.e., $|2\vec{k}_1 - \vec{k}_2 - \vec{k}_3|$, the CARS efficiency will have decreased by an order of magnitude (Ref. 21). Accepting this loss of power for the moment and if a 0.1 cm spatial resolution is desired, then a Δk of 30 cm^{-1} would be tolerable. At wavelengths of 532 nm (ω_1) and 607.3 nm (the N_2 vibrational ground state Stokes wavelength), a 30 cm^{-1} phase mismatch would

CARS PHASE-MATCHING APPROACHES

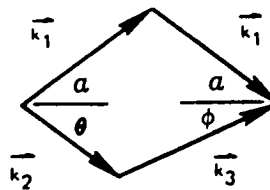
a) GENERAL



b) COLLINEAR



c) BOXCARS



be produced at an angular separation of only 1° assuming no dispersion. Although one could operate in this manner, it is clearly inefficient, and the actual spatial resolution will depend very critically on the precise angular separation.

A method, which was developed at UTRC and permits large angular separation of the input beams while still satisfying phase-matching requirements, is depicted in Fig. 2(c) (Ref. 18). In this approach the ω_1 beam is split into two components which are crossed at a half angle of α . The ω_2 beam is introduced at angle θ producing phase-matched CARS at angle ϕ . Based upon the shape of the phase-matching diagram (Fig. 2(c)), this technique has been termed BOXCARS. The appropriate phase-matching angles are readily related from simple geometric considerations as follows:

$$n_2 \omega_2 \sin \theta = n_3 \omega_3 \sin \phi \quad (1)$$

$$n_2 \omega_2 \cos \theta + n_3 \omega_3 \cos \phi = 2n_1 \omega_1 \cos \alpha \quad (2)$$

Clearly CARS is generated only in the region where all three beams cross leading to greatly enhanced, and perhaps more importantly, unambiguous spatial resolution for sufficiently small intersection volumes. BOXCARS should be extremely useful in the study of highly structured, spatially inhomogeneous flames and has been employed at UTRC to perform spatially resolved temperature measurements in small, sooting laminar propane diffusion flames.

CARS signal magnitudes. - Although CARS has no threshold per se and can be generated with cw laser sources (Ref. 11), high intensity pulsed laser sources are usually employed for the probing of high interference environments to generate CARS signals well in excess of the various sources of interference. Because of the requirements to generate and capture the CARS signal with each laser pulse in limited duration supersonic combustion processes, the individual laser pulses must be energetic enough to provide a statistically large number of CARS photons in each spectral detection interval.

The CARS intensity I_3 and ω_3 can be expressed as

$$I_3 = \left(\frac{4\pi^2 \omega_3}{c^2} \right)^2 I_1^2 I_2^2 |x|^2 z^2 \quad (3)$$

where I_i is the intensity at frequency ω_i ; χ , the third order nonlinear susceptibility, and z , the distance over which the phase matched interaction occurs. The susceptibility can be written in terms of a resonant and nonresonant part, χ^{nr} ,

$$\chi = \sum_j (\chi' + i \chi'')_j + \chi^{nr} \quad (4)$$

χ^{nr} is the contribution from electrons and remote resonances. The resonant susceptibility associated with a Raman transition, j , is

$$(\chi' + i \chi'')_j = \frac{2c^4}{\hbar \omega_j^4} N \Delta_j g_j \sigma_j \frac{\omega_j}{\omega_j^2 - (\omega_1 - \omega_2)^2 - i\Gamma(\omega_1 - \omega_2)} \quad (5)$$

where \hbar is Planck's constant divided by 2π ; N , the total species number density; Δ_j , the population difference between the levels involved in the transition, g_j , the linestrength factor and equal to $(v_j + 1)$ for a Q line; σ_j , the Raman cross section for the transition characterized by frequency ω_j ; and, Γ_j , the Raman linewidth.

It is quite common in the CARS literature in the case of gases to replace Eq. 3 which is in terms of intensities, with an expression in terms of powers for collinear diffraction limited beams, namely

$$P_3 \approx \left(\frac{\omega_1}{\pi c}\right)^2 \left(\frac{4\pi^2 \omega_3}{c^2}\right)^2 P_1^2 P_2 |\chi|^2 \quad (6)$$

Here the interaction occurs in a beam diameter, ϕ , and length, l of

$$\phi = \frac{4\lambda f}{\pi D} \quad l = \frac{\pi \phi^2}{2\lambda} \quad (7)$$

where f is the focusing lens focal length; D , the beam diameter at the lens; and λ the pump laser wavelength. The foregoing corresponds to a diffraction angle, $(4/\pi)(\lambda/D)$ of 0.07 milliradians at 532 nm and $D = 1$ cm. In actuality, most pulsed lasers used for gas phase CARS work are not diffraction limited, but possess divergence angles on the order of 1 milliradian. Due to the cubic dependence on intensity of the CARS signal, the CARS signal generated for a given focal length lens will vary inversely as the sixth power of the divergence angle. In the example above this could lead to an overestimation of the CARS signal intensity by a factor of nearly seven orders of magnitude. In the signal estimates to be made here, the intensity formulations will be employed to show explicitly the spatial resolution and focal lengths employed.

One is not free to choose optical parameters arbitrarily. With the diffraction limited lasers the power formulation should be used instead of the intensity expression with an arbitrary interaction length. CARS calculations using the intensity formulation should be checked to verify that the CARS power calculated doesn't exceed the value obtained with Eq. (6).

If the detuning frequency, $\Delta\omega_j = \omega_j - (\omega_1 - \omega_2)$, is introduced, the resonant susceptibility may be expressed as

$$\chi = K_j \frac{\Gamma_j}{2\Delta\omega_j - i\Gamma_j} \quad (8)$$

where

$$K_j = \frac{2c^4}{\hbar\omega_2^4} N \Delta_j g_j \sigma_j \frac{1}{\Gamma_j} \quad (9)$$

On resonance $\Delta\omega_j = 0$, and $|\chi| = K_j$. Assuming the CARS beam to have the same cross sectional area as the Stokes beam, the CARS power is

$$P_3 = \left(\frac{4\pi^2 \omega_3}{c^2} \right)^2 I_1^2 P_2 K_j^2 z^2 \quad (10)$$

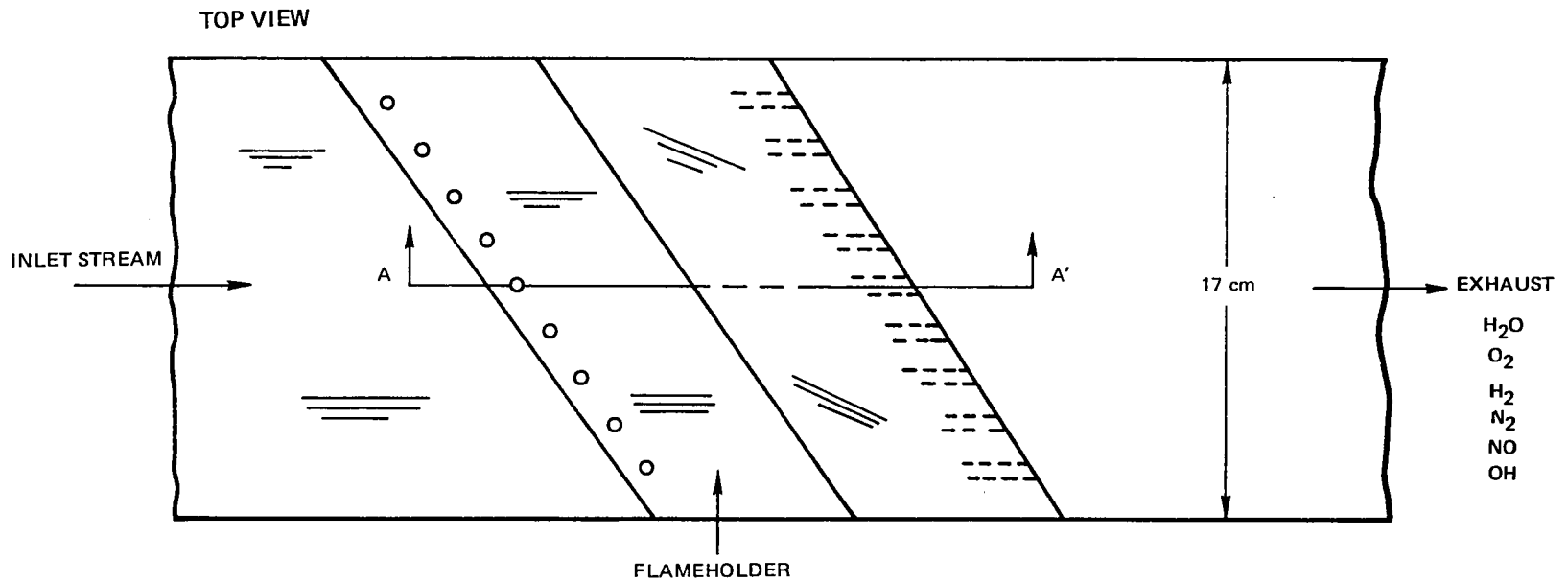
CARS Diagnostics of Supersonic Combustion Processes

In evaluating any diagnostic approach, the ultimate environment of application must be factored into any decision concerning the feasibility of a given technique. The application of interest here is the combustion of H_2 in a supersonic air stream. The supersonic combustion tunnel with one model of flameholder is sketched approximately in Fig. 3. H_2 fuel gas can be injected either parallel or perpendicular to the supersonic air stream. The model flameholder shown is skewed at an angle to the inlet flow and stepped as shown in the cross-sectional view. Anticipated parameter ranges are listed in Table I. Diagnostically this is a benign environment since H_2 - O_2 combustion tends to exhibit low luminosity and is, of course, free of carbonaceous or soot particulates which plague the diagnosis of hydrocarbon-fueled, diffusion flames (Ref. 3). Optical access is available, particularly straight across or transverse to the supersonic stream.

TABLE I - PARAMETER RANGE IN NASA SCRAMJET FACILITY

Temperature:	300 to 2400°K
Pressure:	0.2 to 3 atmospheres
Flow Speed:	2000 m/sec
Species:	O_2 > 1 to 21% by volume
	H_2 > 1 to 100%
	N_2 ~ 78%
	H_2O 0 to 30%
Run Duration:	10-15 sec

SUPERSONIC COMBUSTOR MODEL



SECTION A A'

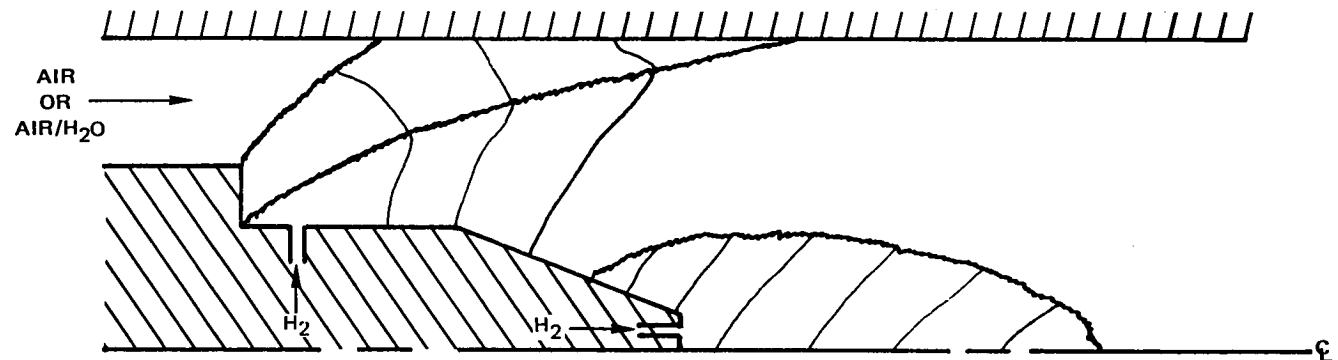


FIG. 3

Although the anticipated interferences, i.e., luminosity, particulate effects, are small, pulsed laser sources are required for rapid time-resolved measurements which can be made at a variety of locations during a run. The very short run duration of 10-15 seconds plays a major role in diagnostic selection as will be seen. One must take care, however, that gas breakdown does not occur. Such an event would preclude any diagnostic interrogation of the medium. From Ref.19 it appears reasonable to assume that an atmospheric pressure combustor at 2000°K would have a breakdown threshold in the visible around 10^{12} W/cm² in the absence of particulate matter above $\sim 1 \mu$ dia, and about 10^{10} W/cm² if large particulates ($\geq 1\mu$) were present. Breakdown thresholds scale inversely with pressure and, hence, would decrease at higher pressures. These thresholds are sufficiently high that they will pose no unusual problem in the present application since the spatial resolution desired, ~ 1 mm, does not require very tight focusing of the input laser beams.

As an example of the calculation of CARS signals relevant to scramjet combustor measurements consider the case of detecting a 50 percent H₂ concentration at 2000°K and one atmosphere pressure. The Raman transition in H₂ at this density will be Doppler broadened with a linewidth $\Gamma_j/2\pi c$ of 0.095 cm^{-1} . Δ_j for the Q(1) CARS transition will be 0.17. For the case of a frequency-doubled neodymium laser (ω_1), K_j can be shown to be $2.62 (10^{-9}) \text{ cm}^3/\text{J}$. The 2xNd laser will be assumed to have a pulse energy of 0.05 J in 10 nanoseconds and a 1 milliradian beam divergence. For a 50 cm focal length lens, the pump intensity would be about $2.5(10^9) \text{ Watts/cm}^2$. For a 1 mm interaction length and a 10 percent collection efficiency, one finds $P_3/P_2 = 6.2(10^{-9})$. If the Stokes beam is broadband, say 100 cm^{-1} , so as to generate the entire H₂ CARS spectrum with each laser pulse, and were 0.01 J in energy, the Stokes laser energy available to drive the Q(1) line [0.095 cm^{-1} wide] would be $2.4(10^{-6})\text{J}$. This would produce a CARS signal of $1.49(10^{-14})\text{J}$ corresponding to $3.25(10^4)$ photons. At a concentration of 1 percent the signal would fall to just 13 photons, clearly inadequate for single pulse measurements. If the spatial resolution were relaxed to 1 cm the 1 percent H₂ signal would increase to 1300 photons, which, at the high photomultiplier quantum efficiencies available in the CARS spectral range ($\sim 435 \text{ nm}$), would lead to statistical fluctuations of about ± 6 percent.

These calculations illustrate that the CARS system has to be carefully designed and that the operating parameter ranges have to be fairly well defined. Under certain circumstances, even the CARS signal levels could be marginal. One may not wish to use a spectrally broadband dye laser for H₂ diagnosis since the CARS H₂ spectrum consists essentially of a set of discrete lines (as will be seen later) and much of the dye laser energy is not utilized in the three wave mixing process.

The measurement parameters of interest for a scramjet combustor are gas temperature and major species, i.e. N₂, O₂, H₂ and H₂O concentrations. The distribution of molecules within the manifold of rotational states is given by Boltzmann equilibrium and depends on the temperature and molecular parameters. Associated with each rotational level, j , there is a frequency given by (Ref. 20)

$$\omega_j = 2\pi[\omega_e - 2\omega_e x_e (v+1) - \alpha_e J(J+1)] \quad (11)$$

for Q branch transitions ($\Delta J = 0$), where ω_e , $\omega_e x_e$ and α_e respectively are the vibrational frequency, anharmonicity and vibrational-rotational coupling constants. The pump beam frequency is ω_p . If the Stokes beam frequency, ω_s is swept then resonances producing enhanced CARS signals will occur at frequencies $\omega_s = \omega_p - \omega_j$. The magnitude of the CARS signal at frequency $\omega_{as} = \omega_p + \omega_j$ depends on the population of j . Therefore the temperature can be related to the shape of the CARS spectrum. As another (preferred) method a broadband dye laser can be used to provide the Stokes beam. CARS is generated at all frequencies $2\omega_p - \omega_s$ and is enhanced when $\omega_p - \omega_s = \omega_j$.

Once the temperature is known the magnitude of the CARS signal can be related to the number density of molecules provided one knows the linewidth and interaction length. Species detection sensitivity is limited for the conventional CARS approach, not due to an inadequacy of signal as is often the case in spontaneous Raman scattering, but due to the presence of the background nonresonant susceptibility. The nonresonant susceptibility is essentially an electronic contribution from all of the molecules present. Species sensitivity limitation is best illustrated by considering the case of a single resonance in the presence of background. The square of the absolute value of the susceptibility (Eq. (3)) is

$$|\chi|^2 = \chi'^2 + 2\chi'\chi^{nr} + \chi^{nr2} + \chi''^2 \quad (12)$$

or in the case of a very weak resonance

$$|\chi|^2 \approx \chi^{nr2} + 2\chi'\chi^{nr} \quad (13)$$

Since χ' varies from negative to positive about line center, the presence of a species in low concentration is apparent by a similar modulation in the CARS background susceptibility profile. In broadband CARS, the background nonresonant susceptibility profile merely mirrors the Stokes laser profile. In narrowband, scanned CARS, it reflects the tuning power variation of the Stokes laser. When the species concentration becomes very low, i.e., $\chi' \ll \chi^{nr}$, the "signal" is lost in the background susceptibility profile. At moderate concentration, i.e., 0.1-10% depending on the gases, the effect of the nonresonant background is to modulate the spectra, producing interferences. In this case too the species concentration can be extracted from the CARS spectrum, however the magnitude of χ^{nr} must be known and a CARS computer code must be used to evaluate the spectra. Examples of these procedures are discussed in later portions of this report. It should be pointed out that some investigators have used the polarization properties of the medium to reject nonresonant background CARS component (Refs. 21-23).

Task I Study

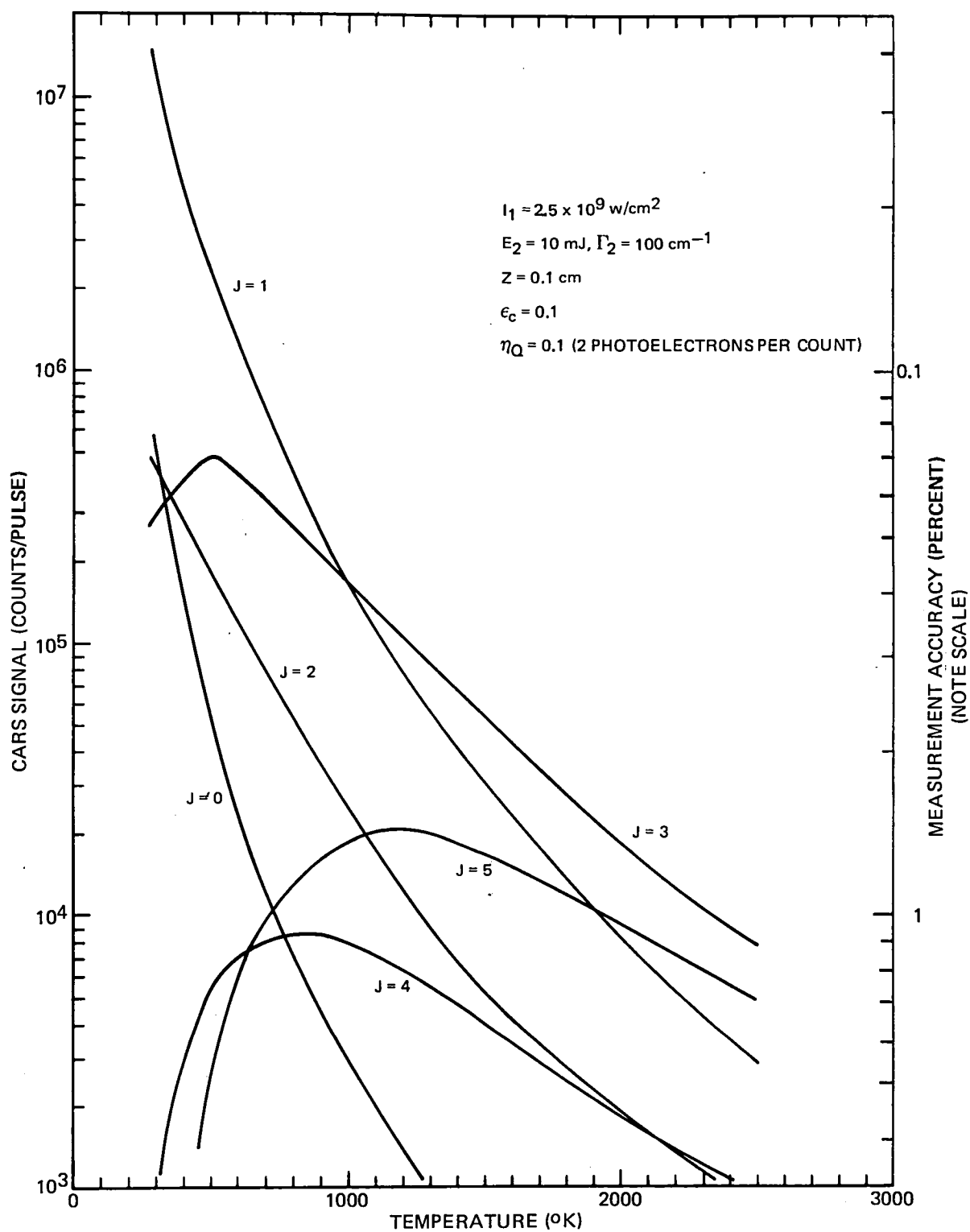
The objective of Task I, investigation of the feasibility of CARS measurements of species concentration temperature for NASA scramjet combustion research, was to investigate preferred diagnostic approaches. This section addresses laser selection, tradeoffs between signal level, data rates and spatial resolution, temperature measurements in hydrogen, and CARS linewidths. The Task I study is summarized, and a general discussion of the Task I results is given at the end of this subsection.

Laser selection. - The ideal laser for CARS work possesses high peak pulse power in the visible and has low-beam divergence, so that high intensities, and thereby, high CARS generation efficiencies are realized. The required power levels dictate a pulsed solid-state laser such as ruby, frequency doubled neodymium-yttrium aluminum garnet or frequency doubled neodymium-glass. Ruby and Nd-glass can generate high-peak powers (1-10 MW) and have good to moderate beam divergence (0.2-3 milliradian), however, the pulse repetition frequency is low, generally less than 0.1 Hz. The long wavelength of the ruby laser (694 nm) implies a smaller Raman cross section and a Stokes frequency which requires an infrared dye laser to study most molecules of interest. On the other hand, frequency doubled Nd-YAG lasers (2xNd) can operate with pulse repetition frequencies up to 25 kHz depending on the mode of operation. For operation in the 1-24 kHz range, the flashlamps which pump the laser rod are operated continuously, and the cavity is Q switched. Typical performance for these lasers is 10 kW peak power with ~2 milliradian beam divergence. The pulsed flashlamp models, on the other hand, can have repetition frequencies up to 10-20 Hz and 20 MW peak power and 1 milliradian beam divergence. Comparing these specifications, the peak intensity for a beam focused with a 50 cm lens is approximately $1.5 \times 10^6 \text{ W/cm}^2$ for the cw flashlamp models and $1.8 \times 10^{10} \text{ W/cm}^2$ for the pulsed flashlamp lasers. Since the CARS generation efficiency depends on the square of the pump intensity, the conversion efficiency can be 100 million times greater for the pulsed flashlamp lasers. Calculations will be presented next which indicate that even the more powerful pulsed flashlamp lasers have limited performance capabilities for measurements at the lowest densities. These calculations will demonstrate the overwhelming superiority of pulsed flashlamp models for scramjet measurements.

Tradeoff studies. - CARS radiation intensities have been estimated for H_2 and O_2 under typical flow conditions in the NASA scramjet facility. The calculated CARS signals for the lowest rotational states in H_2 are shown as a function of temperature in Fig. 4. The calculations assume a 2xNd laser with a pulse energy of 0.1 J in 10 nanoseconds and 1 milliradian beam divergence. For a 50 cm focal length lens, the pump intensity will be about $2.5 \times 10^9 \text{ W/cm}^2$ in a BOXCARS configuration. The pump laser is assumed to drive a broadband dye laser (100 cm^{-1} , FWHM) at modest efficiency (30%). The interaction length is

PREDICTED DOPPLER LIMITED CARS SIGNALS IN H₂
 $P = 1.013 \times 10^5 \text{ Pa (1atm)}$

100% CONCENTRATION



taken to be 1 mm, and the collection efficiency 10 percent. The quantum efficiency of the detector is 10 percent, and two photoelectrons are required to produce a count (typical of an optical multichannel analyzer). The Raman linewidth has been assumed to be Doppler limited. Later in this section this assumption will be shown to be conservative. Scattering from the odd rotational states is higher because of the larger statistical weight factor. These calculations indicate that the CARS signals decrease by three orders-of-magnitude for the temperature range of interest. The calculations are representative of H_2 at 100 percent concentration and 1.013×10^5 Pascal (1 atmosphere) pressure. The CARS intensity at other pressures and concentrations can be estimated by $(pc)^2$ scaling. The measurement accuracy is given on the scale at the right-hand margin.

Figure 5 shows the predicted CARS signal for the Q(15) transition in O_2 . Even numbered rotational levels are totally absent for O_2 . The $J = 15$ level is one of the more populated levels at moderate temperatures. The Raman linewidth for these calculations has been taken to be 0.1 cm^{-1} under all conditions. The CARS intensity of a single O_2 rotational transition is smaller than for a single H_2 transition because of the larger number of rotational levels populated. To completely evaluate the CARS intensities for O_2 , requires consideration of all rotational levels together because of possible interference effects. These calculations require computer calculation and are presented later along with the discussion of the experiments. The simple calculations are adequate for tradeoff studies, however.

The separation between transitions in the vicinity of Q(15) is larger than the Raman linewidth and constructive interferences are negligible. However, at very low concentration, interference between the nonresonant contribution to the susceptibility can occur which limit the ultimate sensitivity. As already mentioned, schemes have been devised which minimize the effect of the nonresonant contribution to the susceptibility (Ref. 21-23).

CARS generation is an integrative growth process. The CARS signal depends on the interaction length. In Figs. 4 and 5, the interaction length is 0.1 cm typical of a large angle BOXCARS configuration. The interaction length can be increased by decreasing the BOXCARS crossing angle or by using a collinear configuration. Figures 6 and 7 show the combined effect of interaction length and pressure-concentration product on the CARS signal in H_2 and O_2 . The upper and lower limits of the range of the pressure-concentration product are shown for the expected scramjet parameters (Table I). The measurement accuracy is also shown. As an example of the use of these curves, consider the prediction of the CARS signal for 20 percent H_2 in 1 atmosphere (2500 °K) for an interaction length of 0.1 cm. Lines perpendicular to the axes at the values $(pc = 0.2)$ intersect near the diagonal line labeled 10^2 counts. Therefore, 100 counts can be expected per pulse under these conditions. The CARS signal at

FIG. 5

PREDICTED CARS SIGNALS IN O_2 $P = 1.013 \times 10^5 \text{ Pa (1atm)}$

100% CONCENTRATION

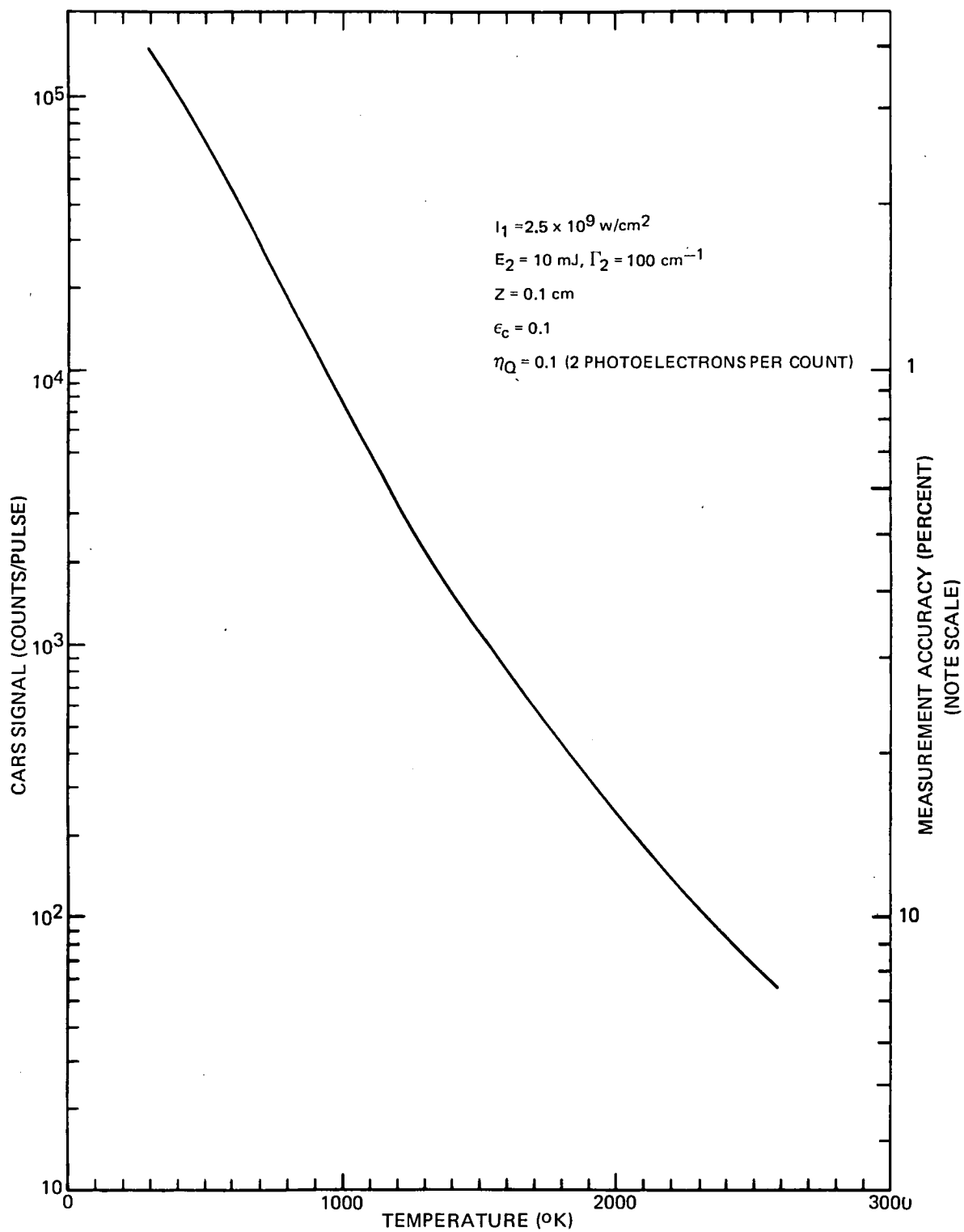
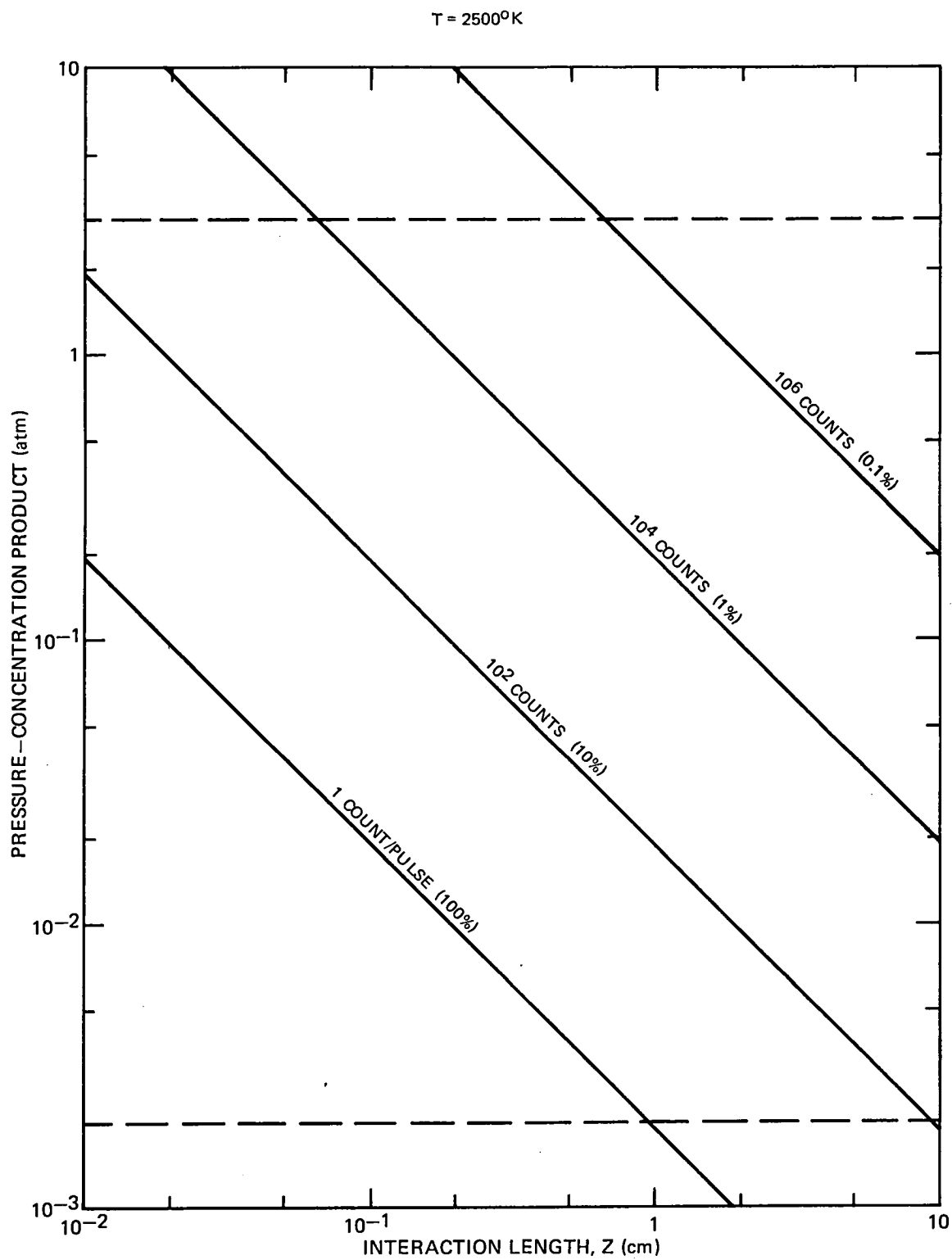
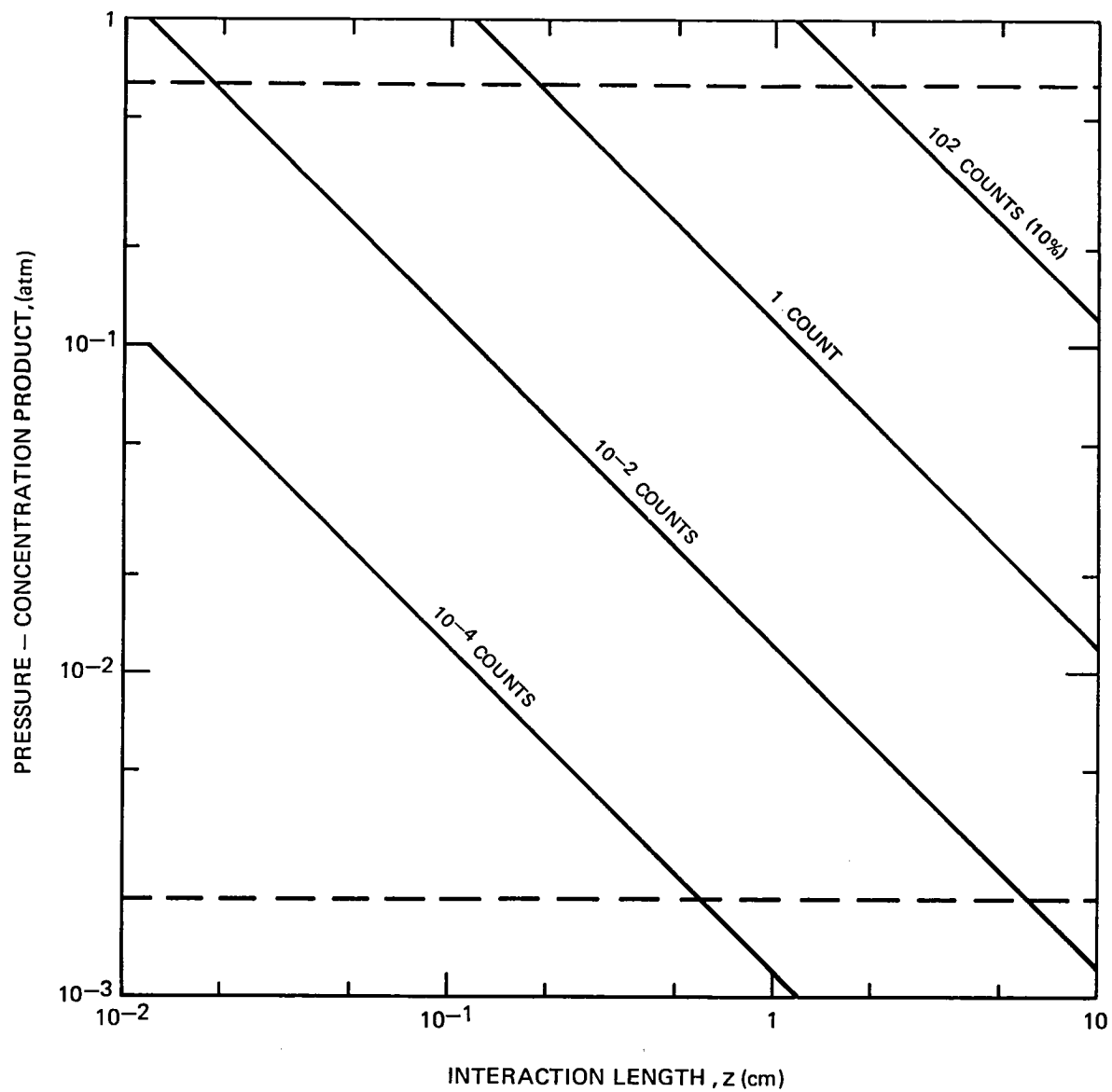
 $\Gamma = 0.1 \text{ cm}^{-1}$ 

FIG. 6

TRADEOFF OF SENSITIVITY VERSUS SPATIAL RESOLUTION FOR H_2 Q(1)

TRADEOFF OF SENSITIVITY VERSUS SPATIAL RESOLUTION FOR O₂ Q(15)

T=2500 ° K



other temperatures can be estimated by reference to Fig. 4. Thus, at 1500 °K the CARS intensity is approximately 10 times larger than at 2500 °K, and 10^3 counts are predicted.

These calculations are quite conservative, because the temperature is taken as 2500 °K. It is probably best to use this worst case since the H₂ and O₂ components of the flow are expected to be lowest in the hottest regions.

Since the spatial resolution of the measurement is effectively the interaction length, it can be seen that under low concentration conditions larger interaction lengths and, consequently, lower spatial resolution will be required.

Temperature measurements from H₂ CARS. - It should be relatively straightforward to make temperature measurements from H₂ CARS because of its simple spectrum. In Fig. 8 are displayed computer calculated CARS spectra of H₂ at a concentration of 1 percent for various temperatures. The separation between adjacent rotational transitions is much larger than the linewidth, therefore the Q(J) intensities are independent under all conditions of interest here. The temperature can be determined from the ratio of intensities among the transitions. The ratios of the strongest transitions are shown in Figure 9. Above 800-900 °K the three ratios can be compared to determine the temperature. The use of three ratios below this temperature would require instrumentation with a dynamic range in excess of 10^4 .

There are several approaches which can be taken to make temperature measurements in hydrogen. The entire spectrum can be generated simultaneously with a broadband dye laser appropriately centered at the Stokes frequency, and the CARS spectrum can be dispersed on a multiple element array such as an optical multichannel analyzer or a diode array. An alternative method of making temperature measurements in hydrogen is to use two narrowband interference filters with passbands which are closely spaced in the H₂ anti-Stokes region. Calculations have been made of the CARS power convolved with typical interference filter bandwidths and transmission profiles. The filters have been assumed to be two cavity, with 1.2 nm bandwidth (FWHM) and equal peak transmissions. The CARS signals with filters centered at 436, 437, and 438 nm have been calculated. The ratios of response of the 437 and 438 nm filters with respect to the 436 nm has been computed and are shown in Figure 10.

If r is the ratio of CARS signals, the variance in temperature can be written as (Ref. 24).

$$\sigma_T^2 = \left(r \frac{dT}{dr} \right)^2 \left(\frac{\sigma_N}{N} \right)^2 + \left(r \frac{dT}{dr} \right)^2 \left(\frac{\sigma_{N'}}{N'} \right)^2 \quad (14)$$

TEMPERATURE VARIATION OF H₂ CARS SPECTRA

1 ATM, 1% H₂, 1 CM⁻¹ SLIT WIDTH

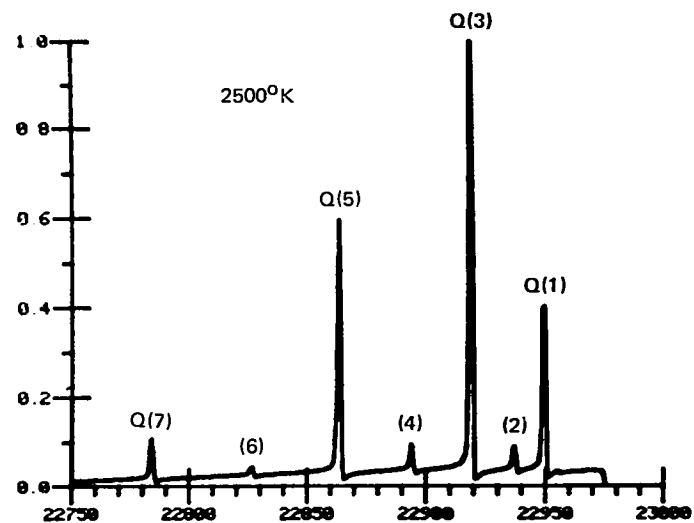
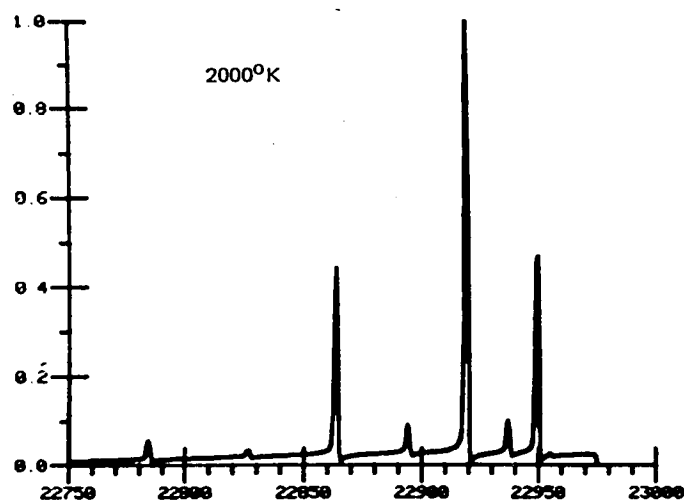
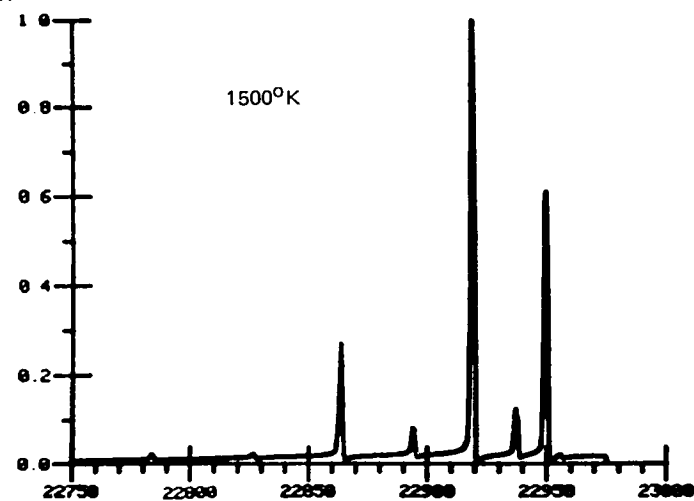
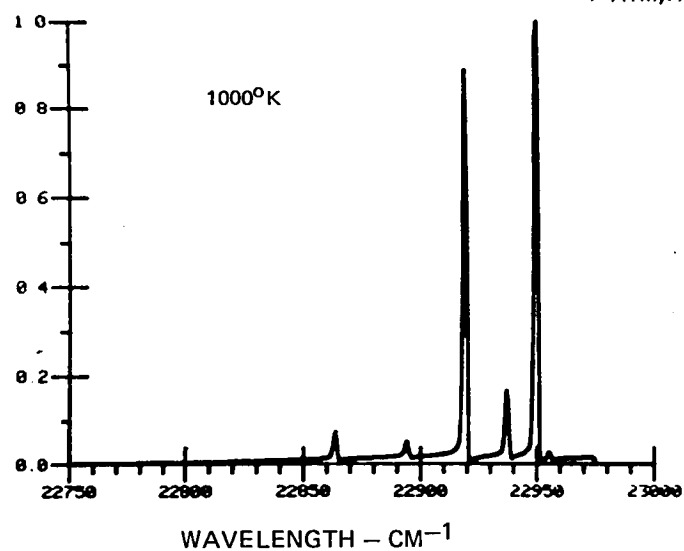
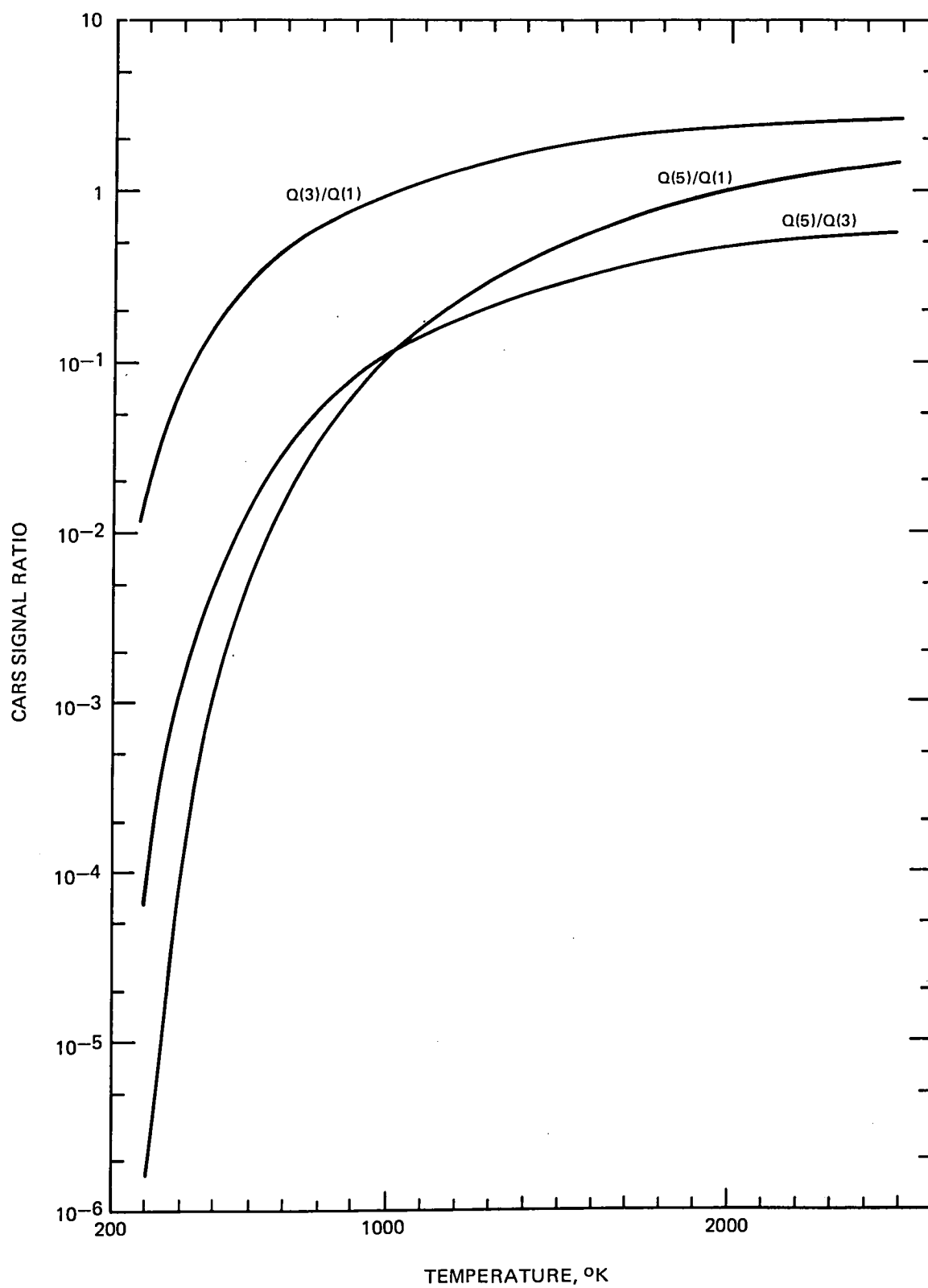


FIG. 8

RATIO OF CARS SIGNALS FOR H_2 Q (J) TRANSITIONS

TEMPERATURE MEASUREMENT IN H₂ CARS WITH FILTERS

1 atm, C=100%

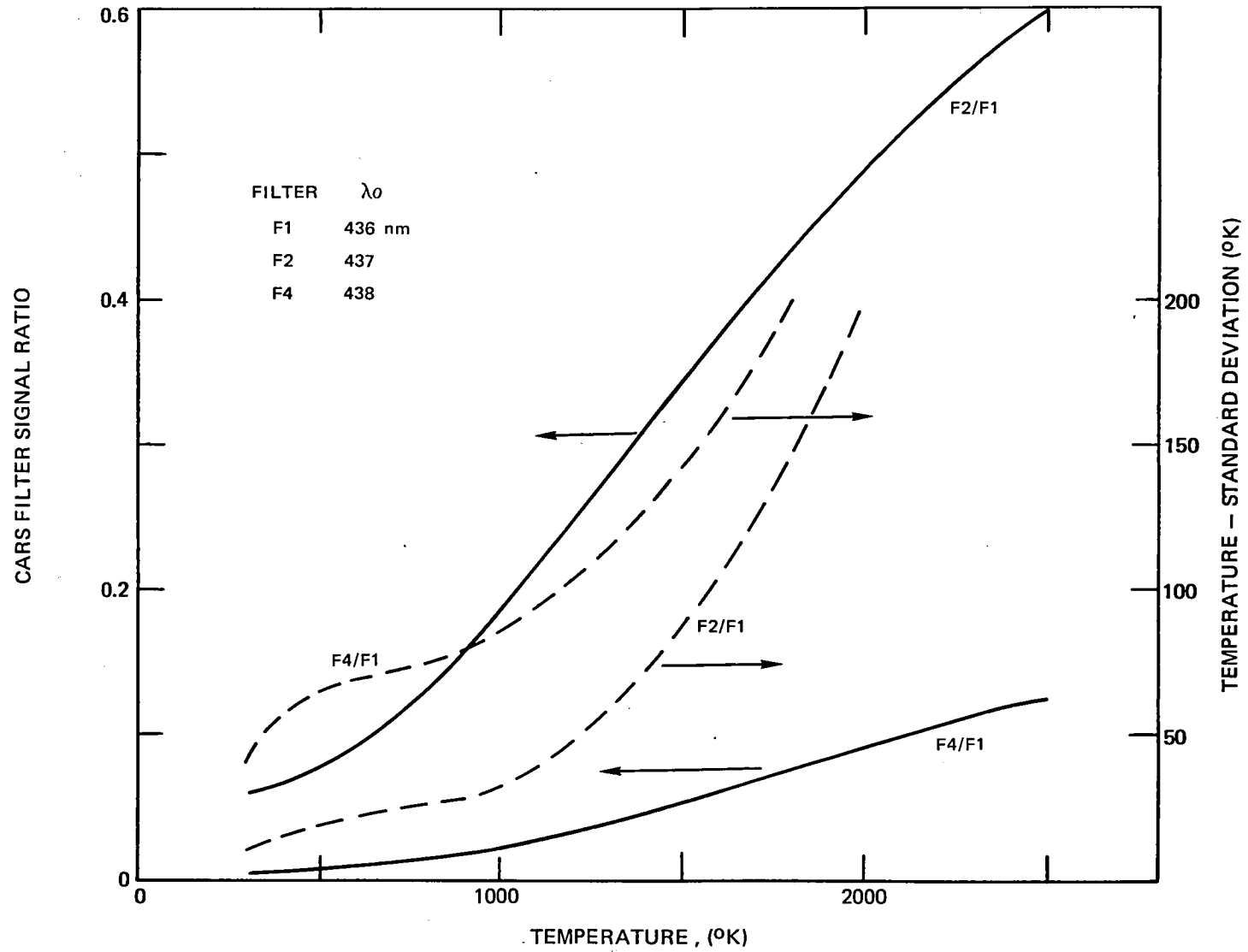


FIG. 10

where N and N' are the CARS signals from each filter with variances σ_N and $\sigma_{N'}$, and $r = N/N'$. For a Poisson distribution of photons $\sigma_N = N^{1/2}$ and

$$\sigma_T = r \frac{dT}{dr} \left(\frac{1}{N} + \frac{1}{N'} \right)^{1/2} \quad (15)$$

The estimated temperature variance for atmospheric pressure, 100 percent concentration hydrogen is shown. The uncertainty increases rapidly at high temperature due to the decrease in CARS signal with temperature. Lower concentration will result in greater uncertainty. For example, in the Doppler broadened limit the number of CARS photons generated varies as the square of the gas density. The uncertainty is proportional to N^{-1} .

Although the signal is derived through filters and some information present in the H_2 CARS signal is thereby lost, this method has some positive points which recommend it. First, it features inexpensive, efficient detection. Capital purchases can be spread out in stages, yet meaningful first results can be generated. Second, analysis of the data could conceivably be done on a small computer, perhaps on line or rapidly after a test.

CARS linewidths. - The generation of CARS depends on the distribution of radiation within the linewidth of the transition as shown in the susceptibility expression presented earlier in this section. The Raman linewidth for a molecular species is a function of gas temperature and density and may depend on the rotational quantum number. Recent investigations have indicated that the CARS linewidth may under certain conditions not be a function of molecular parameters but may be governed by laser characteristics (Refs. 25-26). This is an area of active investigation and will require further study. Discussion here will be confined to Raman linewidths.

At very low density, the linewidth of spectral lines is determined by the Doppler effect due to thermal motion of the molecules. The line profile is Gaussian, and the bandwidth (FWHM)

$$\Delta\nu_D = 2 \frac{\nu}{c} \left(2 \ln 2 \frac{kT}{m} \right)^{1/2} \quad (16)$$

where ν is the center frequency, and m is the molecular mass; and the other symbols have their usual meaning. For Raman scattering with highly unidirectional laser sources the recoil of the molecule imparted by the scattering process must be taken into account. Weber (Ref. 27) has shown that the correct linewidth in this case is given by

$$\Delta\nu_D = \frac{2}{c} \left(2 \ln 2 \frac{kT}{m} \right)^{1/2} \left[4(\nu_o^2 + \nu_o \nu_R) \sin^2 \frac{\theta}{2} + \nu_R^2 \right]^{1/2} \quad (17)$$

where ν_o is the frequency of the exciting radiation, ν_R is the Raman frequency shift and θ is the scattering angle. Note that the linewidth is minimum for forward scattering ($\theta = 0$) and maximum for backward scattering ($\theta = 180^\circ$). These effects have been demonstrated (Ref. 28). Examples and additional references can be found in Weber (Ref. 27). It has been shown (Refs. 29 and 30) that the width of CARS lines in the Doppler limited regime is smaller than the Raman linewidth by a factor of $\sqrt{2}$. The linewidth which is appropriate in the susceptibility calculation, however, is the Raman linewidth.

As the gas density is increased intermolecular forces (collisions) act to modify the linewidth. In the pressure broadened range, the linewidth increases linearly with gas density, and the lineshape is Lorentzian. The linewidth (FWHM) in the usual notation is proportional to $B\rho$ where B is the optical (Raman) broadening coefficient in either $\text{cm}^{-1}/\text{amagat}$ or MHZ/amagat , and ρ is the density. The collisional broadening coefficient depends on the collision partner. Usually the broadening coefficient for foreign molecules is smaller than the self broadening coefficient (Ref. 29). The pressure broadened linewidth for gas mixtures is given by

$$\Delta\nu_L = \sum_i B_i \rho_i \quad (18)$$

In the range of densities between the Doppler limit and the pressure broadening regime, line narrowing, named for Dicke who first described it (Ref. 32), can occur in some molecules (Refs. 33 to 35). As mentioned, Doppler broadening for a scattering event arises from the recoil momentum imparted to the molecule by the scattering photon. If an elastic collision occurs simultaneously, some of the momentum may be taken up by the colliding molecule; and the scattered photon will have a smaller Doppler shift than if no collision occurs. Pressure broadening becomes dominant when the collision rate is so large that a substantial number of inelastic collisions occur, which change the internal state of the molecule. Dicke narrowing occurs when the mean free path for elastic collisions is comparable to the wavelength of the scattered photon and is less than the mean free path for line broadening (internal state changing collisions) (Ref. 31).

Gersten and Foley (Ref. 34) showed that the linewidth is given by

$$\Delta\nu = \frac{k^2 D_o}{\pi \rho} + B\rho \quad (19)$$

where k is the difference between the wavevectors of the incident and emitted photons (i.e., the momentum changed divided by \hbar) and D_0 is the diffusion coefficient at 1 amagat. This formulation will be referred to as the diffusion model. The linewidth is minimum when $\rho = (k^2 D_0 / \pi B)^{1/2}$ and is given by

$$\Delta\nu_{\min} = 2 \left(\frac{k^2 D_0 B}{\pi} \right)^{1/2} \quad (20)$$

It should be noted that k is larger for backward scattering and hence the linewidth at minimum is greater than the forward scattering linewidth at minimum. The wavevector difference is just k_0 , the Raman difference wave-number for forward scattering which is applicable for CARS.

Another type of narrowing occurs at much higher density. As discussed above, pressure broadening occurs when inelastic collisions modify the phase of the vibrational motion. Q branch components can be modified by rotationally inelastic collisions through the rotational-vibrational interaction which causes molecules in different rotational states to have slightly different vibrational frequencies. The effect is probably the dominant source of broadening of the vibrational Raman lines of simple molecules like H_2 , N_2 , and CO (Ref. 36). Alekseyev et al (Ref. 37) first pointed out that when the collision frequency becomes large compared to the rotation-vibration interaction, the Q branch components overlap and such collisions no longer lead to scattering at a slightly shifted frequency. Therefore, broadening should cease at such densities. Splitting of the Q branch components disappears, and the band collapses to the center of the unperturbed band.

The reader is cautioned that an unambiguous nomenclature for these effects has not been adopted. Dicke narrowing and this latter narrowing have both been called collisional narrowing or motional narrowing. In this report, these effects will be referred to as Dicke narrowing and Q branch narrowing.

The density at which collision broadening becomes important is (Ref. 37)

$$N \geq \frac{2\pi\alpha_e J_m^2}{\langle v\sigma_{J-1,J} \rangle} \quad (21)$$

where α_e is the vibration-rotation interaction factor, J_m is the rotational quantum number of the most populated rotational level ($J_m = (kT/2Bhc)^{1/2} - 1/2$) and $\langle v\sigma_{J-1,J} \rangle$ is the rate constant for $\Delta J = 1$ collisions. May, Stryland,

and Varghese (Ref. 38) have observed collision narrowing in nitrogen at densities in excess of 16 amagat. The vibration-rotation interaction factor in O_2 is slightly smaller than that for N_2 , so that a somewhat lower density for collision broadening is expected. The α_e factor in H_2 is very large (2.993 cm^{-1}) so that Q-branch narrowing need not be of concern for the present studies.

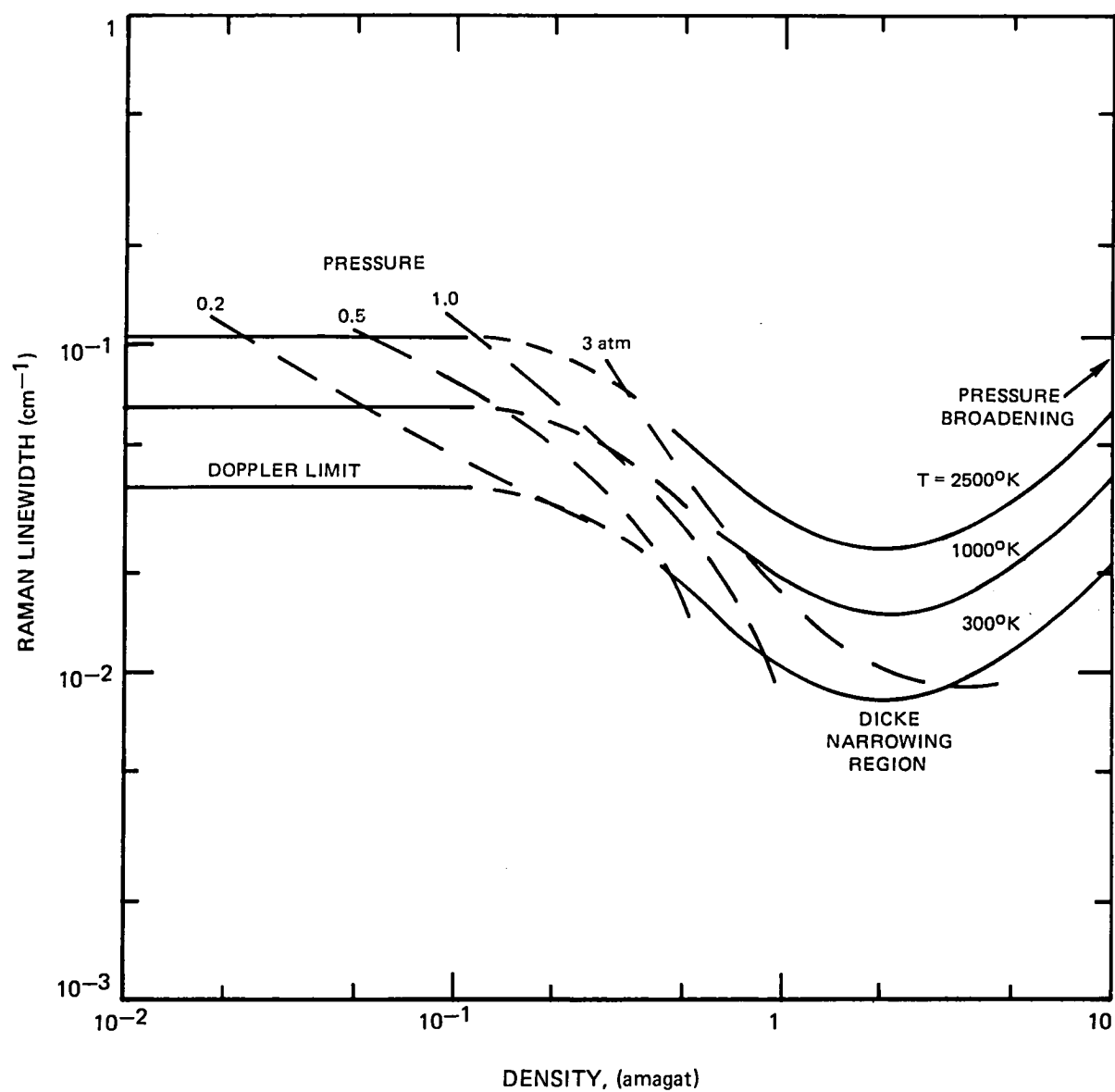
Estimates of the CARS linewidths have been made for H_2 and O_2 . For the nominal range of scramjet experimental parameters, O_2 is within the pressure broadened range. Estimates based on the diffusion model indicate that for H_2 , Dicke narrowing occurs at the higher limit of the density range. The Raman linewidth as a function of density and temperature is shown in Fig. 11. The solid line to the left on this figure gives the Doppler limited linewidth. The solid curves to the right exhibiting minima are based on the diffusion model. Far to the right, the curves assume a linear dependence characteristic of pressure broadening. The pressure broadening coefficient is taken to have a $T^{1/2}$ dependence as has the diffusion coefficient D_0 as defined in Eq.

19. In the region between Dicke narrowing and the Doppler limit, Eq. 19 is not valid. The assumed dependence is shown with a dotted line in the figure. Lines of constant pressure have been included for ready comparison. It can be seen that for low temperatures and moderately high pressures, the linewidth is Dicke narrowed. Under this condition, the linewidth can decrease with increasing density. This will produce higher CARS intensities. Estimates have been made of the CARS signals in H_2 as a function of pressure and temperature; the results are shown in Fig. 12. At low pressure, the CARS intensity is proportional to N^2 . As the pressure is increased, the dependence becomes cubic in pressure and finally goes over to the linear dependence characteristic of pressure broadening. Roh and Schreiber (Ref. 39) have measured the CARS intensity in H_2 as a function of density from 3×10^{-3} to 60 amagat at room temperature. This data shows the same dependence as shown in Fig. 12.

Discussion of task I studies. - Estimates have been made of the CARS signals as a function of spatial resolution for typical scramjet test conditions. These calculations indicate that making measurements in O_2 at the lowest densities will require some tradeoffs. For example, from Fig. 7 the signal for 10 percent concentration at 0.2 atmospheres will be approximately $2(10^{-6})$ counts per pulse for an interaction length of 0.1 cm.

Assuming a BOXCARS configuration is employed, the interaction length can be changed readily by changing the crossing (half) angle α (Ref. 18). Table II gives the geometric resolution as a function of crossing angle for a beam diameter ($1/e^2$) of 300 μm which is typical of a 30 cm lens. It is seen that the resolution can be changed to any desired value.

H₂ Q(1) RAMAN LINEWIDTH-DIFFUSION MODEL



H_2 Q(1) CARS PRESSURE DEPENDENCE – DIFFUSION MODEL

C = 100%

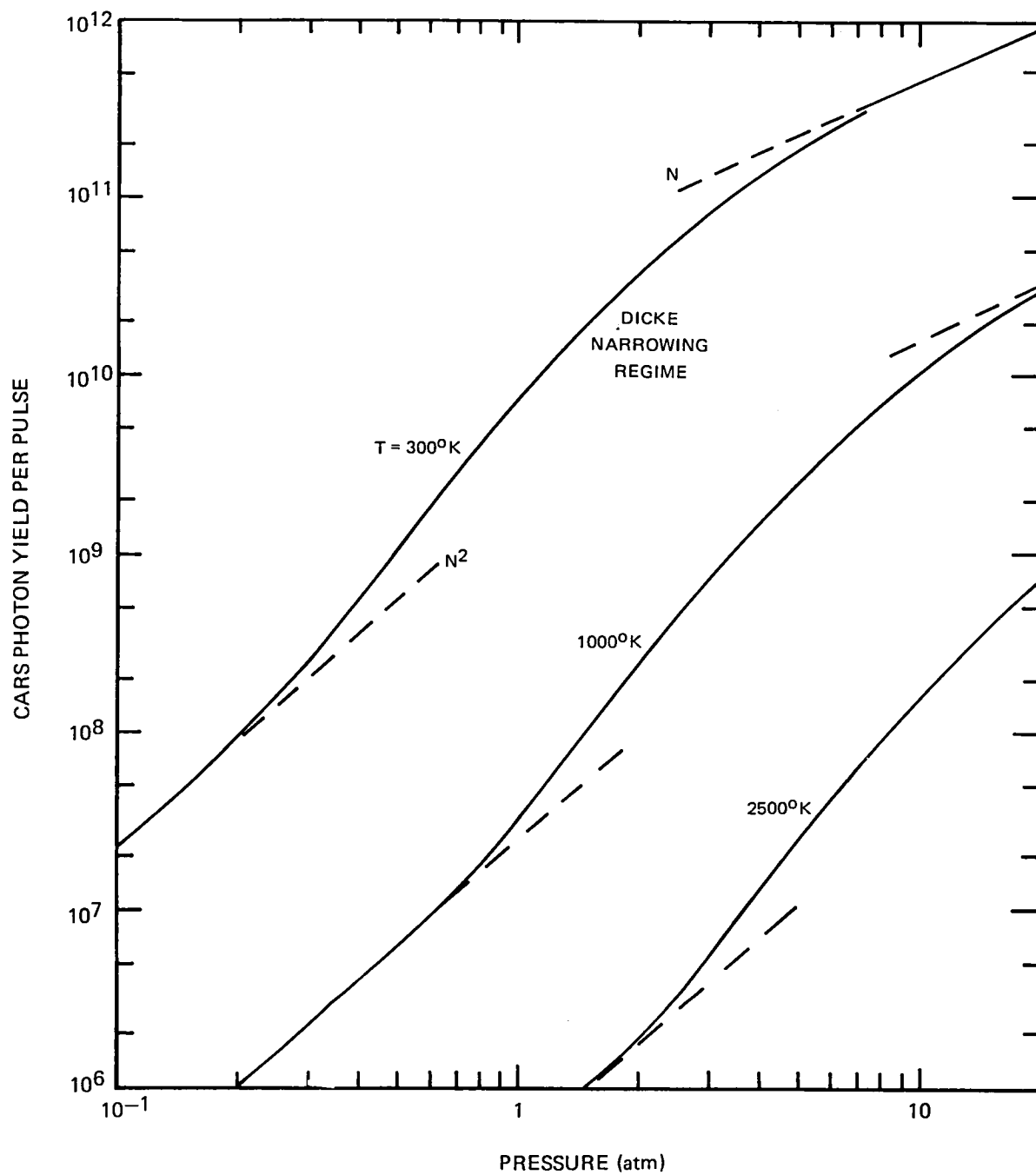


TABLE II - BOXCARS SPATIAL RESOLUTION

<u>2α (degrees)</u>	<u>L (cm)</u>
1	3.1
2	1.6
4	0.77
10	0.31
20	0.16

As an alternative approach, the measurement SNR can be increased by averaging many pulses. At a repetition frequency of 10 Hz, 150 pulses can be accumulated in a 15 second test time. This would result in a signal-to-noise improvement of a factor of 12 for shot noise limited statistics.

Some improvements can be made by using a narrower dye laser spectrum (e.g., an interference filter in the dye laser cavity) or by going to a shorter focal length lens, depending on the available space. It should be noted that the estimates of CARS signals are quite conservative because only a single transition is assumed. In practice, the bandpass of the monochromator necessary for broadband dye laser operation is likely to include several Q(J) transitions. Increasing the bandpass of the monochromator will increase the CARS SNR without affecting the spectral information content too greatly.

The statistics for H₂ CARS are more favorable, however, it appears that measurements at the lowest densities will again require capturing many laser pulses. This presents no difficulties in steady flows. Measurements in turbulent flows cannot be averaged satisfactorily when the CARS signal is a function of the square of the gas density (N²) as in the Doppler limit or when the temperature also fluctuates. When signal strength permits, CARS measurements in turbulent flows can be made in a single shot (Ref. 40).

Temperature measurements in the NASA scramjet facility from H₂ CARS should be relatively simple. Corrections to the data contained in Fig. 9 and 10 would be required to account for the actual dye laser spectral power distribution. Calculations for the filter pair should take into account the actual shape and peak transmission of each filter. A better approach is to calibrate the filter ratio using a heated gas cell. The calculations indicate that the temperature accuracy can be better than 5 percent up to 1400 °K and is approximately 10 percent at 2000 °K for the F2/F1 filter combination. These estimates are for 100 percent concentration and a single shot. At lower concentrations, measurements at the same accuracy can be made by averaging many shots. For

example, measurements at 10 percent concentration can be made at the same accuracy by averaging 100 laser pulses. In regions where the H_2 concentration is very low, the temperature must be determined from other species, such as N_2 .

The principle difficulty for H_2 CARS appears to be in the interpretation of the CARS data to obtain concentrations because of uncertainties in the linewidths. The simple diffusion model which appears to be valid at room temperature was extended to predict linewidths at elevated temperatures. For the calculations, the broadening coefficient, B , was assumed to have a $T^{1/2}$ temperature dependence. This means that the cross section for broadening collisions is independent of temperature. This has been verified for vibrational-rotational Raman scattering up to approximately 420 °K (Ref. 41). The effect of foreign gas broadening has not been fully explored. Roh and Schreiber found Dicke narrowing in H_2 CARS caused by foreign gas (He) broadening (Ref. 39). It is interesting to note that narrowing occurs at the same density as in pure H_2 .

These arguments which are really concerned with Raman linewidth may not be applicable to CARS under all conditions. There is some evidence that linewidths larger than the Raman linewidth are appropriate for pulsed (high intensity) CARS (Ref. 26).

Consideration has not been given under Task I to CARS from H_2O or N_2 . CARS from N_2 in a flame has been studied at this laboratory previously (Ref. 25). Sensitivity estimates for H_2O were not done because of the complicated nature of the spectra. As will become clear in the discussion of experimental results, the calculation of the CARS spectrum of H_2O can only be done on a computer because of the large spectral density of rotational states involved. The Raman cross section for H_2O is two times larger than the O_2 cross section (Refs. 42-43). There are many more rotational states so that the intensity of individual lines is decreased. The sensitivity limits for H_2O CARS will probably be lower than for O_2 .

The estimates of CARS signals presented here indicate that it will be possible under certain conditions to make nonintrusive measurements of gas temperature and species concentrations in the NASA scramjet combustion facility. It appears possible to make some single shot measurements in H_2 at moderate concentrations with excellent (0.1 cm) resolution. Measurements at low concentrations and high temperatures, however, will require some tradeoffs in spatial resolution and/or signal accumulation for several laser shots.

Task II: Experimental Investigations

The objective of Task II was to examine experimentally CARS diagnostic approaches applied to laboratory scale H_2 -air flames. Measurements have been made of CARS spectra of all of the major species, with the exception of nitrogen, which has been studied extensively elsewhere (Ref. 25). The burner and the CARS apparatus employed are discussed first. The results of measurements of H_2O in a premixed H_2 -air burner are described and compared to theoretical predictions of H_2O spectra. Next measurements of O_2 CARS spectra in a H_2 /air diffusion flame are reported. These measurements are compared to theoretical spectral predictions and algorithms for the reduction of O_2 CARS data are presented and used to yield temperature and concentration profiles through the flame. The measurement of oxygen at low concentrations is dependent on the magnitude of the nonresonant contribution to the susceptibility. The results of preliminary measurements of this quantity in the post flame region of stoichiometric H_2 /air and CH_4 /air premixed flames are presented. Finally measurements of CARS spectra of H_2 in a H_2 /air diffusion flame are presented and discussed. The measurements are compared to spontaneous Raman measurements of H_2 in the same burner. The use of reference cells to provide a concentration calibration is discussed in Appendix A.

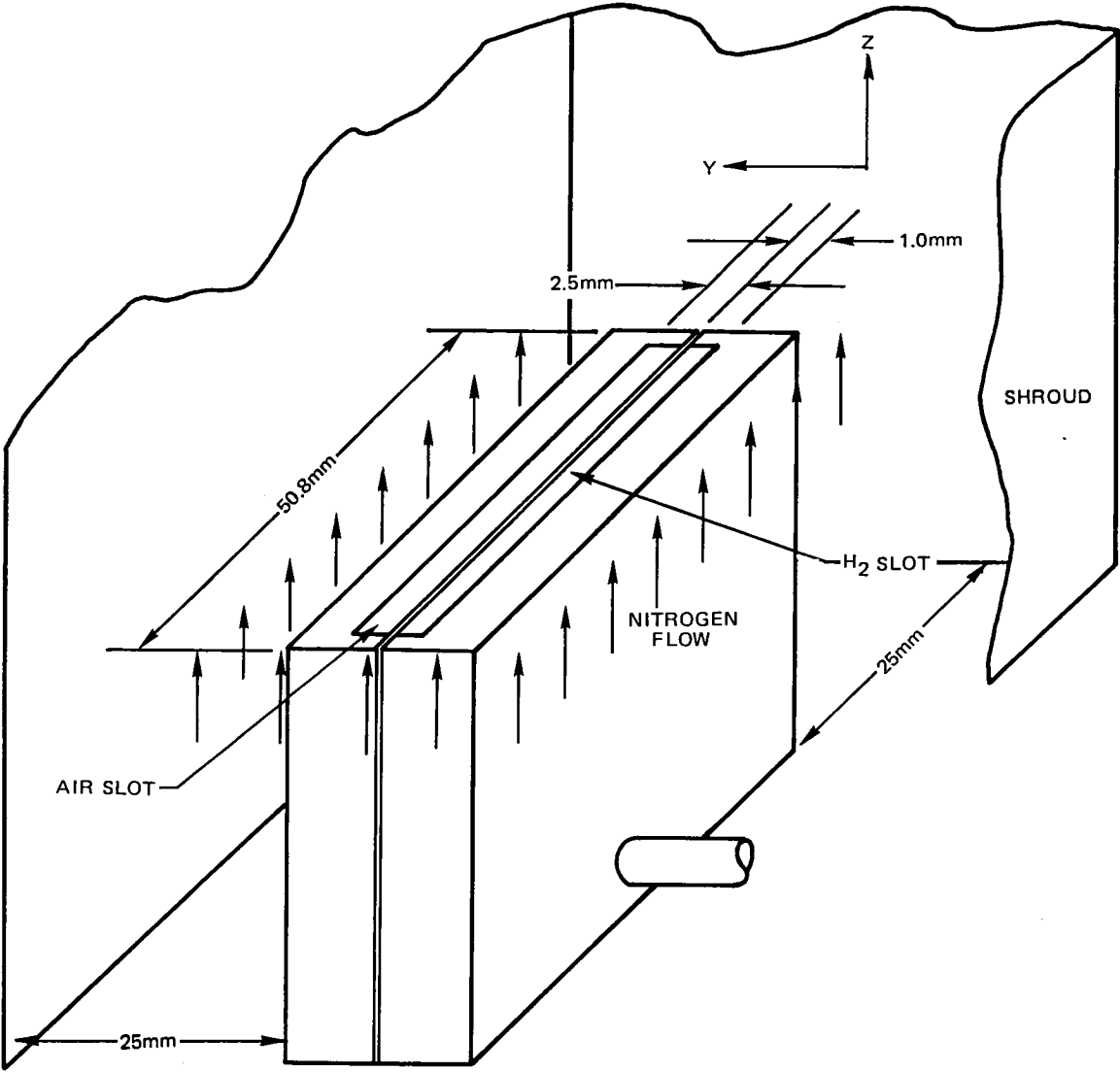
Diffusion flame burner. Most of the measurements reported in this investigation used a flat (two-dimensional) diffusion flame burner patterned after the design of Wolfhard and Parker (Ref. 44). Investigations of this burner have shown that the reactant concentrations are spread out over an extended region affording a large variation in temperature and species concentration. The burner used for these studies is shown in Figure 13. It is composed of two brass blocks into which channels 2.5 mm (0.1 inch) and 1.0 mm (0.040 inch) deep have been milled. These blocks are put together with a "splitter plate" 0.8 mm (0.031 inch) thick. The assembly is uncooled. A curtain of nitrogen surrounds the brass block and acts to stabilize the flame. With the nitrogen flow on, the flame is steady and a small weakly luminous zone is visible starting at the splitter plate and curving into the air side of the flow. For all the measurements reported here, the reactant gas flows are metered on standard rotameters and adjusted to stoichiometric. The flow velocity is approximately 60 cm/sec at the exit of the burner. The areas at the burner exit have been chosen to produce equal velocities in the two streams when the flows are in stoichiometric proportions.

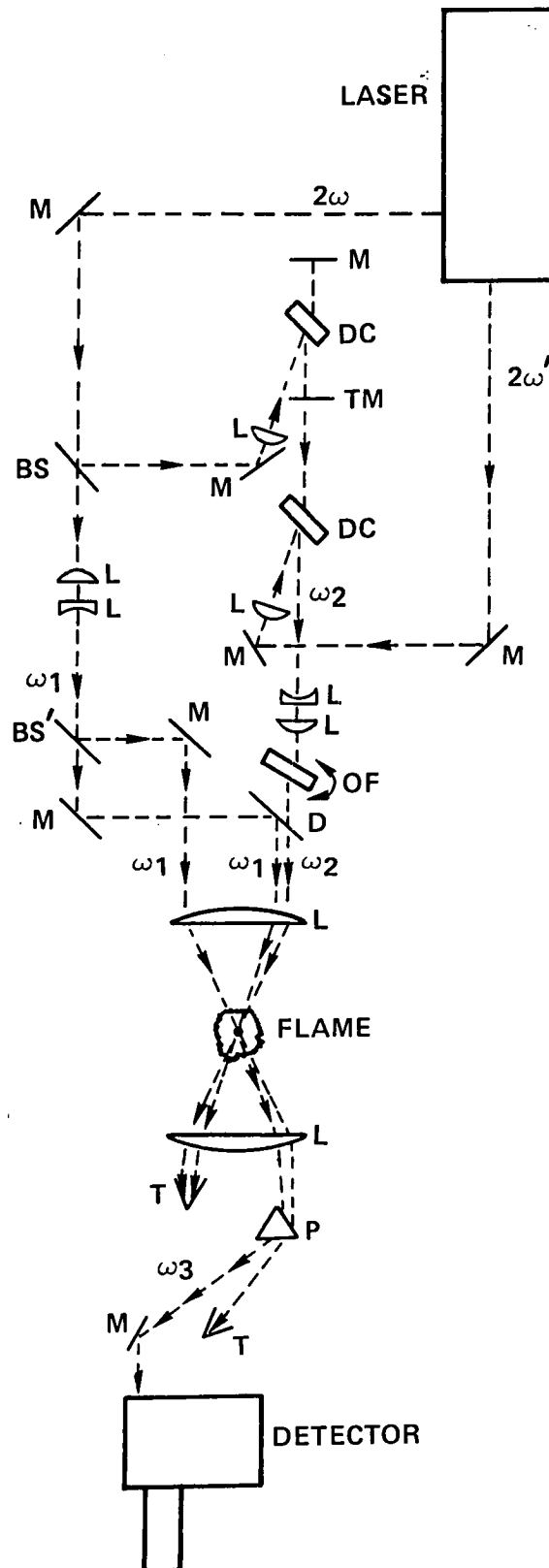
The BOXCARS probe beams are aligned with respect to the burner in such a manner that the axis between the ω_1 pump beams is parallel to the splitter plate and the beams cross at the center of the burner.

CARS experimental apparatus. For the measurements to be described here, a frequency-doubled neodymium laser is used to provide the "pump" frequency as well as to drive the "Stokes-shifted" dye laser as shown schematically in Fig. 14. The output of the neodymium laser (Quanta-Ray Model DCR-1A) is frequency

FIG. 13

FLAT DIFFUSION FLAME BURNER





doubled and produces a horizontally polarized, "primary" green beam at 532 nm. The primary green and residual 1.06 μ m upon leaving the frequency doubler are separated in a splitter section and the residual 1.06 μ m is frequency doubled, generating a "secondary" green beam. Depending upon the condition of the laser, the primary green is typically around 2 W (200 mJ pulses, 10 pps, 10⁻⁸ sec pulse duration) and the secondary about an order of magnitude lower. As seen in Fig. 14 part (about one third) of the primary is split off by the beamsplitter BS, reflected by the mirror M, and focused to pump, slightly off axis, a flowing dye cell oscillator. The output from the dye laser is amplified in another flowing dye cell pumped by the secondary green. The secondary green passes through a piece of KG3 air-cooled Schott glass placed at the Brewster angle to absorb any remaining 1.06 μ m. The dye oscillator and amplifier are in flow series. A small, magnetically-coupled, stainless steel centrifugal pump circulates the dye from a 1.5 liter reservoir through a 0.6 μ filter to prevent any bubbling. The dye cells are oriented at Brewster's angle and produce a horizontally polarized output. To produce the broadband, Stokes-shifted, dye laser output desired for single pulse CARS work, a flat-flat Fabry Perot oscillator arrangement is employed and the bandwidth is appropriately centered by proper dye and dye concentration selection. Bandwidths vary from 100 to 200 cm⁻¹ depending on the oscillator pump energy and whether the dye amplifier is used. By using mixtures of dyes, very broad bandwidths are obtained.

Figure 14 shows the disposition of the three beams at frequencies ω_1 , ω_1 , and ω_2 as utilized for BOXCARS. The primary pump beam after passing through the first beamsplitter is split at the second beamsplitter, BS'. The reflected component passes to the beam crossing lens via the mirror M. The transmitted component is directed to the lens by means of a mirror and the dichroic, D, through which the Stokes-shifted dye laser at ω_2 passes. All three beams ω_1 , ω_1 and ω_2 are aligned parallel to each other in a single plane and sent to the beam crossing lens. If the beams are aligned parallel, they will cross at the focal point of the lens by definition. However, due to wavefront sphericity, they may not necessarily waist at the crossing point. To ensure that the beam waist occurs at the crossing point, adjustable telescopes are added in each leg as shown. At the high laser intensities employed, the beams are readily visualized near the focal region from the room air Rayleigh scattering. The telescopes are then adjusted to visually produce waisting at the crossing point. Also inserted in the ω_2 leg is a rotatable optical flat. Rotation of the flat permits displacement of the ω_2 beams on the focusing/crossing lens permitting the phase-matching angle, θ (Figure 2), to be varied. After passing through the crossing point, the four beams, i.e., CARS @ ω_3 , ω_1 , ω_1 , ω_2 , are recollimated by a second lens generally the same focal length as the focusing lens. Two of the components, ω_1 and ω_2 , are trapped although they could be sent to a reference leg if desired to generate a normalizing signal. At the small crossing angles usually employed for BOXCARS, the

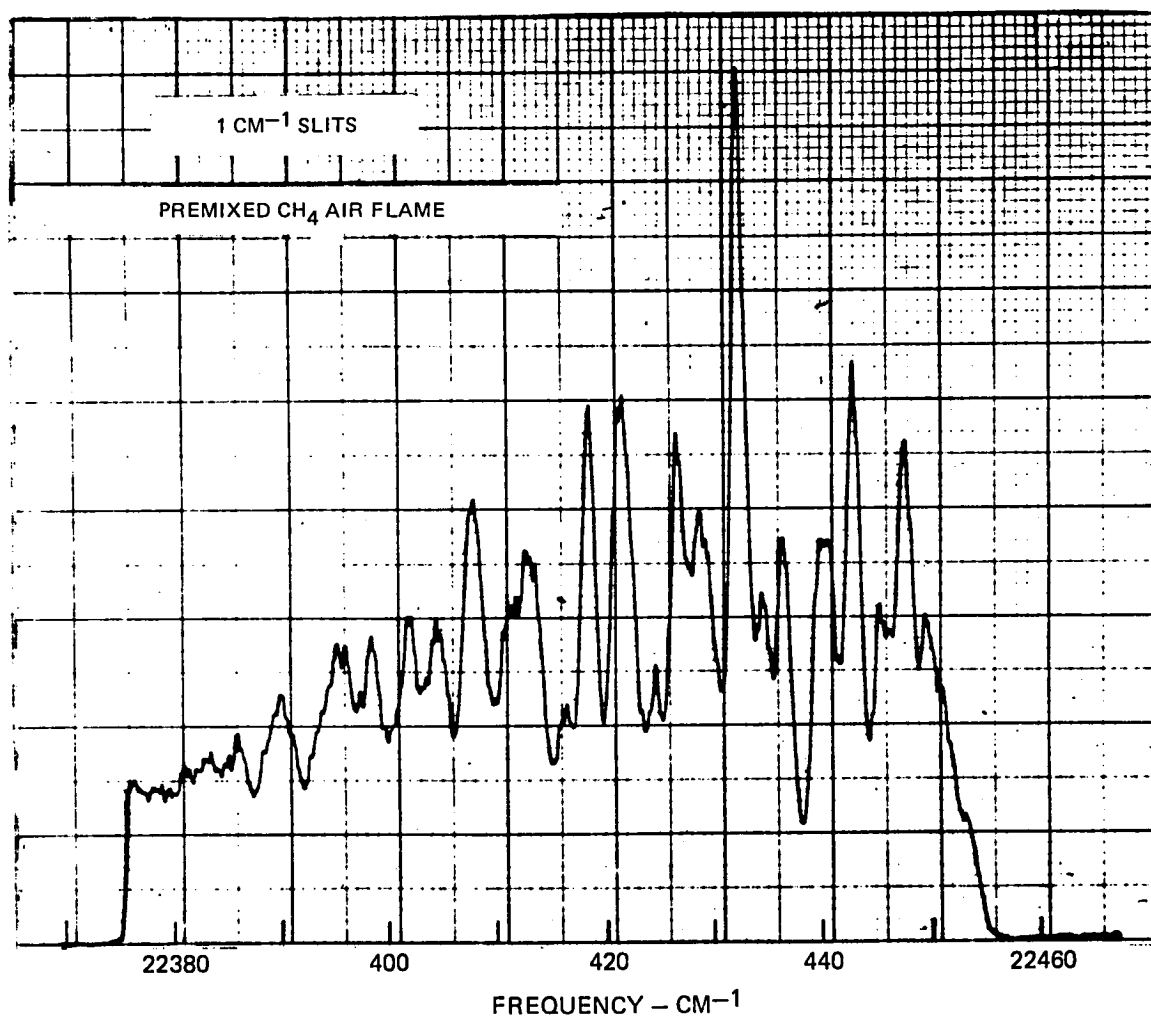
CARS and one pump beam, although angularly separated, are not spatially separated. Additional angular separation is achieved with a double extra dense flint prism. After a suitable distance, the remaining pump component is trapped and the CARS passes through cutoff filters prior to analysis by a 1-m double monochromator (Ramanor HG2S, Jobin Yvon) fitted with an optical multichannel analyzer (SIT, silicon intensified target, PAR). The optical multichannel analyzer captures the entire CARS spectrum with each pulse greatly expediting signal averaging and permitting single pulse measurements. In situations where it is desired to scan the spectrum, the monochromator is fitted with a photomultiplier tube whose output is fed to a boxcar averager (PAR 162/164) which in turn drives a chart recorder. In broadband CARS either the linewidth of the pump laser, the resolution of the spectrometer, or cross-talk on the optical multichannel analyzer determine the ultimate resolution of the spectrum. The 1-m double monochromator has a limiting resolution of about 0.5 cm^{-1} and the pump laser a linewidth of $\sim 0.8\text{ cm}^{-1}$. The CARS spectral resolution was thus limited to about 0.8 cm^{-1} which is more than adequate for most gas phase diagnostics.

CARS spectra of water vapor in flames. Water vapor is the major product of hydrogen combustion and often the dominant product species of hydrocarbon-fueled combustion. Its measurement is an important gauge of the extent of chemical reaction and of overall combustion efficiency. Characterization of the CARS spectrum of water vapor as a function of temperature and concentration is essential to its diagnostic measurement. The spontaneous Raman spectrum of water vapor has been studied in several investigations (Refs. 42, 45), including hydrogen-oxygen flames (Ref. 46).

The experimental apparatus used in these experiments differs from the configuration shown in Fig. 14 only in that collinear phase matching was used. A new laser dye (Ref. 47) was used to generate laser emission at 660 nm. The pump and Stokes beams were combined on a dichroic mirror and focused by a 20 cm focal length lens at a point 2 cm above a pre-mixed methane-air burner. The burner was comprised of a 7.5 cm diameter bundle of 0.3 cm diameter stainless steel hypo tubes pressed in a water cooled ring.

The CARS spectrum of water vapor in the postflame region at a Raman frequency shift of (3651.7 cm^{-1}) corresponding to the symmetric stretch mode is shown in Fig. 15. The flame temperature was measured with a radiation corrected (Ref. 48) thermocouple and found to be approximately 1675°K . The monochromator slits were set at 100, 200, 200, 100 microns corresponding to a nominal 1 cm^{-1} spectra resolution and the CARS spectrum was scanned at $5\text{ cm}^{-1}/\text{min}$. The Stokes dye laser spectrum was initially centered at $15,230\text{ cm}^{-1}$ with a bandwidth (FWHM) of 160 cm^{-1} . As is apparent, the CARS spectrum is very rich in structure even at moderate spectral resolution.

EXPERIMENTAL CARS SPECTRUM OF WATER VAPOR



While only the ν_1 symmetric stretch mode of the H_2O molecule is Raman active (Ref. 42) the involved rotational energy level structure of this asymmetric rotor is expected to give rise to a very complex CARS signature. Each rotational quantum state J possesses $2J+1$ sublevels corresponding to values of the pseudo quantum number τ in the range $-J \leq \tau \leq J$. If all possible transitions obeying the Raman selection rules are considered, approximately $(5/4)(J+1)^2$ transitions would have to be taken into account for each value of J possessing significant population (Ref. 45). It has been shown, however, that the observed spontaneous Raman spectra can be explained in terms of isotropic Q-branch transitions only, a simplification arising from the very small depolarization ($\leq .06$) of the ν_1 mode (Ref. 45). Isotropic Q-branch scattering obeys the greatly simplified selection rules, $\Delta J = 0$, $\Delta \tau = 0$, and the spontaneous cross section will not vary appreciably from line to line.

The success of the theoretical calculation of the H_2O CARS spectrum depends on the accuracy of the vibrational-rotational energy levels used for the calculation of transition wavelengths and state populations. For spontaneous scattering, use of the energy level data of Camy-Peyret, Flaud, and Maillard (Ref. 49) resulted in very good agreement with experiment for temperatures up to $1500^\circ K$ (Refs. 45, 50). In the CARS H_2O calculations reported here, attention is restricted to isotropic Q-branch transitions, and the energy level data of Camy-Peyret, Flaud and Maillard (Ref. 49) is employed. A CARS calculation of the water vapor spectrum places very stringent requirements on energy level accuracy because of strong spectral interference effects which arise from the dependence of CARS intensity on the squared modulus of the third order nonlinear susceptibility.

The energy level data (Ref. 49) are sufficiently complete to permit calculations over a range extending to about 70 cm^{-1} less than the band origin at 3657 cm^{-1} . At the elevated temperatures ($T \geq 1500^\circ K$) of interest for flame diagnostics, the population of the (010) state is significant (> 20 percent), and the contribution of (010) \rightarrow (110) "hot band" transitions, with an origin at 3640 cm^{-1} , should also be considered. Rotational energy levels for these two states have been taken from Camy-Peyret et al (Refs. 51-52). It has been nominally assumed that the fundamental and hot band have the same trace scattering constant.

Given the vibrational-rotational energy levels $E_{vJ\tau}$ of each state, the fractional population $f_{vJ\tau}$ is given by the Boltzman equilibrium relationship,

$$f_{vJ} = \frac{e^{-E_v/kT}}{Q_v} g_\tau \frac{(2J+1)e^{-E_{vJ}/kT}}{Q_r(v)} \quad (22)$$

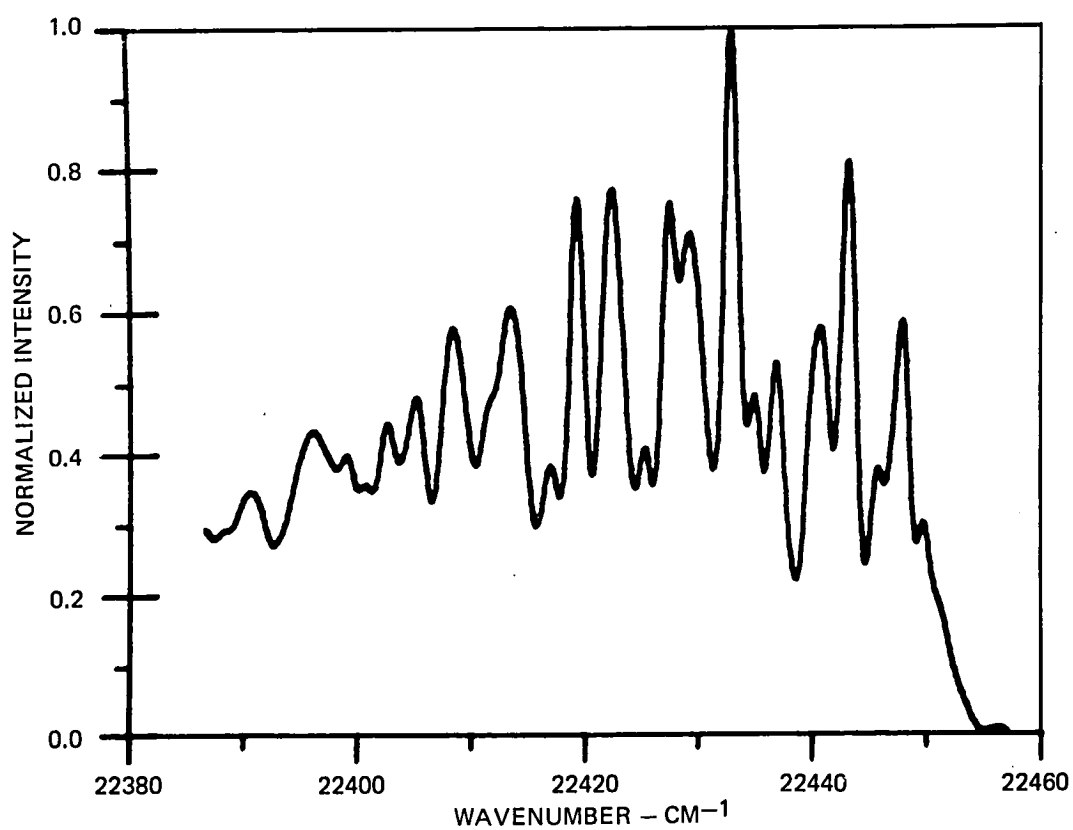
where Q_v is the vibrational partition function, g_τ is a nuclear spin statistical weight ($g_\tau = 1$ for even τ , $= 3$ for odd τ , for the vibrational levels of interest), and $Q_r(v)$ is the rotational partition function for the vibrational state v .

The resonant contribution to the susceptibility can be calculated (Eqn. 5) from the fractional population difference Δ_j between the upper and lower states involved in the transition, $\Delta_j = F_{vJ\tau} F_{v'J\tau}$. For the calculations water vapor was assumed to be present a 10 percent in a nitrogen bath at atmospheric pressure. The nonresonant contribution to the susceptibility (Eqn. 4) was taken to be 4×10^{-18} cm³/erg at room temperature (Ref. 53) and scaled linearly with density. For the broadband, multimode pump and Stokes lasers used in these experiments, the intensity distribution at ω_3 is given by a convolution of $|\chi^{(3)}|^2$ with the measured spectral energy densities of the two exciting lasers.

The predicted CARS signature at the thermocouple indicated temperature is shown in Fig. 16. A comparison of Figs. 15 and 16 shows that the theoretical model reproduces essentially all of the qualitative features of the experimental spectrum. In this calculation the hot band does make a definite contribution, but all of the major features arise from the fundamental, (000) \rightarrow (100). The theoretical reproduction of so much spectral detail is a further indication of the accuracy of the energy level data used (Refs. 49, 51, 52). It is interesting to note that, because of the relatively large spontaneous cross-section for H₂O (Ref. 42), there is little interference from the background susceptibility at the 10 percent H₂O level. This is desirable for thermometry because N and χ_{NR} are then unimportant, leaving temperature as the only unknown parameter. For a background susceptibility approximately equal to that of N₂ (Ref. 53), H₂O CARS spectra should be relatively interference-free down to the few percent level.

The peaks in the H₂O spectrum arise from spectral overlaps of τ states belonging to neighboring J states. In particular, the dominant peak at ~ 22433 cm⁻¹ results from the near coincidence of the J_τ transitions 9₋₅, 10₋₁₀, and 10₋₉ of the fundamental, with a small contribution from 4₋₃ of the hot band. For the assumed homogeneous linewidths ($= .1$ cm⁻¹ for all transitions), the theory does not fully account for the strength of this feature. This and a few other quantitative discrepancies concerning relative peak heights may be due to

COMPUTED CARS SPECTRUM OF WATER VAPOR

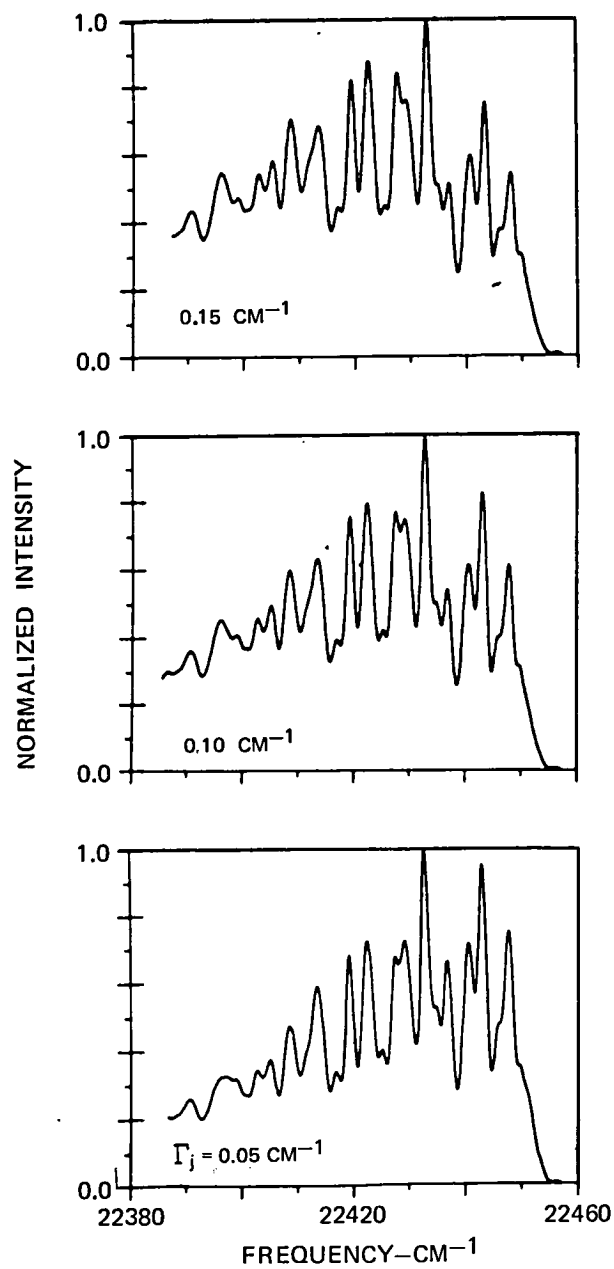


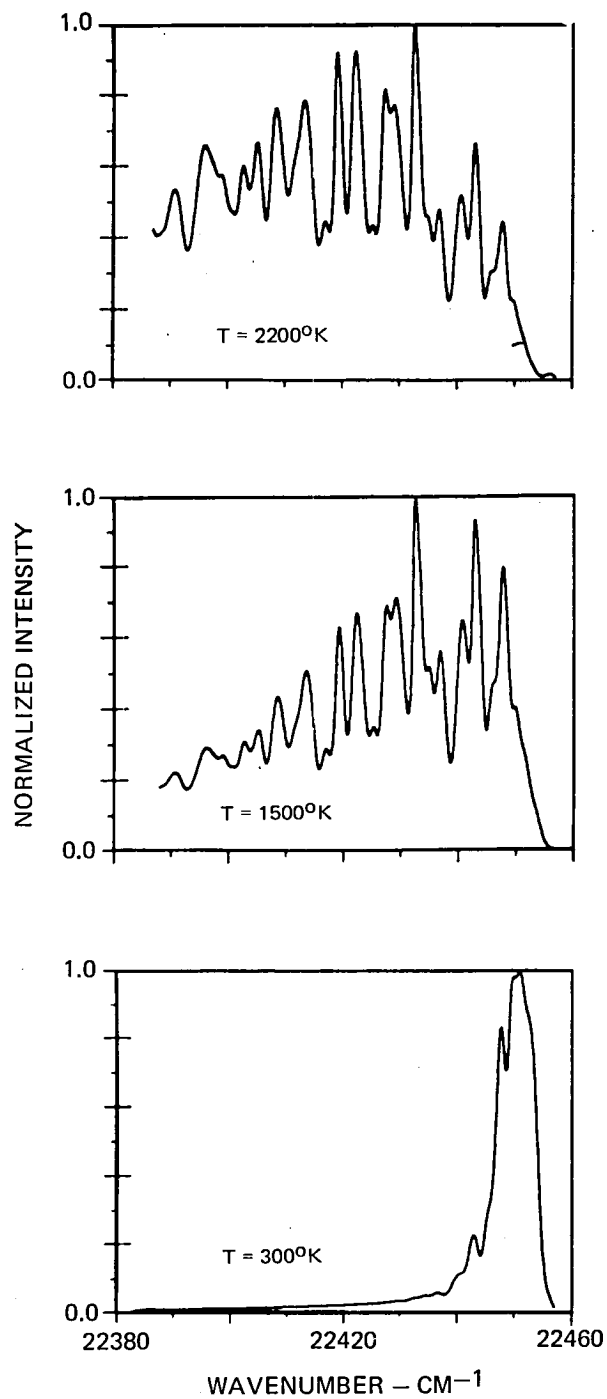
insufficient knowledge of homogeneous linewidths. Calculations have been carried out to study the sensitivity of the CARS computed results to variation of the assumed Raman linewidth. The results of the linewidth sensitivity calculations are shown in Fig. 17. It is seen that although the assumed Raman linewidths are much smaller than the pump laser bandwidth (0.8 cm^{-1}) with which it is convolved in these calculations, important variations can be produced. There are subtle changes, in some cases reversals, in the heights of some adjacent lines in the spectra. More importantly, the CARS contributions from higher rotational levels (i.e. lower frequency) are substantially increased. This observation is significant because a similar effect arises from temperature variations and, experimentally, a shift of the Stokes dye laser spectrum can cause similar effects. Clearly good control of the dye laser Stokes spectrum will be required for accurate temperature measurements. It may be adequate for temperature measurements to infer approximate Raman linewidths from comparison of computed and experimental spectra which can be done for carefully controlled experiments where the temperature is independently determined. However independent measurement of H_2O Raman linewidths under flame conditions will yield more reliable temperature information.

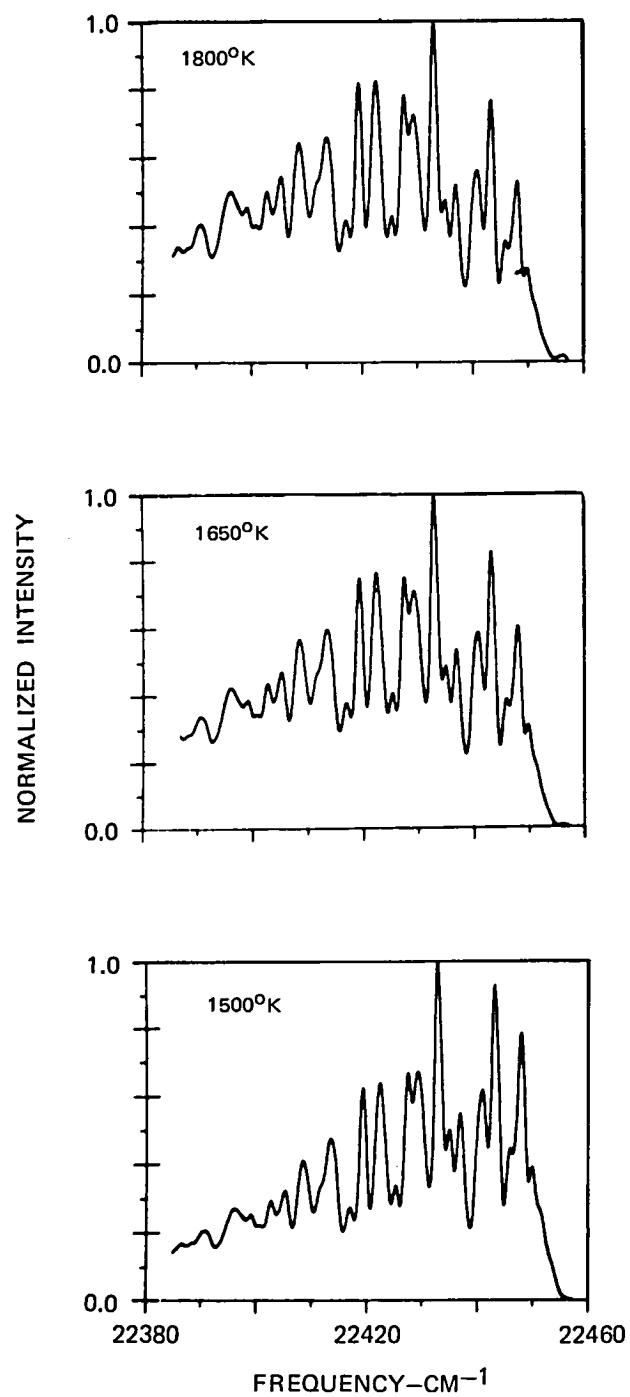
The predicted spectra exhibit a pronounced sensitivity to temperature as shown in Fig. 18. There, normalized CARS spectra are displayed at temperatures of 300, 1500, and 2200°K at 1 cm^{-1} resolution and 0.1 cm^{-1} Raman linewidth. As the temperature increases, higher rotational levels are populated, causing the spectra to become weighted toward smaller Raman shifts. Computer calculations at temperature between 1500 and 1800°K shown in Fig. 19 indicate the CARS spectrum exhibits considerable detail which varies with temperature.

The possibility of performing temperature measurements from the CARS spectrum of flame water vapor appears very promising due to the many rotational transitions involved. Temperature measurements, derived from computer fitting the entire CARS spectrum, would likely be most accurate. Since the water vapor spectrum is relatively broad ($\sim 1.4 \text{ nm}$) at flame temperatures, however, measurements might be made by taking the ratio of selected integrated portions of the spectrum, e.g. through narrowband interference filters centered near the extrema of the spectrum. Number density determination could be performed from integrated intensity measurements after having determined the temperature.

CARS spectra of O_2 in the diffusion flame. The CARS spectra of O_2 in the H_2 -air diffusion flame burner were recorded on the optical multichannel analyzer at several heights above the flame by translating the burner relative to the laser probe volume (determined by the crossing of the pump and probe beams in a low angle ($\alpha = 1^\circ$) BOXCARS configuration). This configuration was found to be necessary to eliminate the effect of cold O_2 from outside the flame

EFFECT OF RAMAN LINEWIDTH ON COMPUTED H_2O CARS SPECTRUM

EFFECT OF TEMPERATURE ON COMPUTED H₂O CARS SPECTRUM

EFFECT OF TEMPERATURE ON COMPUTED H_2O CARS SPECTRUM

region. The data, shown in Fig. 20 which were taken from the air side of the flame through the flame front to the fuel side of the flame, clearly show the cold relatively high concentration O_2 , the O_2 becoming hot and finally being consumed by combustion. The splitter plate is located at $y = 0$ and the air side of the flame corresponds to positive values of y (see Figure 13).

Figure 21 shows a spectrum of O_2 within the air side of the flame averaged on the optical multichannel analyzer for 15 sec. Three bands corresponding from left to right to the $v = 0 \rightarrow 1$ fundamental, and the $v = 1 \rightarrow 2$ and $v = 2 \rightarrow 3$ "hot" bands are apparent. The rotational structure is pronounced because the even numbered rotational transitions are missing (Ref. 20). Interference between the background nonresonant susceptibility and the resonant O_2 contribution causes the 'dip' at the fundamental band head. The CARS radiation to the left of the dip arises from the nonresonant background susceptibility. Photographs taken with less horizontal scale expansion show that the background traces out a curve corresponding to the dye laser spectrum. The dispersion corresponds to $0.44 \text{ cm}^{-1}/\text{dot}$ and the resolution is approximately 1.2 cm^{-1} . The solid curve is a computer calculation of the CARS spectrum for 4.4 percent O_2 at 1700°K assuming a nonresonant susceptibility of $7 \times 10^{-19} \text{ cm}^3/\text{erg}$. Other data show that the height of the first hot band can exceed the fundamental band on the fuel side of the burner where the oxygen is hot and at low concentration. To some extent this behavior is accentuated by the position of the dye laser spectrum. The dye laser spectrum was peaked at 17260 cm^{-1} corresponding to 20334 cm^{-1} in the CARS spectrum or a position between the peak of the fundamental band and the dip of the first hot band. Rhodamine B was used at (5×10^{-5}) moles/liter concentration and gave 12 mJ pulses with a bandwidth of 170 cm^{-1} .

The CARS spectrum of O_2 has been calculated for several concentrations at 1000 and 2000°K . The computer simulated spectra presented in Figures 22 and 23 have been convolved with a 2.7 cm^{-1} slitwidth typical of an optical multichannel analyzer on a 1/4-m spectrometer with high dispersion. The O_2 was assumed to be present in a background of H_2 and H_2O . The nonresonant susceptibility of water vapor has been assumed equal to methane. As seen, the CARS spectrum at 20 percent concentration rises well out of the nonresonant background and the CARS hot band is quite prominent. As the concentration decreases, significant modulation of the nonresonant background occurs; however the depth of modulation becomes less with decreasing O_2 concentration. To the extent that the nonresonant susceptibility is known or can be approximated, the concentration can actually be obtained from the shape of the CARS spectrum obviating the requirement for absolute intensity measurements.

Spectra have been recorded at 0.5 cm, 1.0 cm and 1.5 cm above the burner exit. The spectra shown in Figure 21 were analyzed by fitting computer simulated spectra to the measured spectra. To simplify the data reduction algorithms using the ratio of spectra band features were developed from simulated spectra.

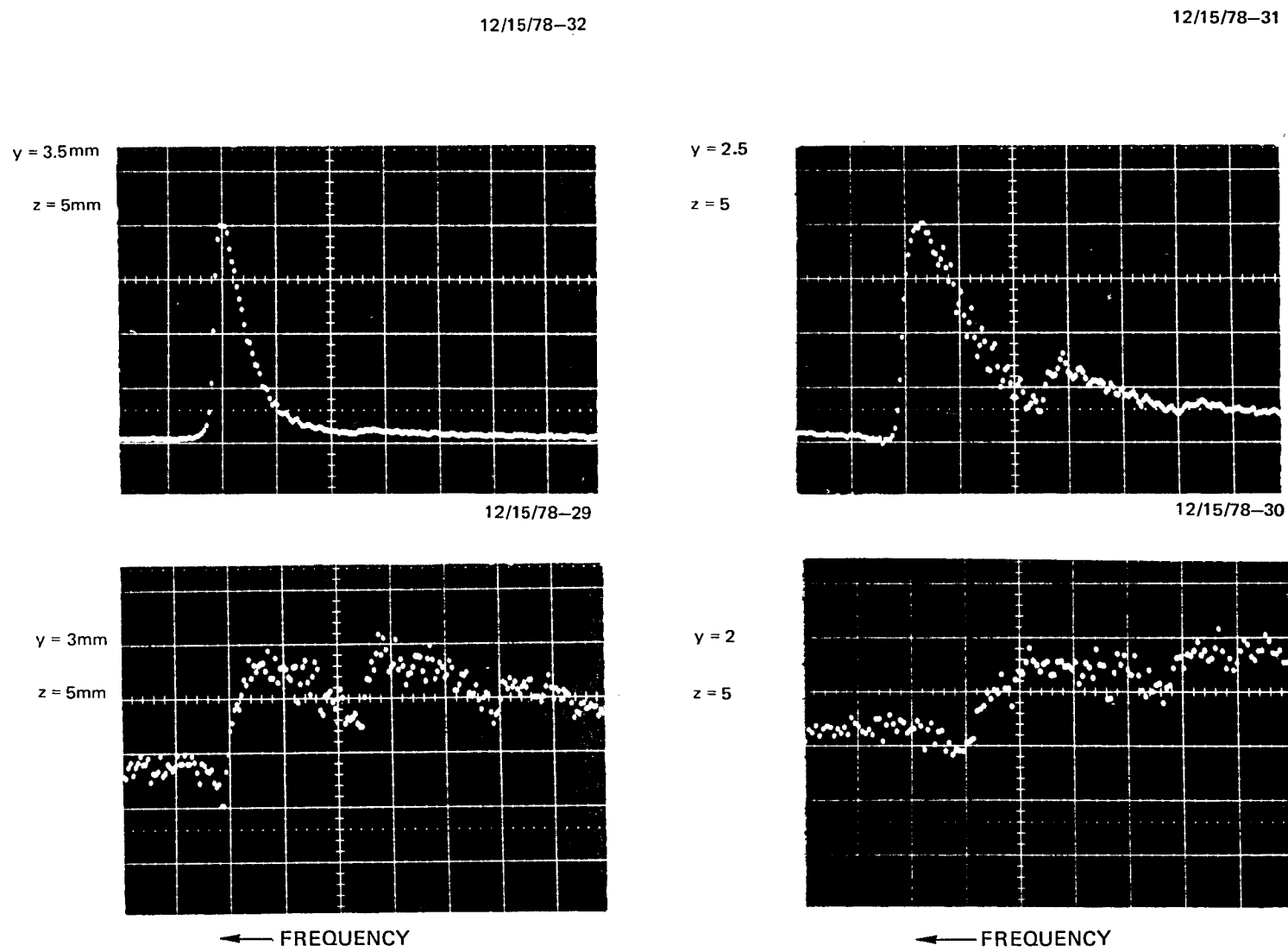
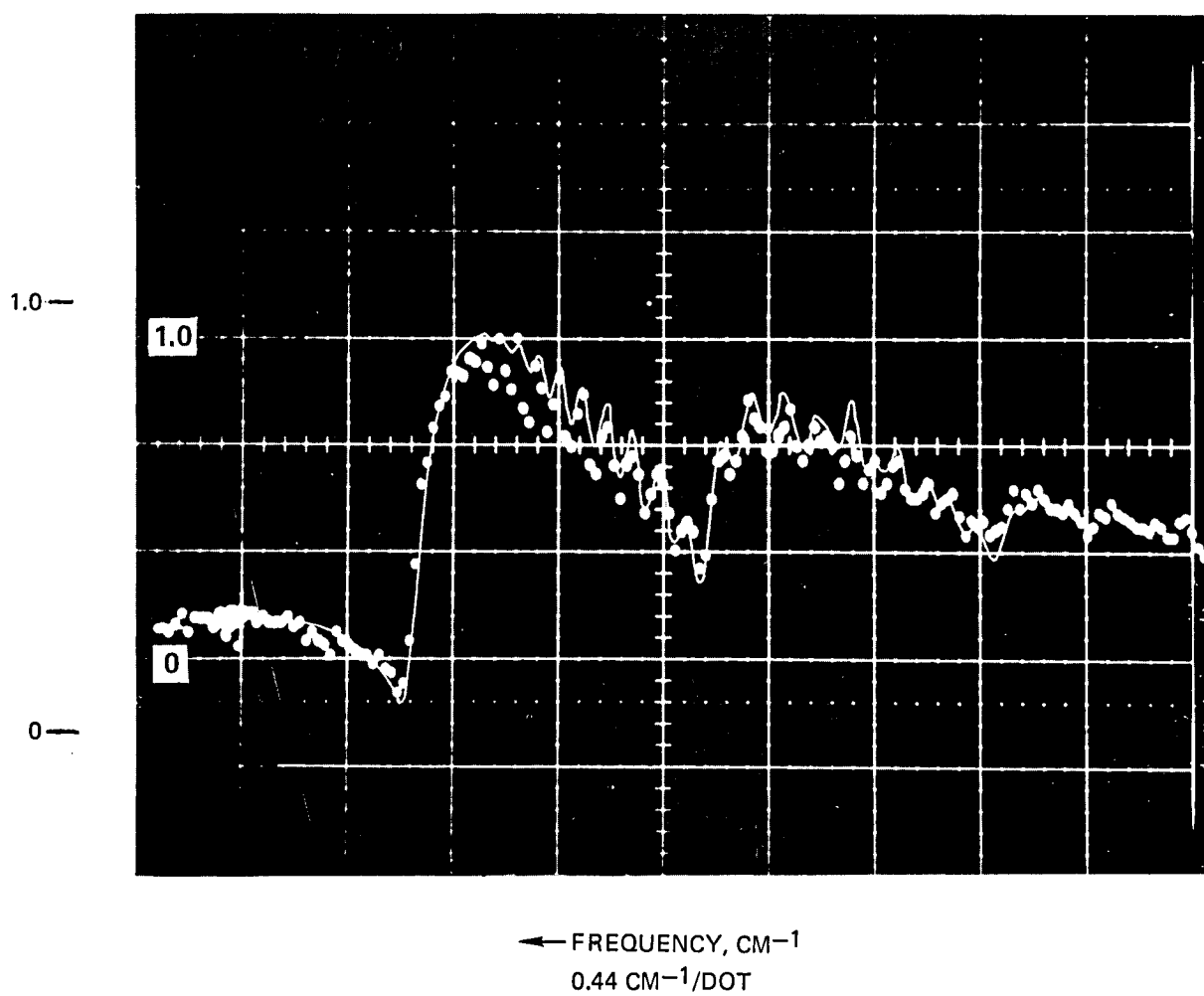
CARS SPECTRA OF O_2 IN H_2 -AIR DIFFUSION FLAME

FIG. 20

CARS SPECTRUM OF O₂ IN H₂-AIR FLAME $T = 1700^{\circ}\text{K}$, $C = 4.4\%$, $\chi_{\text{NR}} = 7 \times 10^{-19} \text{ CM}^3/\text{ERG}$ 

COMPUTED CARS SPECTRA OF OXYGEN

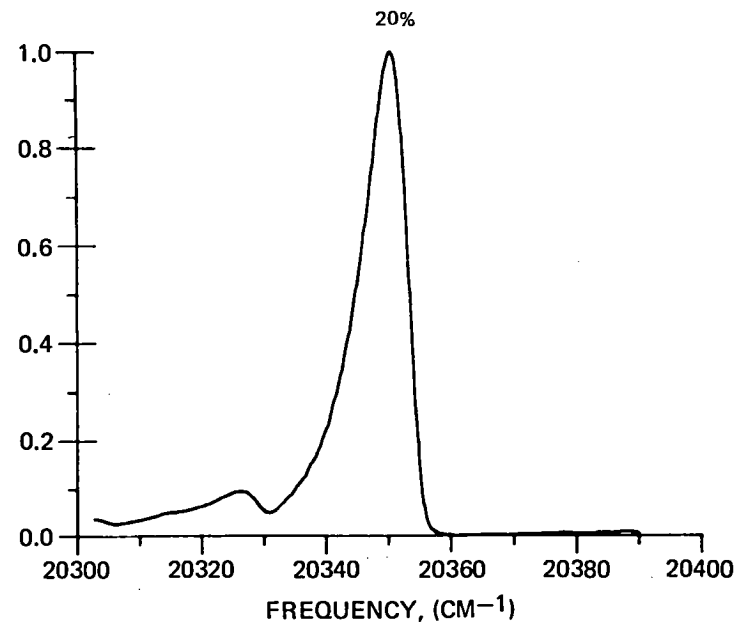
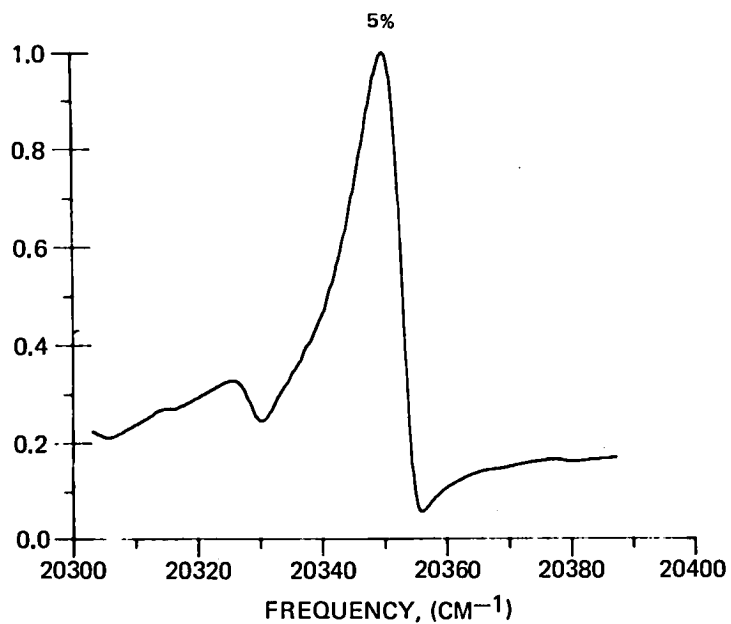
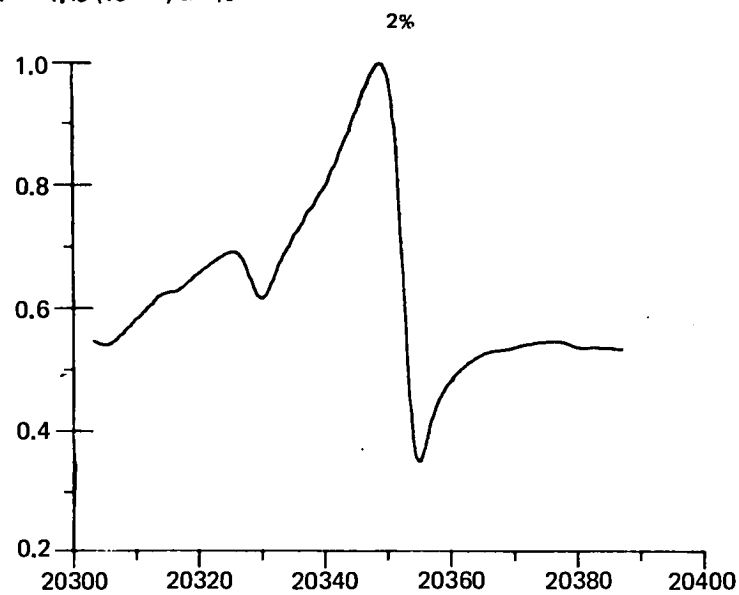
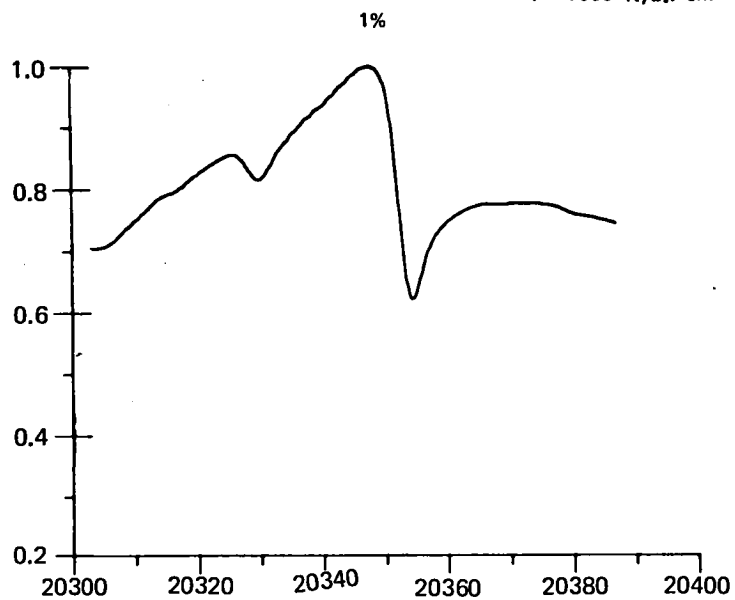
 $T = 1000^{\circ}\text{K}$, 2.7 cm^{-1} SLIT WIDTH, $X^{nr} = 1.49 (10^{-11})\text{ cm}^3/\text{J}$ 

FIG. 22

COMPUTED CARS SPECTRA OF OXYGEN

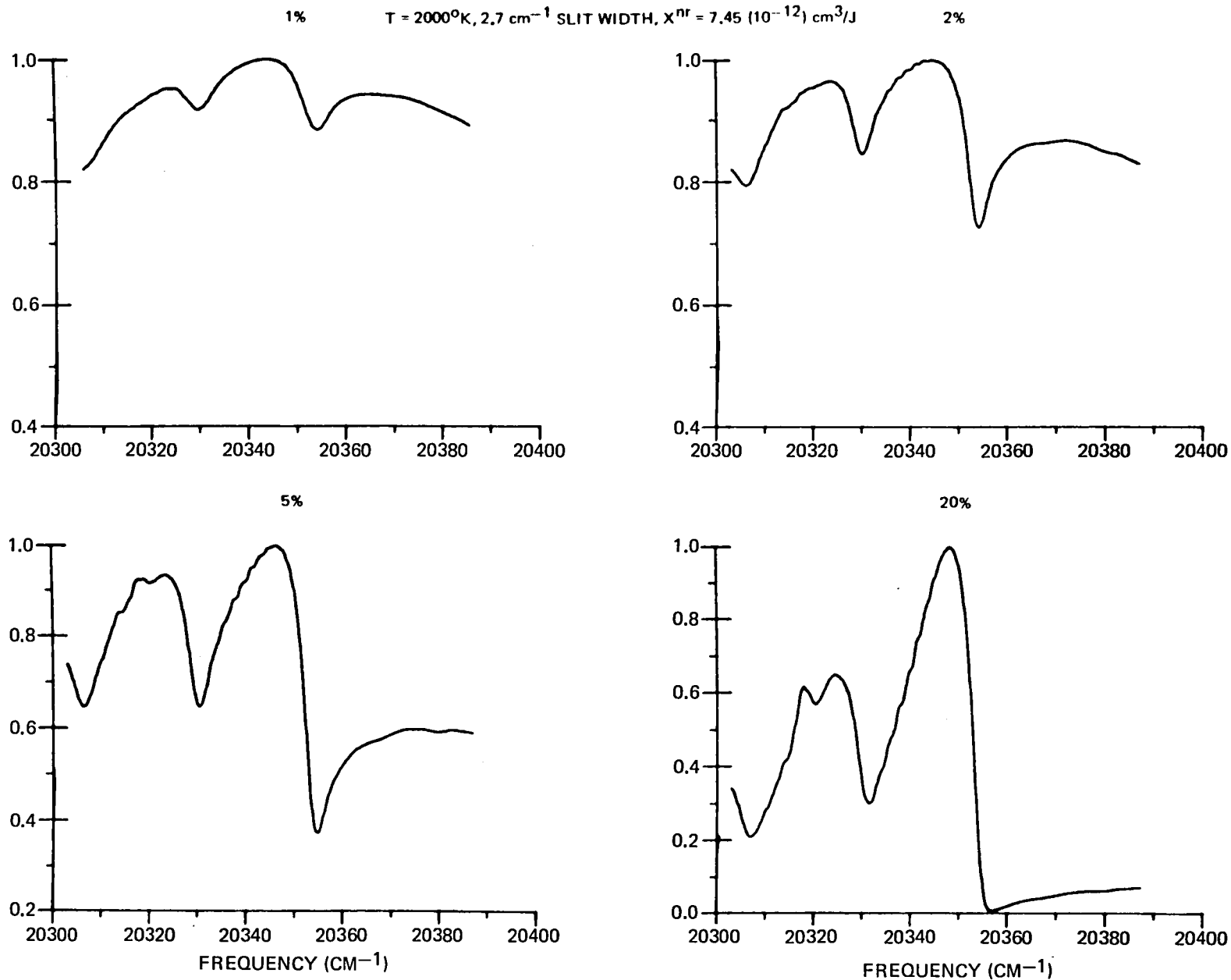
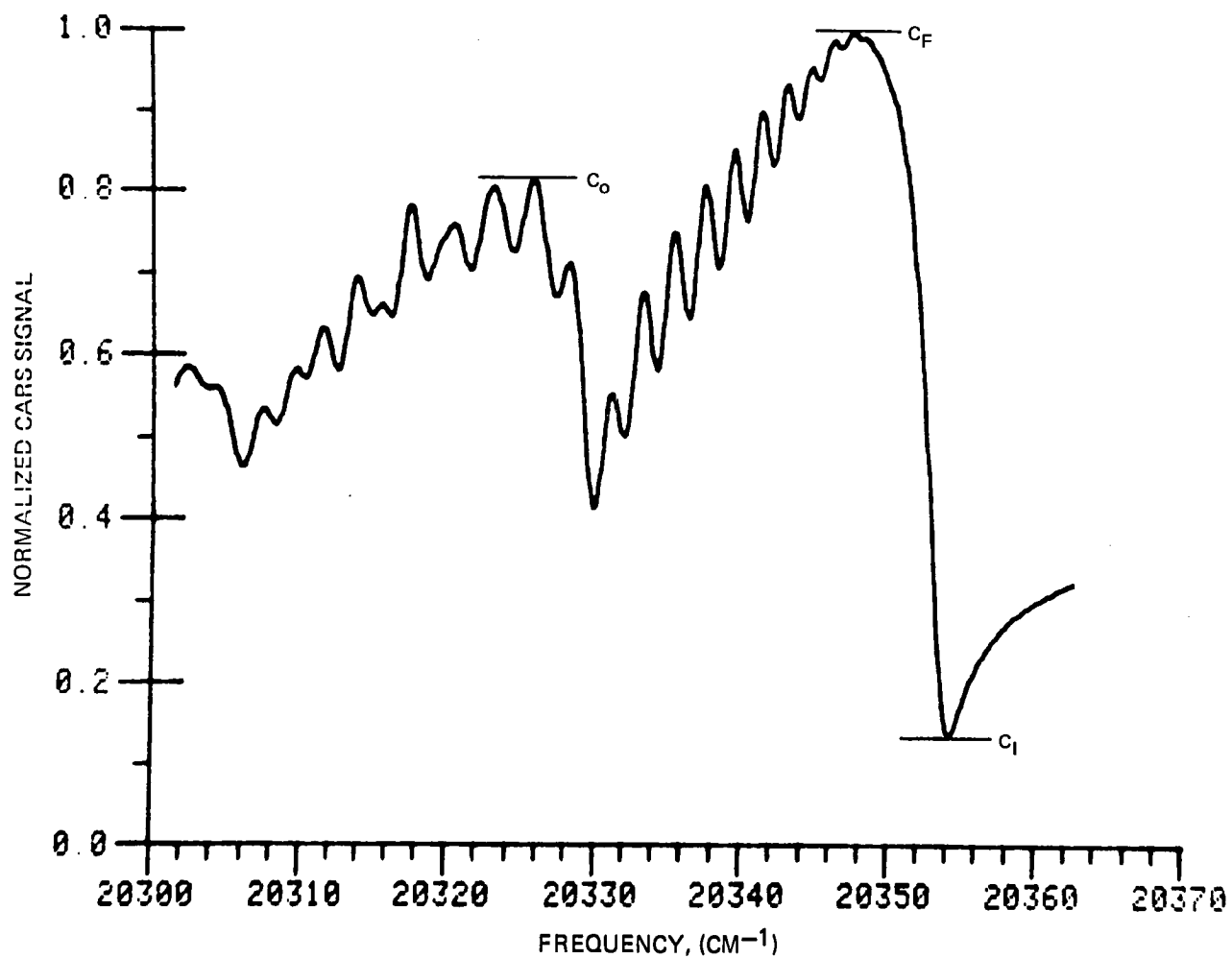
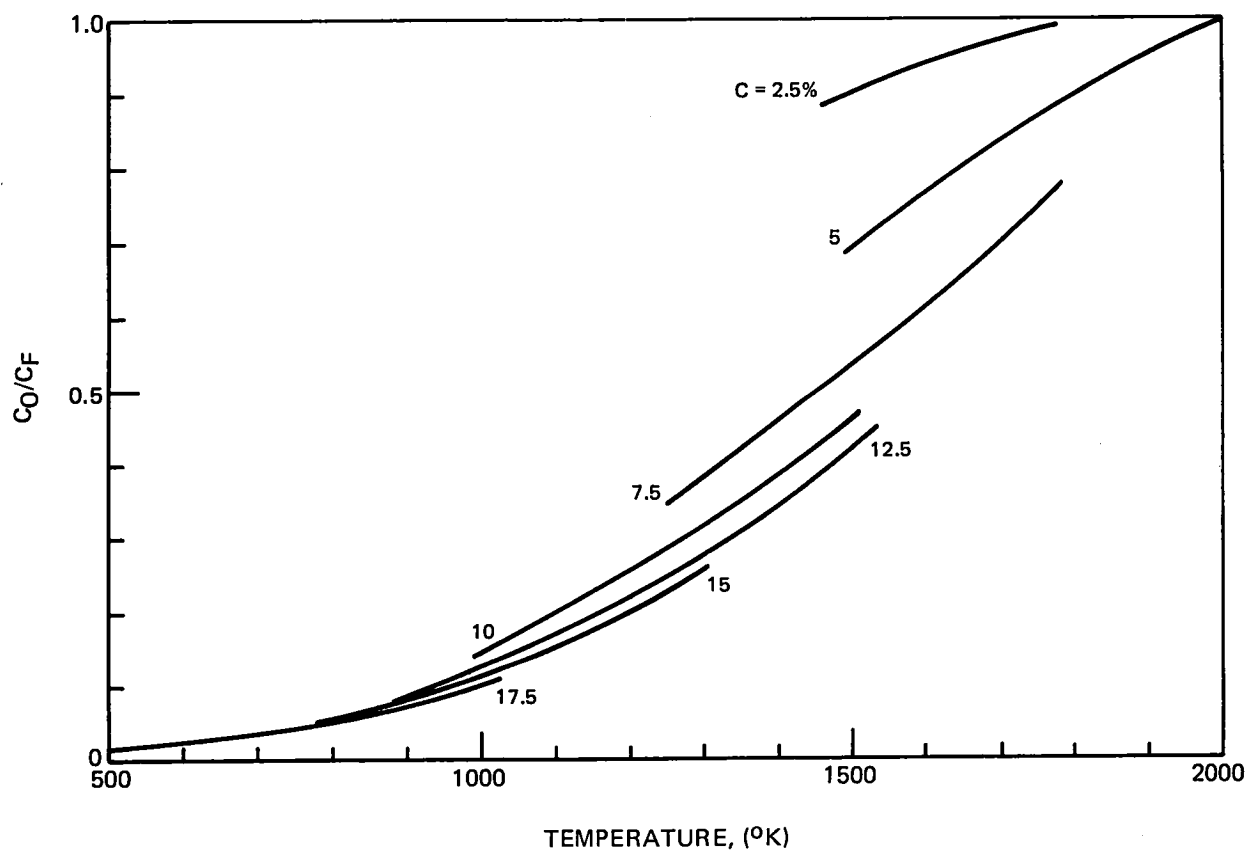


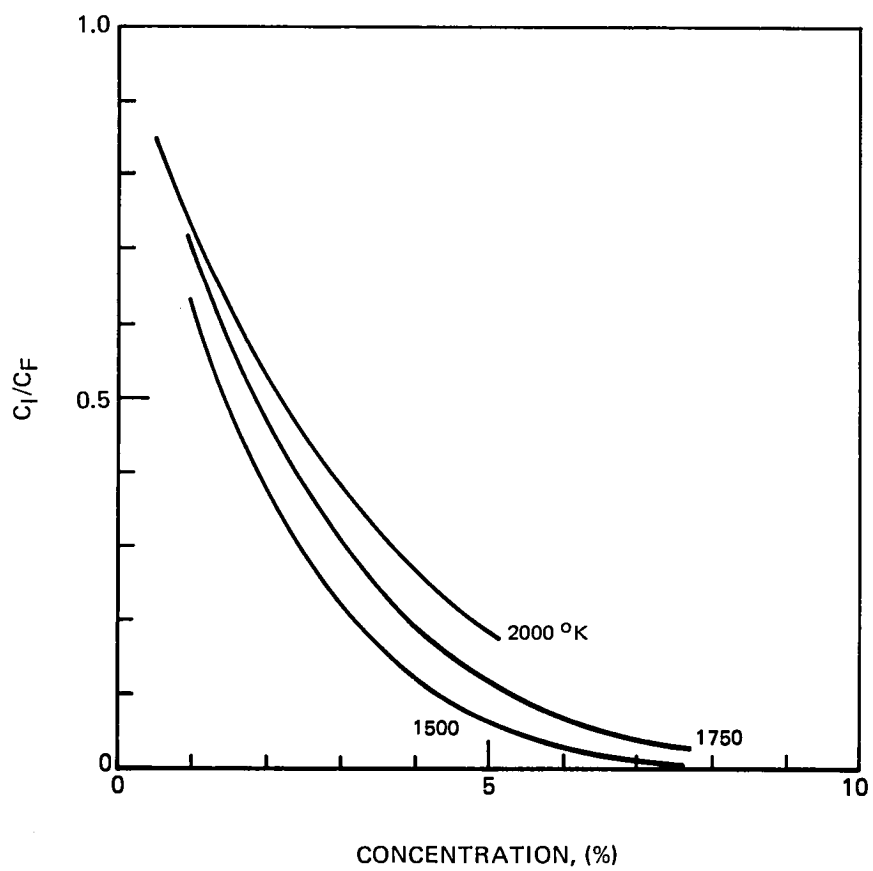
FIG. 23

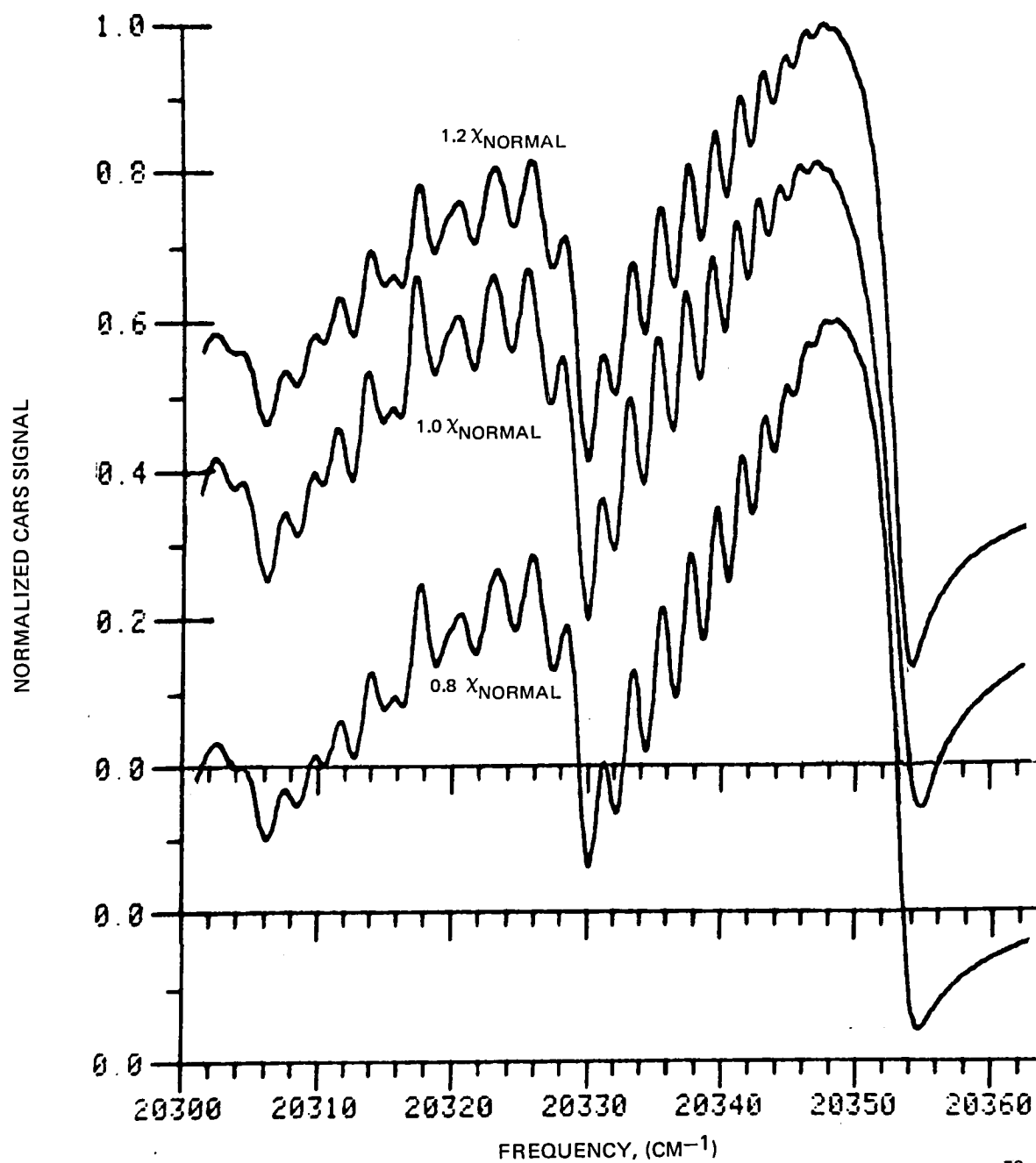
The ratio of the height of the hot band to the height of the fundamental band is a measure of the temperature. The ratio of the height of the interference minimum to fundamental band depends on the concentration. The definition of these quantities is illustrated in Figure 24. C_F , C_O and C_I are the signal counts at the extrema of the fundamental band, overtone band and interference minima, respectively. It seems reasonable to determine temperature down to approximately 900°K from these curves. Temperatures below this value can be determined from the width of the fundamental band. Figure 25 shows the ratio C_O/C_F as a function of temperature with concentration c as a parameter. The dependence of C_O/C_F on concentration introduces some ambiguity into the determination of temperature. The calculated C_I/C_F ratio is illustrated in Figure 26 as a function of concentration with temperature as a parameter. Again there is some ambiguity in the determination of concentration. The calculations indicate that the highest concentration that can be determined depends on the temperature. Clearly the effects illustrated by these curves depend on the magnitude of the nonresonant susceptibility. The sensitivity of the computed spectra to the value of χ^{nr} is shown in Figure 27. The value of χ^{nr} depends on the gas composition. The value of χ^{nr} for most atmospheric gases has been measured (Ref. 53), however the nonresonant susceptibility of water vapor has not been measured. Preliminary results of its measurement are presented in the next topic of this section. Assuming χ^{nr} for H_2O is the same as for methane a change of 40 percent is estimated for the composition change (neglecting the temperature effect which affects χ^{nr} through the density) as a result of combustion. Figure 27 shows that the ratios C_F/C_I are affected by the assumed value of χ^{nr} . This result demonstrates the need for a measurement of the H_2O nonresonant susceptibility, and suggests that CARS minority species measurements would be most accurately performed in conjunction with computer modeling of the majority species concentration profiles. If the nonresonant susceptibility of H_2O is comparable to that of O_2 and N_2 , which are nearly equal, concentration measurements can be performed without the requirement to know the gas composition very accurately. In such an instance, changes in composition would have little effect on the value of the nonresonant susceptibility. Because the temperature is a measure of the degree of combustion, it may be possible to make a "smart guess" of the composition from a knowledge of the temperature, and thereby estimate χ^{nr} .

The oxygen data have been analyzed using these algorithms. The diffusion flame data will be presented later along with the discussion of H_2 CARS in Figures 30 and 32. Temperatures from 400 to 2000°K and concentrations from 1 to 10 percent have been determined. It appears possible to determine O_2 concentrations down to 0.5 percent using these techniques (at 1 atmosphere).

DEFINITIONS FOR O₂ DATA REDUCTION

O₂ CARS COMPUTED OVERTONE TO FUNDAMENTAL BAND RATIO

O₂ CARS COMPUTED INTERFERENCE TO FUNDAMENTAL BAND RATIO

COMPUTED EFFECT OF x_{NR} ON O_2 CARS SPECTRUM $T = 1600^\circ K, C = 5\%$ $x_{NORMAL} = 7 \times 10^{-19} \text{ CM}^3/\text{erg}$ 

χ^{nr} in H_2 /air flame. The nonresonant susceptibility of post flame gases of several flames has been determined from CARS generated in the low angle BOXCARS configuration shown in figure 28. A portion of the combined pump and dye beams incident on the flame is split off by an uncoated microscope slide (BS). The beams focus into a reference cell (10 cm long) and are collected, dispersed and sent to a photomultiplier equipped with a cutoff filter. The reference provides a normalization for the CARS generated from the nonresonant susceptibility in the flame, eliminating the effect of fluctuations in laser pulse energy. The CARS reference signal generated with the microscope slide beam splitter was too weak with air in the cell. Therefore the cell was filled with 1,3 butadiene which has a large Raman cross section at 1647 cm^{-1} (Ref. 54) 91 cm^{-1} from the O_2 bandhead at 1556 cm^{-1} . The dye laser was operated with a grating in the cavity which facilitated shifting the output spectrum to generate CARS from butadiene. In practice the dye laser grating was tuned to generate the maximum CARS signal in the reference leg and the monochromator was tuned to the peak CARS signal.

The CARS signal from the post flame gases of premixed flames burning methane-air, methane-oxygen and hydrogen-oxygen in various burners were compared to CARS generated from atmospheric air. For methane-air combustion the ratio of the CARS signal for the flame with respect to air is 1:21. Since the CARS signal is proportional to $(\chi^{nr})^2$ the ratio of the nonresonant susceptibility of the flame to that of the surrounding air is 1:4.6. The nonresonant susceptibility of a mixture of gases is the sum of the individual susceptibilities

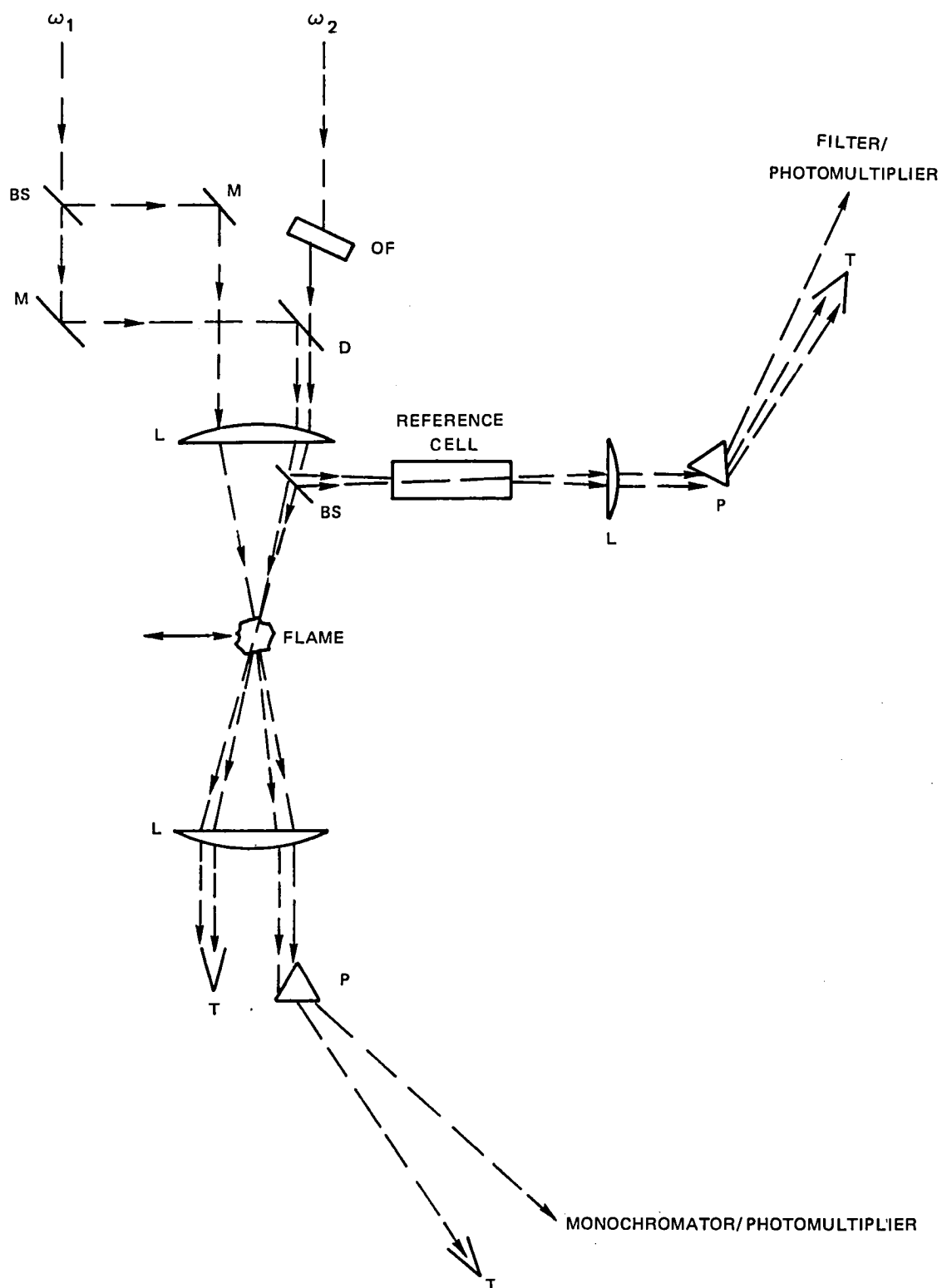
$$\Sigma \chi^{nr} = \Sigma n_i \chi_i^{nr} = \frac{p}{kT} \Sigma c_i \chi_i^{nr} \quad (23)$$

The ratio of the susceptibility of the post flame mixture to the susceptibility of air is

$$\frac{\chi^{nr}(\text{flame})}{\chi^{nr}(\text{air})} = \frac{T_a}{T_f} \frac{\Sigma c_i \chi_i^{nr}}{\chi_i^{nr}(\text{air})} \quad (24)$$

where T_a and T_f are the room and flame temperature respectively. The non-resonant susceptibility of air can be calculated from Reference 53: $\chi^{nr}(\text{air}) = 1.3 (10^{-18})\text{ cm}^3/\text{erg}$. The flame temperature is approximately 1700°K . Therefore the nonresonant susceptibility of the post flame mixture is $\chi^{nr}(\text{flame}) = 2.2 (10^{-19})\text{ cm}^3/\text{erg}$. Assuming the composition of the product gas is 57 percent N_2 , 14 percent CO_2 and 29 percent H_2O corresponding to complete (stoichiometric) combustion the nonresonant susceptibility of H_2O at NTP is estimated to be $\chi^{nr}(H_2O) = 2(10^{-18})\text{ cm}^3/\text{erg}$.

NONRESONANT SUSCEPTIBILITY EXPERIMENTAL ARRANGEMENT



Similar estimates for the $\text{H}_2\text{-O}_2$ flame indicate that $\chi^{\text{nr}}(\text{H}_2\text{O}) = 3(10^{-18}) \text{ cm}^3/\text{erg}$. These values compare very well with the value which was previously assumed for H_2O in the oxygen calculations, which was $3(10^{-18}) \text{ cm}^3/\text{erg}$.

CARS spectra of H_2 in a diffusion flame. - Measurements have been made of the CARS spectra and spontaneous Raman scattering signals from H_2 in the H_2 -air flat diffusion flame. Measurements were made at 0.5, 1.0 and 1.5 cm above the burner exit using a low angle BOXCARS configurations similar to that employed for the oxygen work. A mixture of 7.7×10^{-5} molar cresyl violet perchlorate and 3.9×10^{-5} molar oxazine 725 pumped with the 2xNd-YAG laser produced broadband emission (4.4 mJ) centered at 14700 cm^{-1} (670 nm) with a 110 cm^{-1} bandwidth (FWHM). The CARS signal ($\sim 22900 \text{ cm}^{-1}$) was dispersed and recorded on an optical multichannel analyzer. Figure 29 shows a selected set of CARS spectra taken at various positions within the flame, illustrating the effect of gas temperature. Approximate temperatures deduced from the ratios of the CARS intensities among the $Q(1)$, $Q(3)$ and $Q(5) \nu=0 \rightarrow 1$ (See Fig. 9) transitions are shown. Correction has been made for the distribution of power in the dye laser spectrum. Agreement among the temperatures deduced from the three $Q(J)$ intensities ratios was good. The standard deviation, $\chi(T)$, of the three temperatures varied from 2 to 8 percent for temperatures from 900 to 2100°K. The variation of $\chi(T)$ with the temperature reflects the variation in signal strength because the concentration was low in the hottest parts of the flame. Below approximately 900°K the temperature was determined from the $Q(3)/Q(1)$ ratio alone because of the low intensity of the $Q(5)$ transition at these conditions. Repeated measurements in a low temperature region of the flame resulted in a mean of 590°K and a standard deviation of 22°K (4%). The H_2 spectra normally were averaged for 300 cycles. The CARS beam was attenuated for some data points with neutral density filters of up to 2.6 optical density (1/400 attenuation).

The results of temperature profiling the diffusion flame are shown in Fig. 30 along with the position of the burner. The temperature determined from H_2 and O_2 CARS is compared to the temperature from a Pt-Pt 10 percent Rh, $\text{BeO-Yt}_2\text{O}_3$ coated thermocouple (radiation corrected). The measured temperatures agree quite well (5-10%) especially in cooler regions of the flame. Larger discrepancies are anticipated in hot regions of the flame where the concentrations are low. The discrepancy between H_2 CARS and the thermocouple temperatures in the cool fuel side of the flame at 0.5 cm may result from heat transfer to the flow from the uncooled burner.

Spontaneous Raman measurements of H_2 concentration were made under identical burner conditions for comparison to the CARS signals. The apparatus employed is shown schematically in Fig. 31. Light scattered at nearly 90 degrees from one leg of the 2xNd-YAG pump beam is detected by a phototube equipped with an interference filter centered at 680 nm with 10 nm bandwidth.

H₂ CARS THERMOMETRY

1 ATMOSPHERE, FLAT H₂/AIR DIFFUSION FLAME

Q BRANCH TRANSITIONS IDENTIFIED

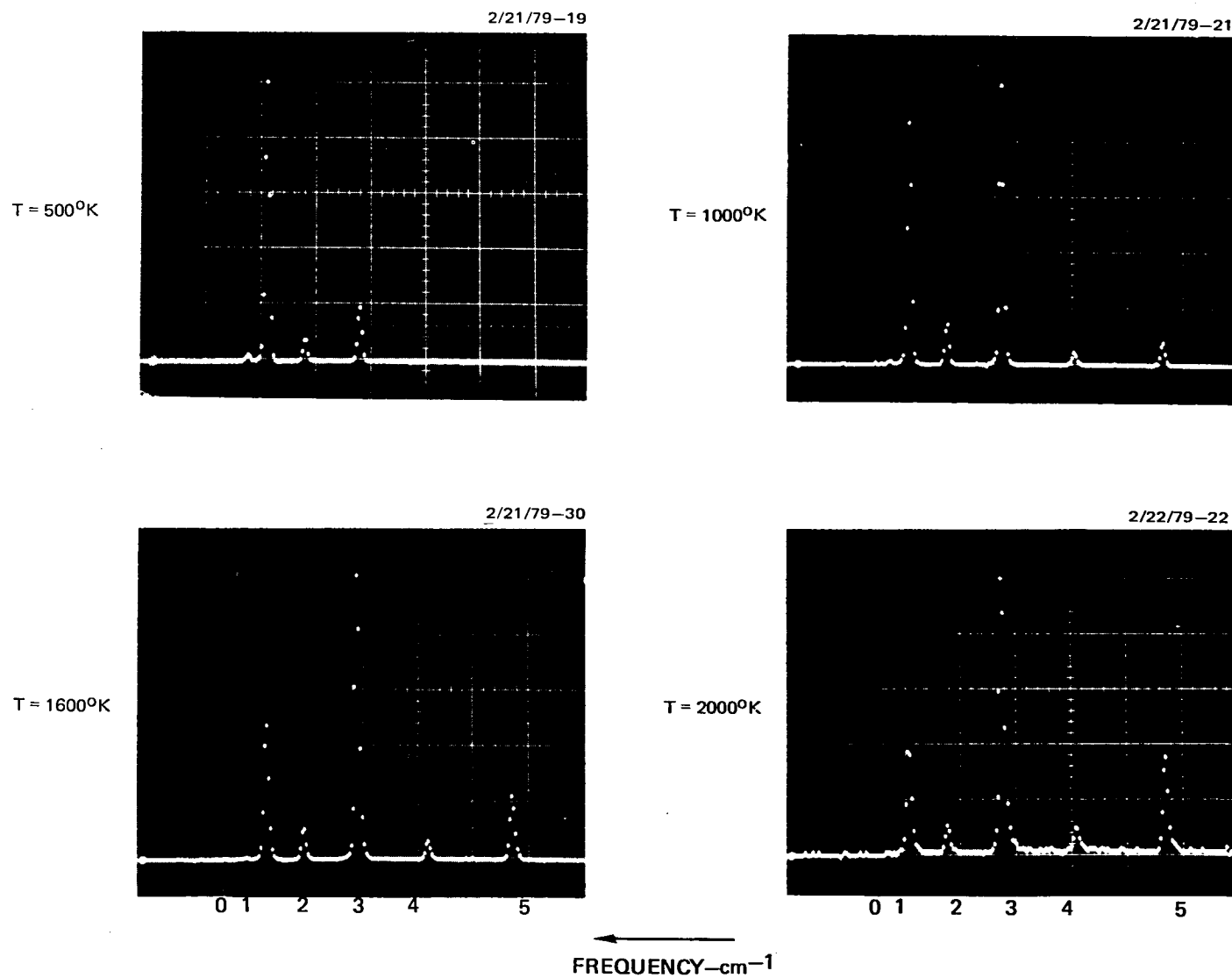
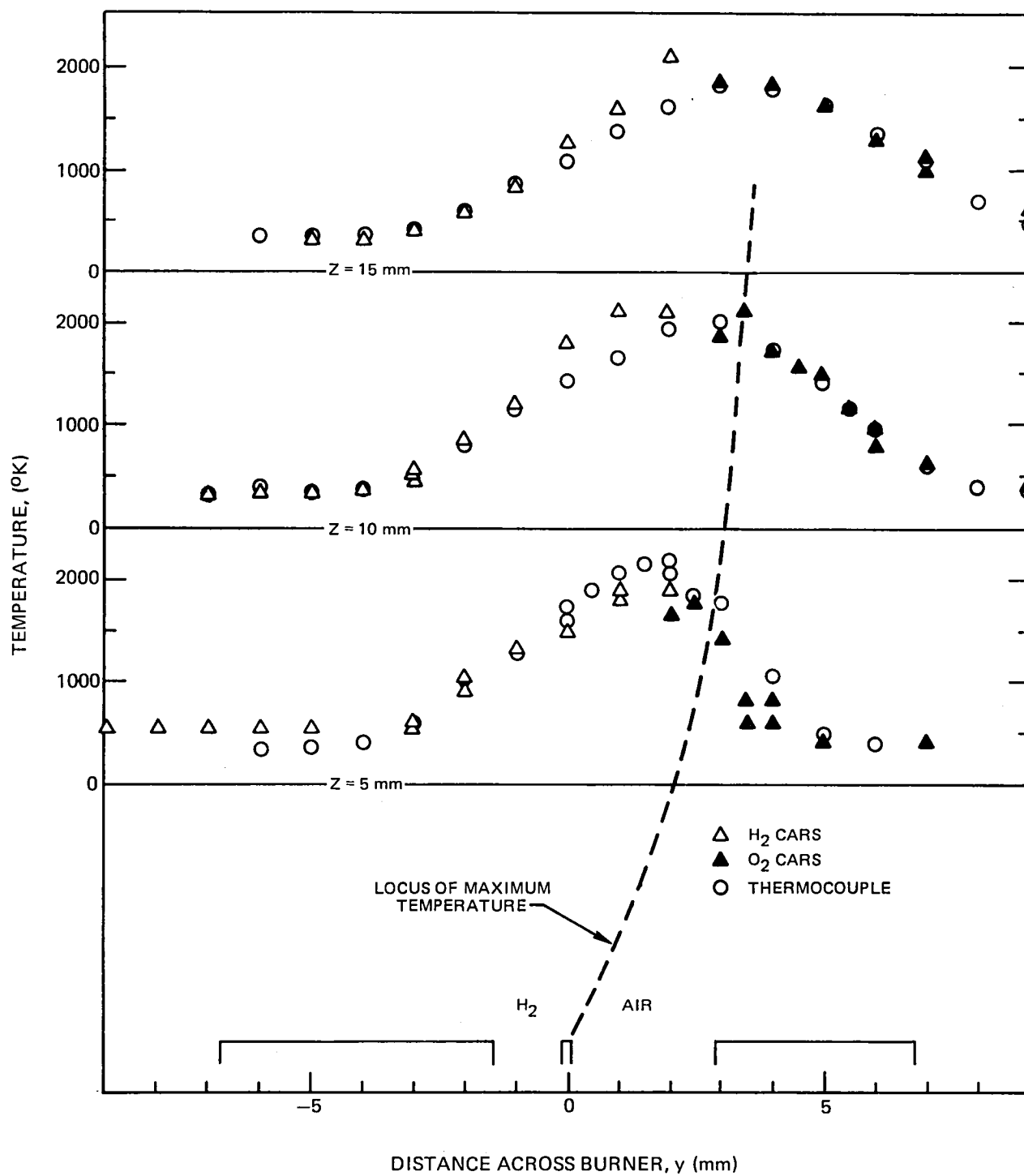
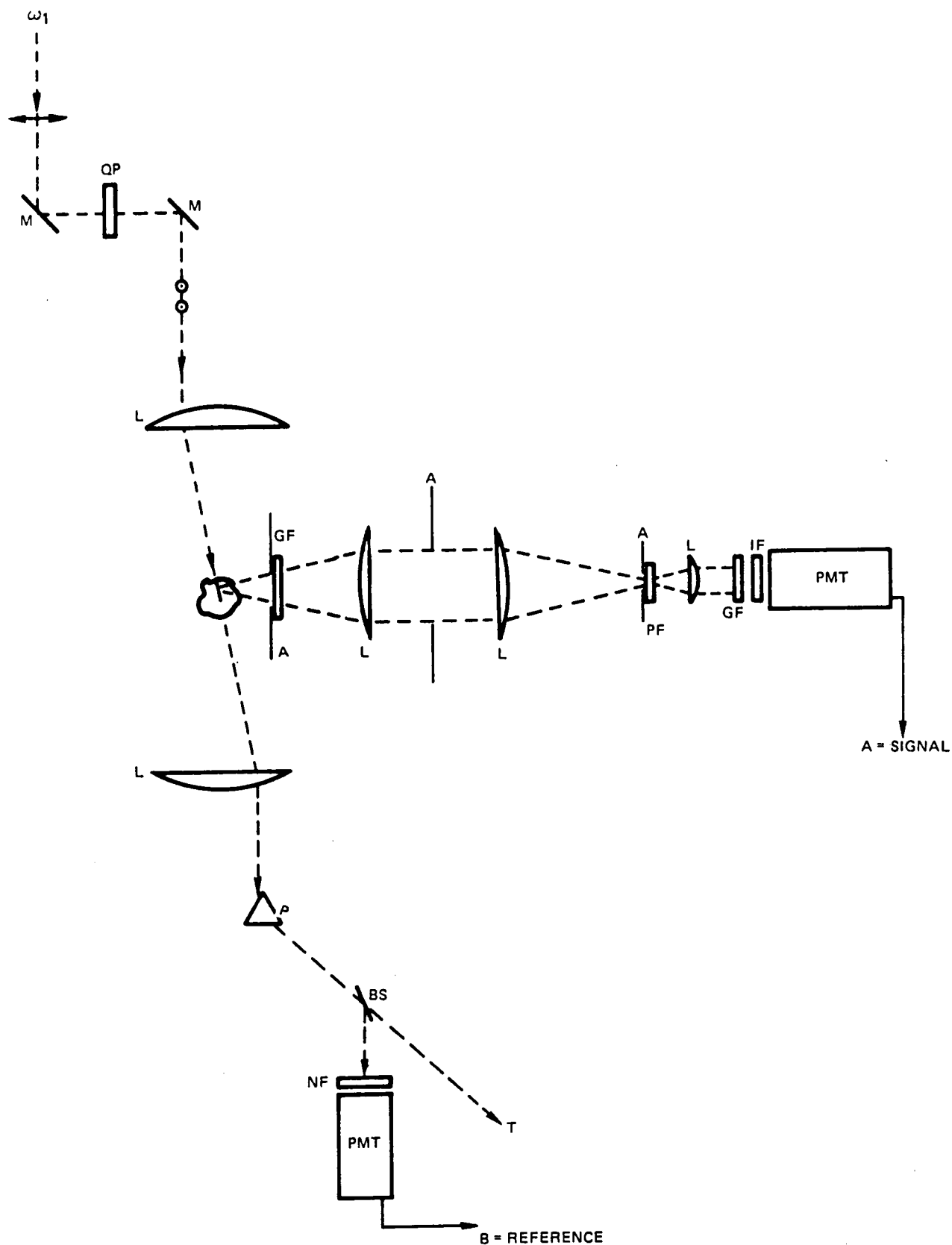


FIG. 29

TEMPERATURE MEASUREMENTS IN H_2 - AIR DIFFUSION FLAME

79-03-26-2

H₂ SPONTANEOUS RAMAN EXPERIMENTAL ARRANGEMENT



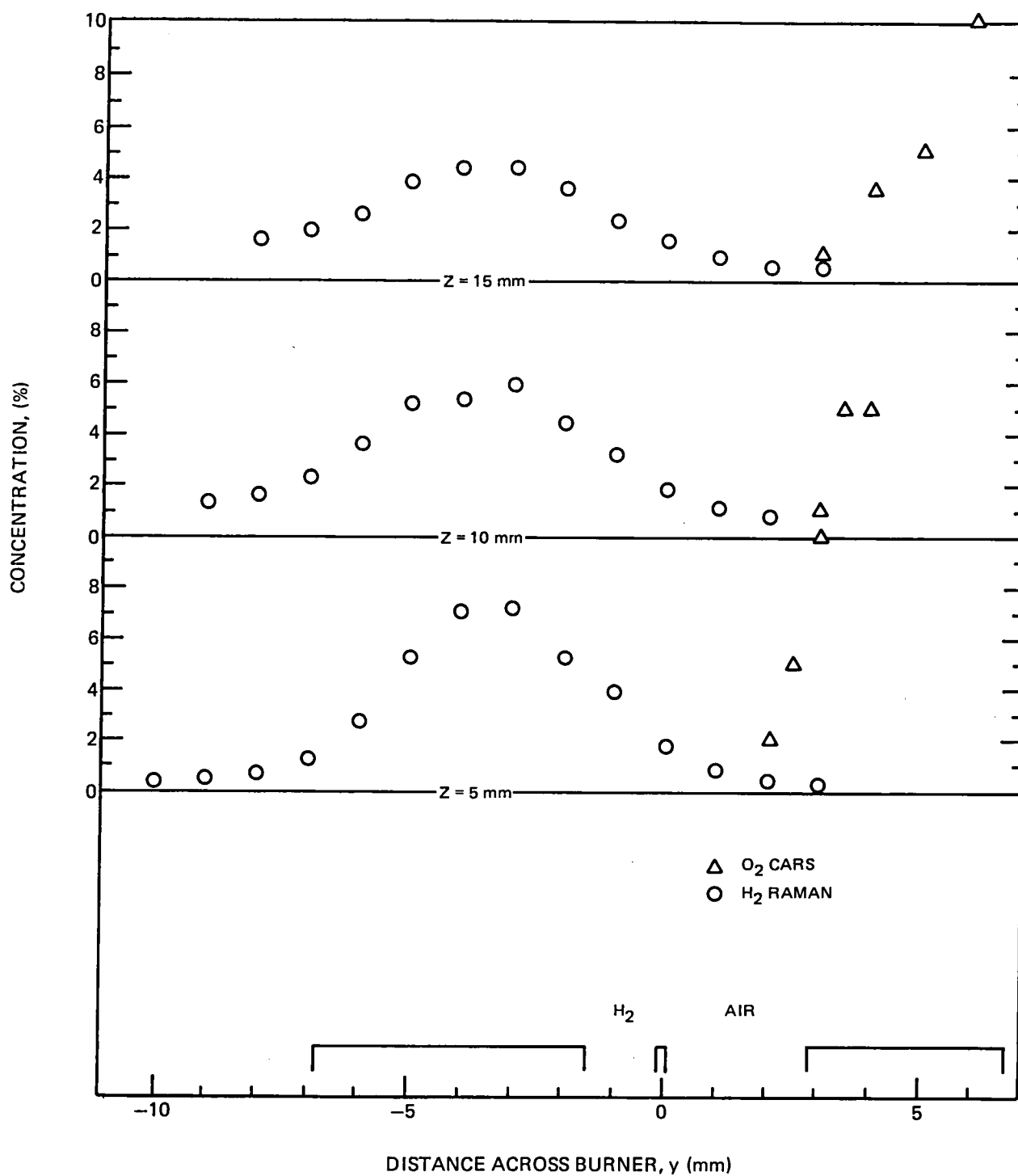
The dye laser was blocked and the usual horizontal polarization of the pump beam was rotated to the vertical with a half wave plate. Phototube pulses were averaged by a gated integrator and normalized to the laser pulse energy by a phototube observing the residual pump beam. The spontaneous Raman signal reached a maximum at a position 3 to 4 cm to the fuel side of the splitter plate. Since the relative distribution of Raman scattered radiation depends on the temperature, a correction must be calculated to account for the effect of this shift on the H_2 Raman signal within the passband of the filter (Ref. 55). The Raman signals from the flame were normalized by comparing the flame H_2 Raman signal to the signal from a cell filled with pure hydrogen. The concentrations in the H_2 -air flame determined in this manner are shown in Fig. 32 along with the concentrations from the O_2 CARS interference measurements. The H_2 concentration attains a maximum approximately 3mm from the splitter plate at all the measured heights above the burner. The peak concentration is greatest at the 0.5 cm height, reaching a maximum of 7.5 percent. In the hottest parts of the flame the concentration is less than 0.5 percent. The maximum O_2 concentration measured from interference between the resonant O_2 and the nonresonant background contribution to the susceptibility is 10 percent. The O_2 concentration decreases toward the center of the flame. The profile of O_2 in the cool outer portions of the flame is probably similar to the H_2 profile but with a steeper concentration gradient. Determination of O_2 concentration in this region would require measurement of the integrated CARS signal because the interference effects in O_2 are too weak to use at low temperature.

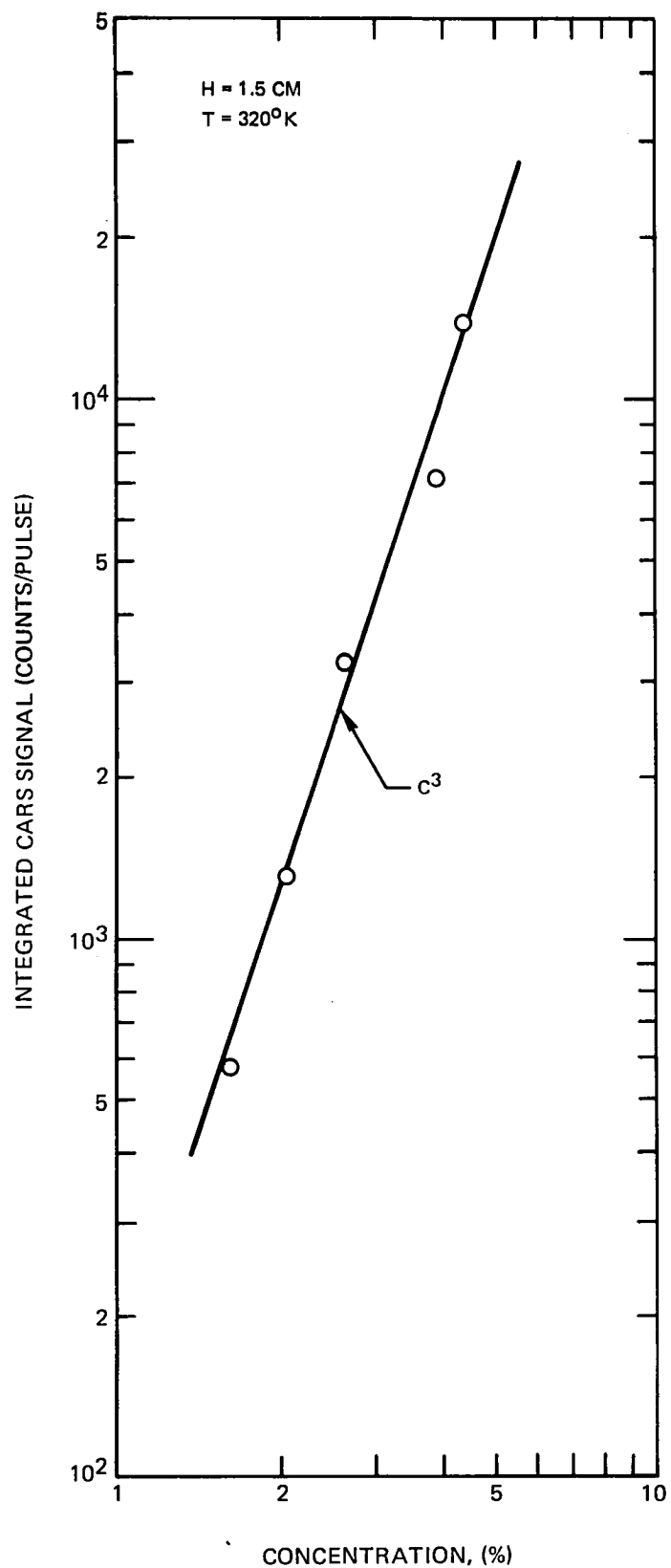
The H_2 data analysis shows that there is a region on the fuel side of flame where the temperature is constant while the concentration changes by a factor of almost 3. Figure 33 shows the CARS signal summed over all $Q(J)$ transitions compared to the concentration determined from spontaneous Raman scattering. The CARS intensity follows a cubic dependence on H_2 concentration. This is in agreement with the estimate of the behavior of the H_2 CARS signals (See Figure 12) at this temperature (320°K).

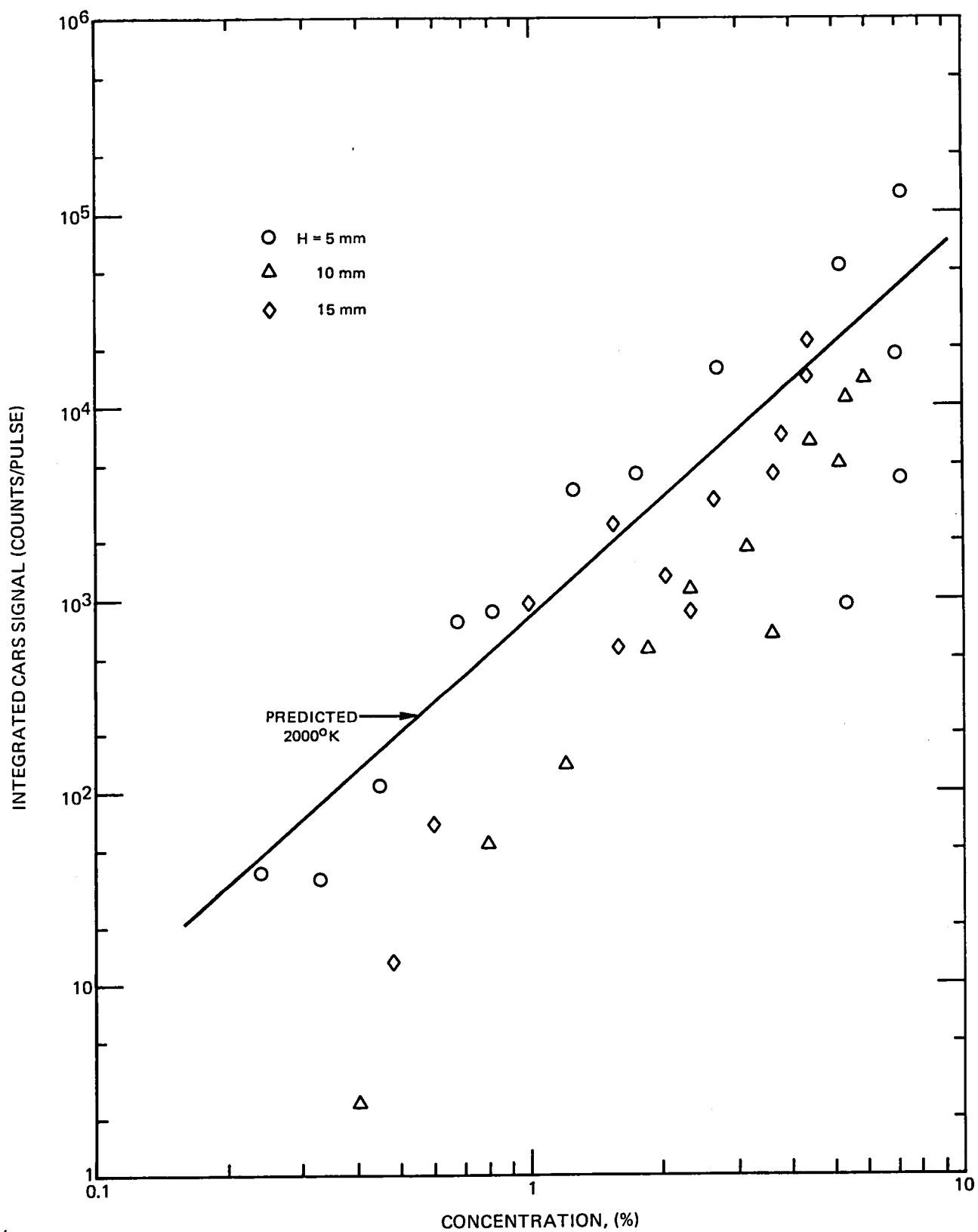
All of the H_2 CARS data are shown in Figure 34 irrespective of temperature. Also shown in this figure is the CARS signal predicted for the laser intensities measured in these experiments. The values assumed for the experimental parameters are shown in Table III.

TABLE III - H_2 CARS EXPERIMENTAL PARAMETERS

Interaction length, $z = 0.3$ cm
Pump intensity, $I_1 = 1.6 (10^{10})$ W/cm² (0.11 J, 300 μ m focal diameter)
Dye laser energy, $E_2 = .025$ J
Dye laser bandwidth, $\Gamma_2 = 112$ cm⁻¹
Collection efficiency, $\epsilon_c = 0.23$

CONCENTRATION MEASUREMENTS IN H_2 - AIR DIFFUSION FLAME

PRESSURE DEPENDENCE OF INTEGRATED H₂ CARS SIGNAL

H_2 INTEGRATED CARS SIGNAL VS. CONCENTRATION

The line shown is calculated for 2000°K and is scaled with the square of the concentration. The agreement between theory and experiment is good. The scatter of the data is probably caused by the lack of normalization on the CARS signal. CARS generation depends strongly on the alignment of the laser, and the scatter to some extent reflects changes in the laser alignment. That some data points exceed the prediction is not surprising. The temperature for all these points is less than 2000°K so that the density therefore the CARS generation is greater. This comparison validates the calculations of Task I.

Comparing Fig. 34 to the H₂ CARS prediction in Fig. 12 it is apparent that the experimental CARS signals have a smaller range of variation at constant concentration than shown in Fig. 12. The prediction is for Q(1) and the data include all the Q-branch transitions for which less variation is expected (see Fig. 8).

Although single shot H₂ CARS measurements were not attempted, the fact that some measurements were made with an attenuation of 1/400 for a 300 cycle average indicates that single shot measurements are possible. The single shot accuracy can be estimated from the curve in Fig. 34. Table IV shows the accuracy (standard deviation σ) of measurements estimated for a temperature of 2000°K and atmospheric pressure.

TABLE IV - H₂ CARS ESTIMATED SINGLE SHOT ACCURACY

1 Atmosphere, 2000°K

<u>Concentration (%)</u>	<u>σ_N/C (%)</u>	<u>σ_T (°K)</u>
0.5	7	70
1	3.5	35
5	0.7	7
10	0.35	3.5

The accuracy of single shot measurements at other pressures can be estimated by scaling the values in this Table according to the square of the pressure.

CARS spectra of the major molecular species in H₂-air combustion, with the exception of N₂, have been investigated experimentally in this study. The CARS spectrum of flame H₂O has been measured and compared with computer calculated spectra. The agreement at the 1675°K temperature of the experiments is good, somewhat validating the code and the energy level data. Further checks of the code at other temperatures are desirable to test the validity over the full range of scramjet experimental temperatures. O₂ CARS spectra

also shows good agreement between calculated and measured spectra. The temperatures deduced are in very good agreement with thermocouple measurements. The concentrations determined from interference between the background nonresonant susceptibility and the resonant O_2 susceptibility are reasonable, but need to be checked independently. For positions in the flame where the O_2 concentration is high and the temperature is low, approaches for normalization and calibration should be employed. The nonresonant background susceptibility near the oxygen frequency has been determined in the postflame region of a premixed, stoichiometric H_2 -air flame. The nonresonant background at various positions in the diffusion flame should be determined and the impact on the O_2 spectrum assessed. The nonresonant susceptibility for virtually any composition in the H_2 -air flame could be predicted if χ^{nr} for H_2O were known. A preliminary measurement of this quantity has been made. To determine this quantity precisely, measurements should be made in a cell under known concentration and temperature conditions. Finally, measurements have been made of the CARS spectra of H_2 in a hydrogen-air diffusion flame. Agreement between temperatures determined from the spectra and thermocouple measurements is again found to be good. Measured CARS signal magnitudes are in good agreement with the analytical predictions, but the requirement for reference cells to eliminate the effects of minor misalignments (Appendix A) is pointed out. Questions concerning the Raman linewidth of hydrogen in a variety of mixtures, temperatures and pressures and its impact on CARS intensities must be addressed. As was the case for O_2 , measurement approaches for calibration and normalization should be investigated experimentally.

Task III Conceptual Design Study

The components which comprise a CARS system are the laser sources, optics, detectors, and signal processors. In this section, comments are first made on the selection of each of these components, then the section is concluded with a discussion of a suggested CARS installation in the NASA scramjet facility.

Laser selection. - Laser selection was discussed earlier in this section where it was noted that at the present time only Nd-YAG lasers have sufficient intensity and repetition rate to fulfill the requirements of diagnostics for the scramjet facility. Models developed by several manufacturers can be found in the Laser Focus Buyer's Guide (Ref. 56). If measurements at the lowest densities are paramount, then models producing more than 200 millijoules at 532 nm are recommended.

For the calculations and measurements performed in this study, a single laser provides the ω_1 pump beam and drives a dye laser for the Stokes beam. The low density sensitivity of the technique would be improved by the use of

two Nd-YAG lasers, one to provide the pump and one to separately drive the dye laser(s). The lasers must be synchronized; however, this is not difficult as the jitter is generally less than a few nanoseconds.

In a novel approach, two Nd-YAG lasers can be used to drive two dye lasers with different dyes chosen for two individual molecular species. The geometry of the beams incident on the primary focusing lens can be arranged to focus the beams from the two dye lasers at one point in the test region. One method is to use a larger crossing angle for one dye/pump pair. Alternatively, the beams can be oriented so that one dye/pump pair crosses in a horizontal plane, and the other crosses in a vertical plane. In this manner, simultaneous measurements of two species can be made.

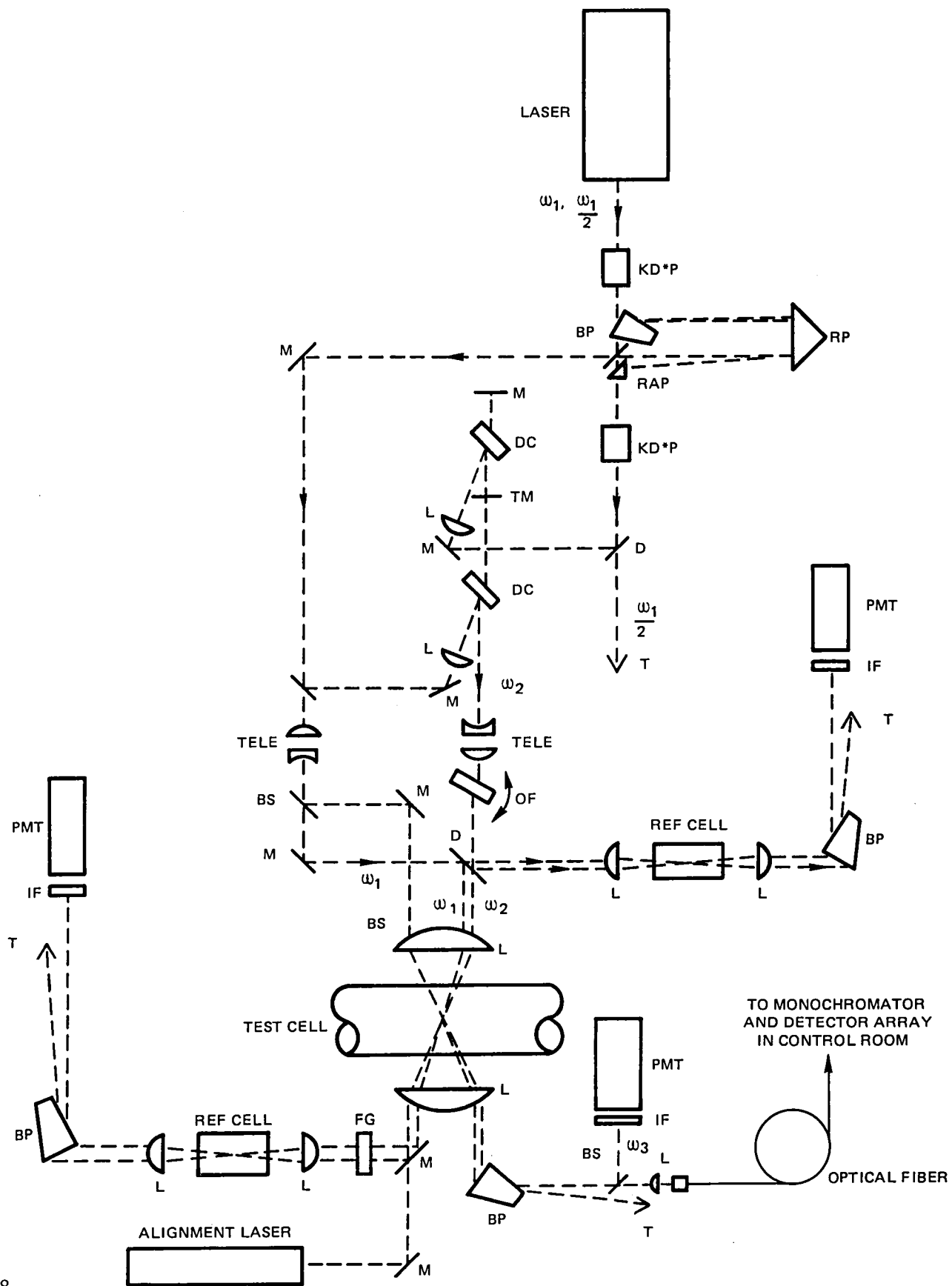
The dyes recommended for CARS measurements in the molecular species of interest are shown in Table V along with a summary of the required frequencies (wavelengths). The choice of dye is most uncertain for the case of water vapor. The dye recommended, LD690, was the only dye tested to give useful energy at 15147 cm^{-1} . As noted previously, stability may be a problem with this dye. The manufacturer (Ref. 47) has pointed out that these dyes (oxazines) generally possess superior stability and suggested that it may be necessary to de-oxygenate the solvent to prevent dye deterioration. These hypotheses have not been tested. For H_2 , it was necessary to use a dye combination. Cresyl violet perchlorate alone with $2\times\text{Nd}$ pumping does not overlap the H_2 Stokes region, and oxazine alone is very inefficient. A possible alternative dye for H_2 CARS is carbazine. Dyes appropriate for generation of Stokes radiation for N_2 and O_2 are efficient and stable.

TABLE V - DYE LASER CHARACTERISTICS FOR Nd-YAG PUMP

Molecule	Raman Shift (cm^{-1})	ν_s (λ_s)	ν_{AS} (λ_{AS})	Recommended Dye
H_2	4160	14674 cm^{-1} (681.5 nm)	22920 (436.3)	Ox725+CVP, carbazine
H_2O	3652	15147 (660.2)	22447 (445.5)	LD 690
N_2	2331	16466 (607.3)	21124 (473.4)	Rhodamine 6G
O_2	1556	17241 (580.0)	20348 (491.5)	Rhodamine B

CARS optical configuration. - An optical configuration suitable for scramjet CARS measurements is represented in Fig. 35. More optical components (turning mirrors) than actually shown will be required to fold and compact the system so that it will fit into the scramjet test bay and be easily moved for

PLANAR REPRESENTATION OF SCRAMJET CARS OPTICS



model changes. The central portion of the layout is similar to the UTRC experimental apparatus which has been described previously, so only additional features will be pointed out here. The KD*P frequency doubling crystals are shown. The efficiency of the doubling crystals are such that it is beneficial to redouble the residual 1.06 μm radiation. For this purpose, the 1.06 μm radiation can be separated from the 532 nm radiation with a 90° deviation Brewster prism. The remaining 1.06 μm radiation, after the second doubler, can be separated with a dichroic mirror, as shown, or with heat-absorbing glass. For the remote operation required for scramjet measurements, it may be necessary to thermally stabilize the doubling crystals with a temperature-controlled oven. Otherwise, approximately 10 minutes of laser operation and crystal angle adjustment are necessary to keep the crystal axis oriented for efficient doubling.

Following along the optical train, the features of most of the optical components have been pointed out already. Focussing attention on the detector output shows that a phototube has been added to observe a portion of the CARS signal which is split off with a beamsplitter (BS). The passband of the interference filter (IF) is chosen to admit anti-Stokes radiation from the entire band of the molecule of interest. This phototube serves to normalize the main signal with respect to possible laser pulse energy fluctuations (typically 2-5% depending on the manufacturer). The main CARS beam is shown coupled into an optical fiber. Since the detector element arrays required for single pulse spectral measurements are sensitive to vibration, it is best to operate them in a control room or other low-vibration environment. Measurements with an output system similar to this will soon be made at UTRC in a research combustor test bay with a 0.3 meter monochromator/detector located in the control room and connected to the output end of the CARS systems with a 100 μm optical fiber. Output from the fiber is at f3 and is ideally suited to a small, fast monochromator.

Two CARS reference cells are shown in Fig. 35, arranged before and after the test cell. These are required to normalize the CARS signal generated in the test cell to the CARS generated from a known concentration of gas contained in the reference cell. These cells would be filled with a known amount of the gas of interest. Pulse-to-pulse fluctuations of the laser, and alignment changes thus would be compensated for by normalization to CARS generated from these cells. CARS generation in the test section can be related to gas concentration by normalization to the CARS generated in the reference cell. The signal generated in the post sample volume reference cell can be used to reject poor data points.

CARS signal detection and data processing. - CARS measurements in the scramjet combustor will require spectral resolution to make O_2 interference measurements and H_2 temperature measurements. To make these measurements on

a single shot requires a detector element array attached to the exit or photographic plane of a spectrograph. The spectrograph must have a flat field to image onto the detector array. The primary requirements for the detector are large dynamic range and short scan cycle time. All of the candidate detector arrays can be scanned in a time (5-10 ms) which is short compared to the laser pulse period. Manufacturers should be consulted on the recycle time of the particular device.

The calculations and experiments indicate that the CARS signal dynamic range can be 10^5 to 1 for the full range of desired measurements. None of the currently available detector types have a dynamic range of this magnitude. The two types of possible detectors are a silicon vidicon or an intensified diode array. Vidicon detector models are available with 5000-10,000 to 1 dynamic range. Diode arrays are available with 4096:1 dynamic range. The large 10^5 dynamic range is not required on a single shot, rather this range is required for spatial scanning from high-species density regions to regions of low-species density. A neutral density filter can be used to attenuate the beam as has been done in most of the experiments reported here. Introducing identical neutral density filters simultaneously into the reference legs would automatically normalize the data.

Data acquisition from the spectrally resolved primary CARS signal and the reference channels can be read onto magnetic tape or floppy disc between laser pulses. Under some conditions, the main CARS signal can be averaged on the detector and read after several pulses, while the signal from the reference channels can be averaged on gated integrators. Detailed CARS computer codes run on a large computer can be used to generate a library of spectra or algorithms. These in turn, can be stored on magnetic tapes or disks and can be used with a small dedicated computer to reduce CARS data at the test site.

Conceptual scramjet installation. - Two views of a possible CARS installation in the NASA Langley scramjet facility are shown in Figs. 36 and 37. The system components would be located on small modular structures which can be easily assembled and disassembled. Most of the optics are located on two small (2' x 6') optical tables which are placed one over the other. The laser and doubling crystals are on the lower table. The primary and secondary 2xNd beams are sent up through the upper table where the dye oscillator and amplifier are located. The pump and Stokes beams are combined and sent to a lens which focuses and crosses the beams in the test section. The collection optics are located on the opposite side of the test section on an I-beam which is independently supported by pillow blocks sliding on ground steel rods. The optical tables carrying the lasers also slides perpendicular to the axis of the test section on pillow blocks and rails. The movement of the lasers/optics and detector/optics are linked by a rigid beam passing under the test section. A reference cell, input to the fiber optic and alignment laser are located together on the detector I beam. The envisioned CARS diagnostic apparatus can be easily disassembled and moved out of the way for model changes.

CONCLUSIONS

The feasibility of measuring temperature and major molecular species concentration in H_2 -air scramjet combustion using coherent anti-Stokes Raman spectroscopy (CARS) has been investigated. On the basis of the analytical and experimental investigations, it is concluded that temperature and concentration measurements of molecular species occurring in H_2 -air combustion can be made with CARS. Calculations predict that accurate and spatially precise measurements can be made, however, tradeoffs in spatial or temporal resolution will be required at the lowest species density conditions. CARS spectra of H_2O , O_2 , and H_2 have been measured in laboratory flames. Computer code calculated spectra agree very well with measured spectra. The agreement for H_2O is remarkable because of the complex nature of the CARS spectra resulting from the nonlinear interaction of many vibrational-rotational transitions. CARS H_2O measurements have been made only in a narrow temperature range. In order to confirm the computer code predictions, measurements should be made over a larger temperature range. Temperature and concentration measurements of O_2 and H_2 have been made in a H_2 -air diffusion flame. CARS temperature measurements in both species generally agree within 5 percent with radiation corrected thermocouple measurements. Measured H_2 CARS signal magnitudes are in good agreement with the analytical predictions, but the requirement for the use of reference cells to eliminate the effects of small optical misalignments has been identified. The use of such techniques is discussed in Appendix A. The feasibility of measuring O_2 concentrations from the interference between the nonresonant background susceptibility and resonant O_2 susceptibility at low concentrations has been demonstrated. The accuracy of these measurements and of measurements from integrated CARS signals at higher concentrations remains to be investigated. The post flame nonresonant background susceptibility of H_2 -air and CH_4 -air flames has been measured. A preliminary measurement of the nonresonant susceptibility of water vapor has been made. Calculations indicate that the nonresonant susceptibility can vary by about 40 percent due to composition changes (neglecting the effect of temperature) through the flame.

A conceptual design for the LaRC scramjet combustion facility has been formulated. Specifications of key components have been prescribed, and auxiliary apparatus required for measurements have been identified.

Measurements have been confined to laboratory, atmospheric pressure flames. Although the range of pressure in the scramjet combustion facility is small, verification of predicted CARS signals at the pressure extremes might be critical in the light of questions raised about the Raman linewidth in H_2 . Finally, it should be pointed out that the feasibility of making measurements in a supersonic flow has not been demonstrated. The influence of shock waves

SCRAMJET CARS CONCEPTUAL INSTALLATION – SIDE VIEW

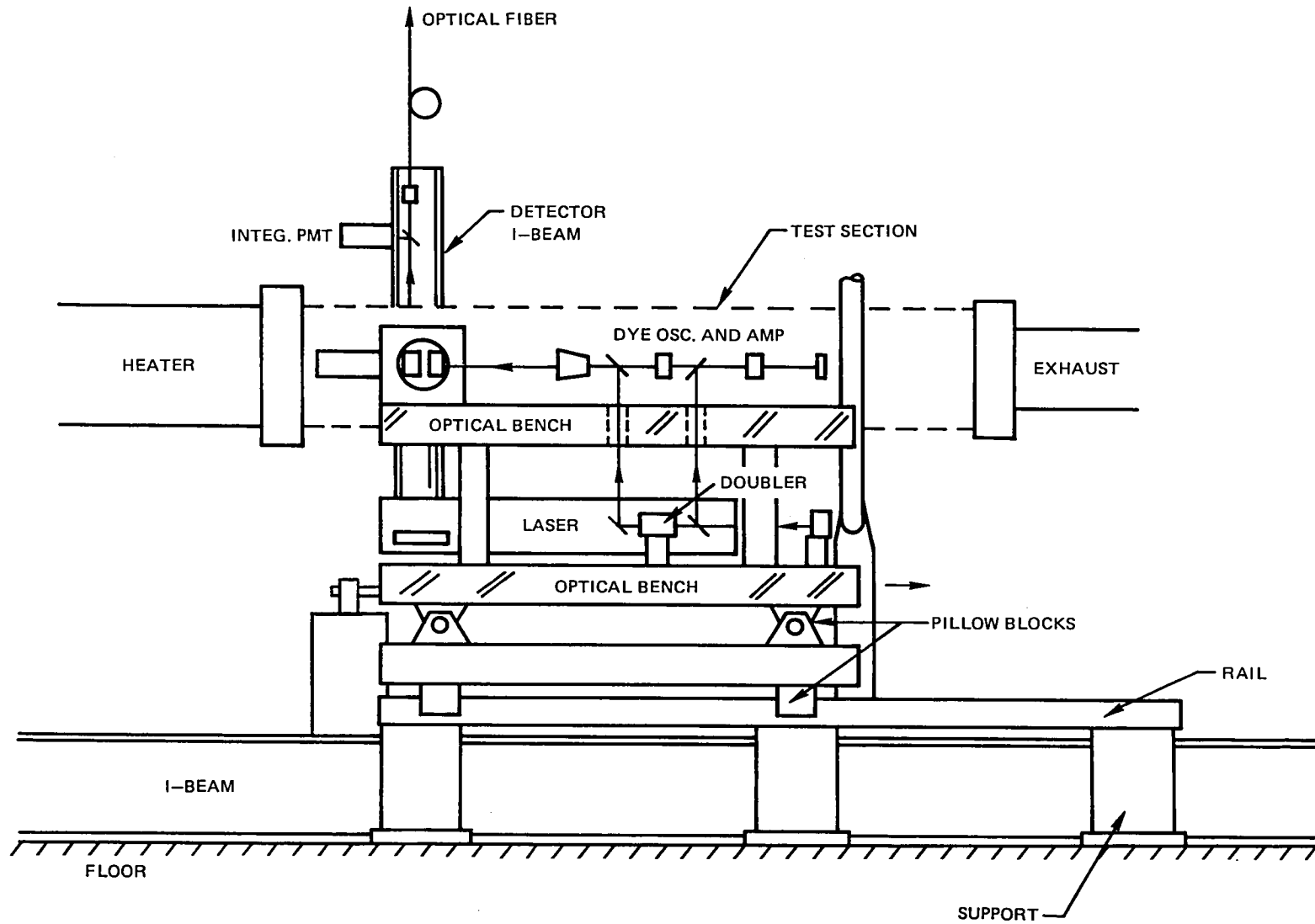


FIG. 36.

SCRAMJET CARS CONCEPTUAL INSTALLATION—TOP VIEW

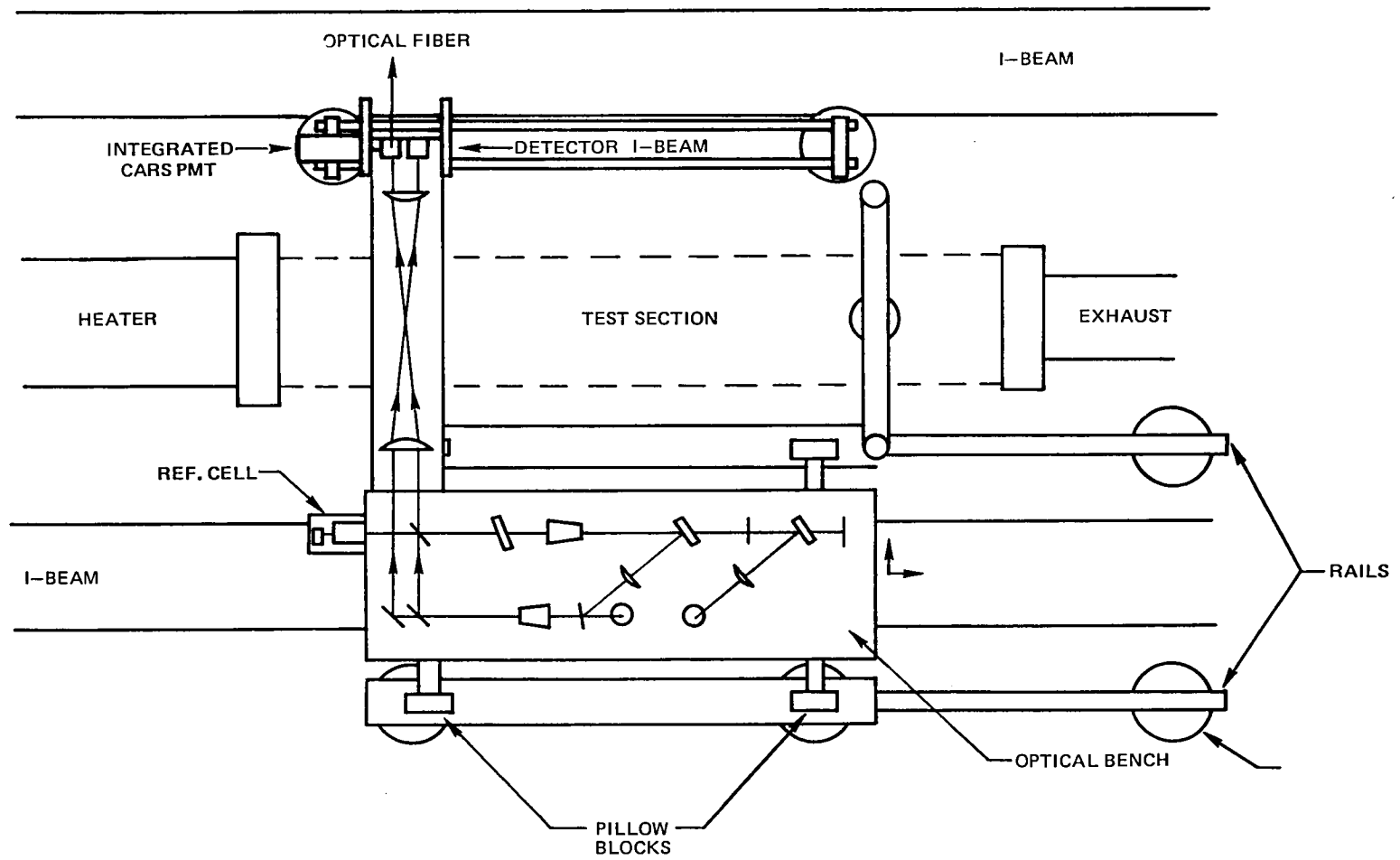


FIG. 37

and thermal boundary layers on CARS measurements should be investigated. These effects can be assessed without resort to actual CARS measurements. Steering effects can be determined by propagating a laser beam through the test section at several locations. The influence of flowstream nonuniformities on BOX-CARS can be measured with apparatus similar to a laser Doppler velocimeter. The fringe field formed at the LDV focal volume can be imaged onto a screen, and the influence of the flow on the projected fringe image can be determined.

REFERENCES

1. Zinn, B. T., ed.: Experimental Diagnostics in Gas Phase Combustion Systems, AIAA, New York, N.Y. 1977, pp. 549-575.
2. Regnier, P. R. and J. P. E. Taran: On the Possibility of Measuring Gas Concentrations by Stimulated Anti-Stokes Scattering. Appl. Phys. Letts., Vol. 23, September, 1973, pp. 240-242.
3. Regnier, P. R., F. Moya and J. P. E. Taran: Gas Concentration Measurement by Coherent Raman Anti-Stokes Scattering. AIAA Paper 73-702, July 1973.
4. Moya, F., S. A. J. Druet, and J. P. E. Taran: Gas Spectroscopy and Temperature Measurements by Coherent Raman Anti-Stokes Scattering. Opt. Comm., Vol. 13, February 1975, pp. 169-174.
5. Regnier, P. R., F. Moya and J. P. E. Taran: Gas Concentration Measurement by Coherent Raman Anti-Stokes Scattering. AIAA J., Vol. 12, June 1974, pp. 826-831.
6. Maker, P. D. and R. W. Terhune: Study of Optical Effects Due to an Induced Polarization Third Order in Electric Field Strength. Phys. Rev., Vol. 137, February 1965, pp. A801-A818.
7. Nibler, J. W., J. R. McDonald and A. B. Harvey: CARS Measurements of Vibrational Temperature in Electric Discharges. Opt. Comm., Vol. 18, August 1976, pp. 371-373.
8. Begley, R. F., A. B. Harvey and R. L. Byer: Coherent Anti-Stokes Raman Spectroscopy. Appl. Phys. Letts., Vol. 25, October 1974, pp. 387-390.
9. Harvey, A. B., J. R. McDonald and W. M. Tolles: Analytical Applications of a New Spectroscopic Tool: Coherent Anti-Stokes Raman Spectroscopy (CARS), in Progress in Analytical Chemistry, Plenum Press, 1977.
10. Tolles, W. M., J. W. Nibler, J. R. McDonald and A. B. Harvey: A Review of the Theory and Application of Coherent Anti-Stokes Raman Spectroscopy (CARS). Appl. Spect., Vol. 31, 1977, pp. 253-272.
11. Barrett, J. J. and R. F. Begley: Low Power CW Generation of Coherent Anti-Stokes Raman Radiation in CH_4 Gas. Appl. Phys. Letts., Vol. 27, 1975, pp. 129-131.

REFERENCES (Cont'd)

12. Barrett, J. J.: Generation of Coherent Anti-Stokes Rotational Raman Radiation in Hydrogen Gas. Appl. Phys. Letts., Vol. 29, December 1976, pp. 722-724.
13. Roh, W. B., P. W. Schreiber, and J. P. E. Taran: Single-Pulse Coherent Anti-Stokes Raman Scattering. Appl. Phys. Letts., Vol. 29, August 1976, pp. 174-176.
14. Harvey, A. B., J. R. McDonald, and W. M. Tolles: Analytical Applications of a New Spectroscopic Tool: Coherent Anti-Stokes Raman Spectroscopy (CARS), in Progress in Analytical Chemistry, Plenum Press, 1977.
15. Tolles, W. M., J. W. Nibler, J. R. McDonald, and A. B. Harvey: A Review of the Theory and Application of Coherent Anti-Stokes Raman Spectroscopy (CARS). Appl. Spect., Vol. 31, 1977, pp. 253-272.
16. Nibler, J. W., W. M. Shaub, J. R. McDonald, and A. B. Harvey: Coherent Anti-Stokes Raman Spectroscopy. J. R. Durig, Ed., Vibrational Spectra and Structure, Vol. 6, Elsevier, Amsterdam 1977, pp. 173-225.
17. Nibler, J. W., and G. V. Knighten: Coherent Anti-Stokes Raman Spectroscopy in A. Weber, Ed., Topics in Current Physics, Chapter 7, Springer Verlag, Stuttgart 1977.
18. Eckbreth, A. C.: BOXCARS: Cross-Beam Phase-Matched CARS Generation in Gases. Appl. Phys. Letts., Vol. 32, April 1978, pp. 421-423.
19. Eckbreth, A. C., P. A. Bonczyk, and J. F. Verdick: Review of Laser Raman and Fluorescence Techniques for Practical Combustion Diagnostics. Report EPA-600/7-77-066, June 1977.
20. Herzberg, G.: Molecular Spectra and Molecular Structure I. Spectra of Diatomic Molecules. Van Nostrand, Princeton, N.J. (1945).
21. Song, J.J., E. L. Eesley, and M. D. Levenson: Background Suppression in Coherent Raman Spectroscopy. Appl. Phys. Letters, Vol. 29, November 1976.
22. Akhmanov, S. A., A. F. Bunkin, J. E. Ivanov, and N. I. Korsteev: Polarization Active Raman Spectroscopy and Coherent Raman Ellipsometry. Sov. Phys. JETP, Vol. 47, April 1978, pp. 667-678.

REFERENCES (Cont'd)

23. Rahn, L., L. J. Zych, and P. L. Mattern: Background-Free CARS Studies of Carbon Monoxide in a Flame. Opt. Comm. Vol. 30, 1979, pp. 249-253.
24. Bowker, A. H., and G. J. Lieberman: Engineering Statistics. Prentice Hall, Englewood Cliffs, NJ, 1972.
25. Hall, R. J., and A. C. Eckbreth: Flame Diagnosis by Coherent Anti-Stokes Raman Spectroscopy. Proc. SPIE Volume 158, August 1978, pp. 59-73.
26. St. Peters, R. L.: Augmented Coherent Anti-Stokes Raman Spectroscopy Line-width Parameter from Laser-Mode Structure. Opt. Letts. Vol. 4, 1979, pp. 401-402.
27. Weber, A.: High Resolution Raman Studies of Gases, Chapter 9 in The Raman Effect. A. Anderson, Ed., Marcel Dekker, New York, NY, 1973.
28. Murray, J. R., and A. Javan: Motional Narrowing in Hydrogen Raman Scattering. J. Mol. Spectrosc., Vol. 29, 1969, pp. 502-504.
29. Henesian, M. A., L. Kulevskii, R. L. Byer, and R. L. Herbst: CW High-Resolution CAR Spectroscopy of H₂, D₂, and CH₄. Optics. Commun., Vol. 18, 1976, pp. 225-226.
30. Roh, W. B., R. F. Weber, and P. W. Schreiber: Linewidth Determination by Integrated Power Measurement of Coherent Anti-Stokes Raman Scattering. Optics Commun., Vol. 27, October 1978, pp. 142-146.
31. Hinkley, E. D., K. W. Nill, and F. A. Blum: IR Spectroscopy with Tunable Lasers. Chap. 2 in Laser Spectroscopy, H. Walther Ed., Springer Verlag, Berlin, 1976.
32. Dicke, R. H.: The Effect of Collisions Upon the Doppler Width of Spectral Lines. Phys. Rev., Vol. 89, January 1953, pp. 472-473.
33. Galatry, L.: Simultaneous Effect of Doppler and Foreign Gas Broadening on Spectral Lines. Phys. Rev., Vol. 122, May 1961, pp. 1218-1223.
34. Gersten, J. I., and H. M. Foley: Combined Doppler and Collision Broadening. J. Opt. Soc. Am., Vol. 58, July 1968, pp. 933-937.
35. Nelkin, M., and A. Ghatak: Simple Binary Collision Model for Van Hove's Gs(r, t). Phys. Rev., Vol. 135A, July 1964, pp. 4-9.

REFERENCES (Cont'd)

36. Dion, P., and A. D. May: Motional Narrowing and Other Effects in the Q Branch of HD. Can. J. Phys., Vol. 51, 1973, pp. 36-39.
37. Alekeseyev, V., A. Grosiuk, V. Ragulsky, I. Sobel'man, and F. Faizulov: Stimulated Raman Scattering in Gases and Gain Pressure Dependence. IEEE J. Quant. Electronics, Vol. QE-4, October 1968, pp. 654-656.
38. May, A. D., J. C. Stryland, and G. Varghese: Collisional Narrowing of the Vibrational Raman Band of Nitrogen and Carbon Monoxide. Can. J. Phys., Vol. 48, 1970, pp. 2331-2335.
39. Roh, W. B., and P. W. Schreiber: Pressure Dependence of Integrated CARS Power. Appl. Optics, Vol. 17, May 1978, pp. 1418-1424.
40. Eckbreth, A. C.: CARS Investigations in Sooting and Turbulent Flames. UTRC Report, R79-954196-3 under SQUID Contract 8960-28 and ONR Contract N00014-75-C1143, February 1979.
41. Lallemand, P., and P. Simova: Stimulated Raman Spectroscopy in Hydrogen Gas. J. Mol. Spectrosc., Vol. 26, 1968, pp. 262-276.
42. Penney, C. M., and M. Lapp: Raman-Scattering Cross Sections for Water Vapor. J. Opt. Soc. Amer., Vol. 66, May 1976, pp. 422-425.
43. Eckbreth, A. C., P. A. Bonczyk, and J. F. Verdieck: Laser Raman and Fluorescence Techniques for Practical Combustion Diagnostics. Appl. Spectrosc. Rev., Vol. 13, 1978, pp. 15-164.
44. Wolfhard, H. G., and W. G. Parker: A New Technique for the Spectroscopic Examination of Flames at Normal Pressures. Proc. Phys. Soc. A, Vol. 62, 1949, pp. 722-730.
45. Bribes, J. L. et al.: Raman Band Contours for Water Vapor as a Function of Temperature. App. Phys. Lett., Vol. 28, 1976, pp. 336-337.
46. Lapp M.: Raman Scattering from Water Vapor in Flames. AIAA J., Vol. 15, 1977, pp. 1665-1666.
47. LD-690, Exciton Chemical Co., Inc., Dayton, OH, 1979.
48. Tourin, R. H.: Spectroscopic Gas Temperature Measurement, Elsevier Publishing Co., Amsterdam, 1966.

REFERENCES (Cont'd)

49. Flaud, J. M., C. Camy-Peyret, and J. P. Maillard: Higher Ro-vibrational Levels of H_2O Deduced from High Resolution Oxygen-Hydrogen Flame Spectra Between $2800-6200\text{ cm}^{-1}$. Mol. Phys. Vol. 32, 1976, 499-521.
50. Bribes, J. L., R. Gaufres, M. Monan, M. Lapp, and C. M. Penney: Detailed Study of the Q-branch Profile of the ν_1 Mode of the Water Molecule from $293\text{ }^\circ\text{K}$ to $1500\text{ }^\circ\text{K}$. Proceedings of the Fifth International Conference on Raman Spectroscopy, edited by E. E. Schmid, et. al., University Freiburg, September 2-8, 1976, Hans Ferdinand Schulz Verlag, Freiburg, 1976.
51. Camy-Peyret, C., and J. M. Flaud: Line Positions and Intensities in the ν_2 Band of $H_2^{16}O$. Molecular Physics, Vol. 32, 1976, pp. 523-537.
52. Camy-Peyret, C., and J. M. Flaud: Vibration-Rotation Intensities for the $3\nu_2$, $\nu_1 + \nu_2$, and $\nu_2 + \nu_3$ bands of H_2O . Journal of Molecular Spectroscopy, Vol. 67, 1977, pp. 117-131.
53. Rado, W. G.: The Nonlinear Third Order Dielectric Susceptibility Coefficients of Gases and Optical Third Harmonic Generation. Appl. Phys. Lett., Vol. 11, 1967, pp. 123-125.
54. Stephenson, D. A.: Raman Cross Sections of Selected Hydrocarbons and Freons. J. Quant. Spectrosc. Radiat. Transfer, Vol. 14, 1974, pp. 1291-1301.
55. Eckbreth, A. C.: Laser Raman Gas Thermometry. AIAA Paper 74-1144, October 1974.
56. 1979 Laser Focus Buyer's Guide, Advanced Technology Publications, Inc.

APPENDIX A

CARS MEASUREMENT OF H_2 NUMBER DENSITIES IN A FLAME

Solid state lasers used for CARS experiments typically exhibit pulse-to-pulse instability of 2-5%. In a system which uses the primary (ω_1) laser to optically pump a dye laser in the saturation limit, the CARS power is proportional to the primary laser power cubed. Therefore, laser power fluctuations would be expected to produce CARS signal fluctuations of 6-15% even in static gases. This uncertainty in density measurement is unacceptable for most applications. One technique which has been used normalizes the dispersed CARS signal to the so-called integrated CARS by coupling off a portion of the CARS beam before it enters the monochromator. With this technique, however; it is not possible to distinguish laser power fluctuations from concentration fluctuations and thus is applicable only to steady-state situations. Furthermore, it is desirable to have a reference signal which normalizes against power fluctuations and, in addition, provides a signal by which the single shot test volume signal can be related to the absolute concentration, i.e., a calibrating reference. In principle, this can be accomplished by generating a reference CARS signal in a separate optical leg with a reference cell maintained at known pressure and temperature. There are several approaches which can be followed in setting up the reference.

Measurement Approach

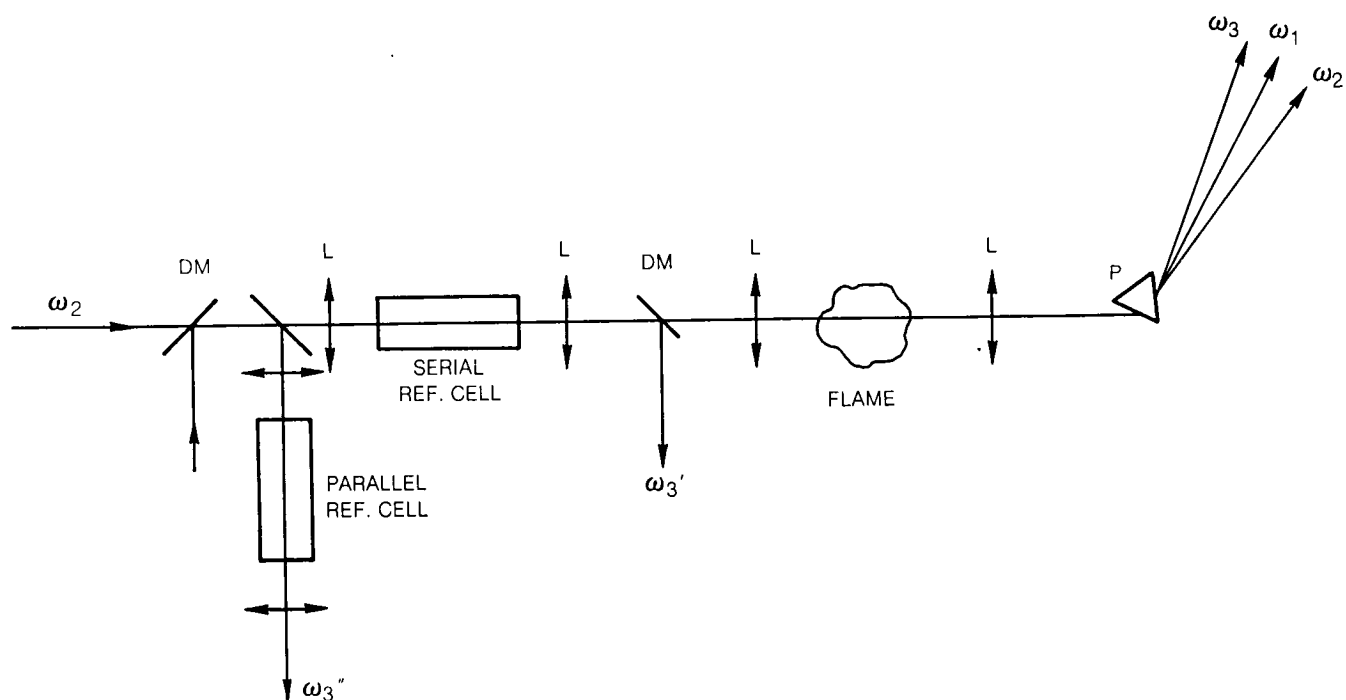
First, the reference signal can be generated resonantly or nonresonantly, according to whether the gas in the sample cell is identical to the test gas (for which the Stokes laser frequency has been selected) or not. The best argument against nonresonant generation is that it is usually very weak. It is shown later that, under some circumstances, the reference signal is photon-statistics limited, and, therefore, it would be preferable not to use an already weak process.

Second, the reference cell must be positioned with respect to the probe volume in such a way that CARS generation in the reference cell responds to angular deviations in the optical train in exactly the same manner as CARS generation in the probe (test) volume.

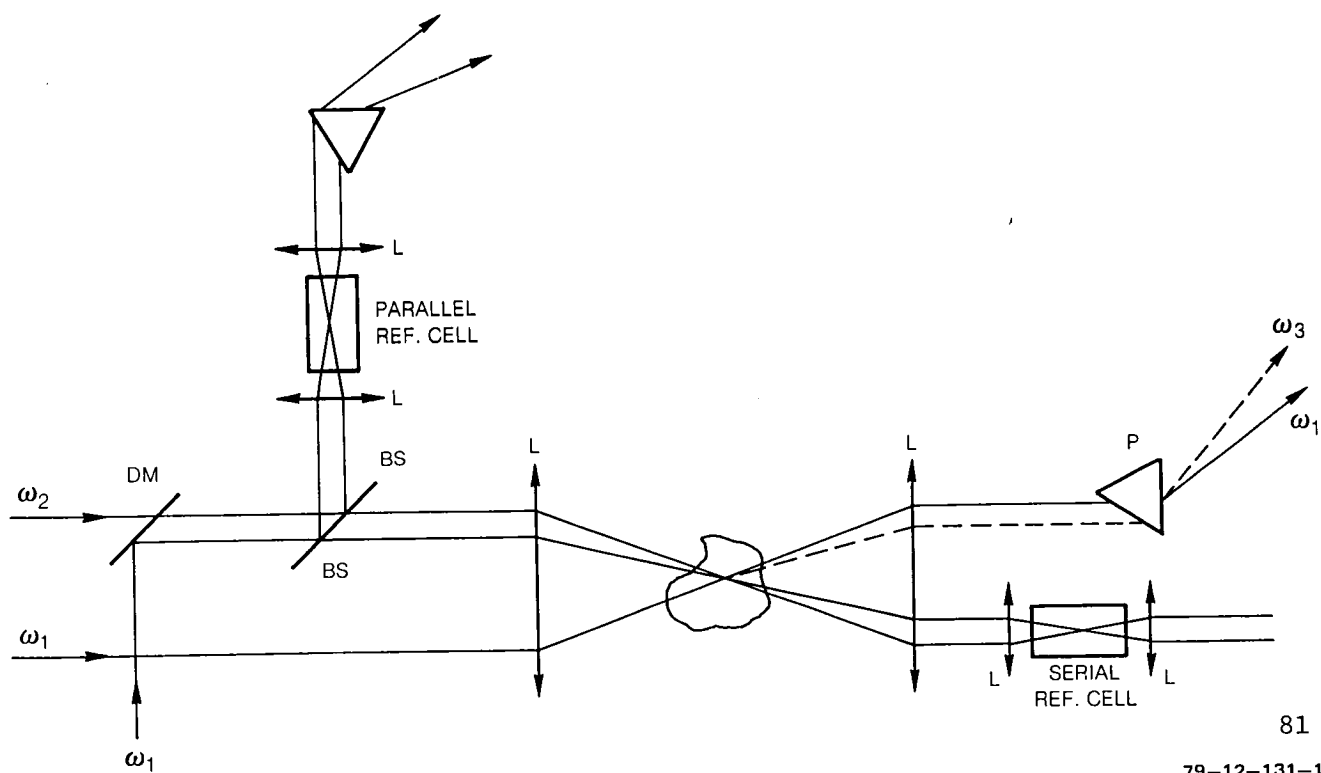
Options for phase matching for the arrangement of the reference cell relative to the test volume are shown in Figs. A-1 and A-2. The upper portion

REFERENCE CELL APPROACHES

(1) COLLINEAR ARRANGEMENT



(2) BOXCARS ARRANGEMENT



SCHEMATIC OF BOXCARS REFERENCE ARRANGEMENT

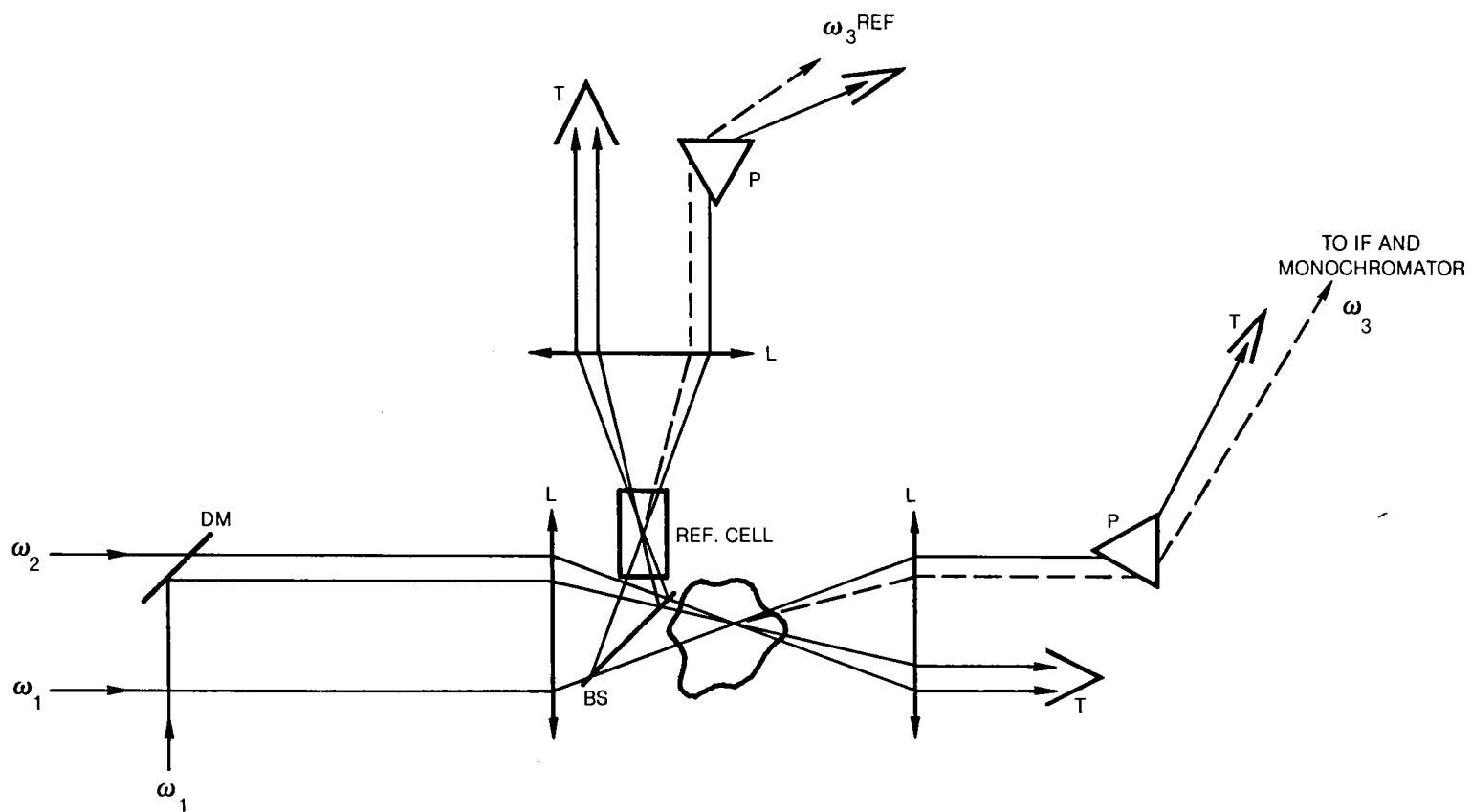


FIG. A-2

of the figure shows collinear phase matching with both a serial and a parallel arrangement of the reference cells. In this configuration, the pump beam, ω_1 , is combined with the Stokes beam, ω_2 , on a dichroic mirror, labelled DM. The combined beams, as shown, are split, focussed, and collimated through a serial and a parallel reference cell. After passing through the parallel reference cell, the beams are dispersed and filtered (not shown in Fig. A-1 for simplicity) to isolate the ω_3'' CARS component. A dichroic mirror DM is used after the serial reference cell to remove the ω_3' reference CARS component from the beam before it is focused into the test region. The application of reference cells in this collinear arrangement should be confined to situations where fine spatial resolution is not required.

A BOXCARS configuration using reference cells is shown in the lower portion of Fig. A-1. The illustrated configuration sends a portion of one ω_1 pump beam and the ω_2 Stokes beam through parallel and serial reference cells. Note that CARS generated in the reference cells in this configuration is not BOXCARS phase matched but is phase-mismatched collinear, or more likely two beam BOXCARS (Ref. A-1).

A true BOXCARS reference can be generated by using a larger beam splitter, to reflect a portion of both pump beams into the parallel reference cell, as shown in Fig. A-2. This configuration was used in the experiments reported here. A single lens was used to focus the beams in the probe volume and reference cell. Tracking between the signal and reference legs should be closer in this configuration than in either of the configurations shown in Fig. A-1. A microscope slide placed at an angle to the beam was used to reflect a portion of the incident beams into the reference cell. The beams leaving the reference cell were collimated, dispersed, and sent through interference and cutoff filters before being detected by a photomultiplier.

Using the beamsplitter in the focussing beams introduces a small amount of astigmatism into either the test leg or the reference leg, depending on which side of the beamsplitter is reflection coated. There are measures which can be taken to minimize or eliminate the effect of astigmatism. A weak cylindrical lens can be used to compensate for the change in focal length caused by the optical thickness of the beamsplitter, thus eliminating astigmatism. On the other hand, astigmatism can be introduced into both legs using a anti-reflection coated flat in the appropriate leg.

The coupling fraction can be changed somewhat by changing the angle of the beam splitter. The angular separation of the beams in the BOXCARS arrangement gives rise to a difference in reflection coefficient between the two convergent beams. In these experiments, the wave is p-polarized so that the reflection coefficient is zero at the Brewster angle. CARS generation in the reference leg is larger if the leg containing the pump component alone is closer to the

Brewster angle than the leg containing the pump and Stokes beam together so that the reflectivity is higher for the two beams than it is for the single beam. Practical limitations, however, usually restrict the angle to close to 45 degrees. In these experiments, the included angle between the BOXCARS beams was 3° , so that the angles of the beams with respect to the beamsplitter were 43.5° and 46.5° . With an index of refraction for glass of 1.5, the reflection coefficients are 0.010 and 0.006, respectively for the smaller and larger angles.

CARS generation in the reference leg also can be enhanced by increasing the gas pressure in the reference cell. The dependence of CARS signal on pressure depends on the broadening mechanism of the Raman linewidth. Using a broadband Stokes laser and detection with an interference filter, the CARS measured signal is proportional to the CARS intensity convolved with the wavelength interval of the bandpass filter. For isolated Lorentzian shaped lines with a full width at half maximum, Γ , it can be shown that the integrated CARS intensity is proportional to N^2/Γ (Ref. A-2). Therefore, in the pressure broadened limit, the integrated CARS signal is directly proportional to the density since $\Gamma \sim N$. In the Dicke narrowed regime, the linewidth is inversely proportional to the density so that the CARS signal varies as the cube of the density. The rotational components in H_2 are spaced far enough apart to be isolated, but in nitrogen and oxygen, cross terms in the CARS intensity dependence will introduce small corrections to this density dependence. The dependence of integrated CARS signal on pressure was measured for both N_2 and H_2 by varying the pressure in the reference cell. The results are nearly linear for both molecules. There may be evidence for Dicke narrowing in H_2 ; however, these tests were not definitive. The main point of these tests was to show that the reference signal could be enhanced by increasing the reference cell pressure.

One problem which must be considered when using a reference cell is CARS generation in the cell windows. This problem can be put in perspective by noting that the nonresonant susceptibility for glass is 0.92×10^{-14} cm³/erg (Ref. A-3) whereas a typical (resonant susceptibility) for a molecular gas such as H_2 is 10^{-15} cm³/erg at one atmosphere pressure. CARS generation in the windows depends on the reference cell size and optical parameters, such as the focal length of the focussing lens. Window generation would not normally be expected in a BOXCARS configuration; however, CARS can be generated from the collinear (phase-mismatched) leg of a BOXCARS configuration. In these experiments, a collinear CARS component was sometimes observed when the signal should have been all BOXCARS. The magnitude of BOXCARS and collinear CARS components were checked by blocking the relevant pump beam component. The collinear CARS component could be made to be less than 5% of the BOXCARS component by peaking up the BOXCARS signal by first adjusting the orientation of the mirror reflecting the BOXCARS pump beam and then the mirror reflecting the pump beam generating the collinear CARS component. It is not known how the collinear component could be emitted in the BOXCARS direction. Presumably, the collinear CARS component may also result from a diffuse reflection.

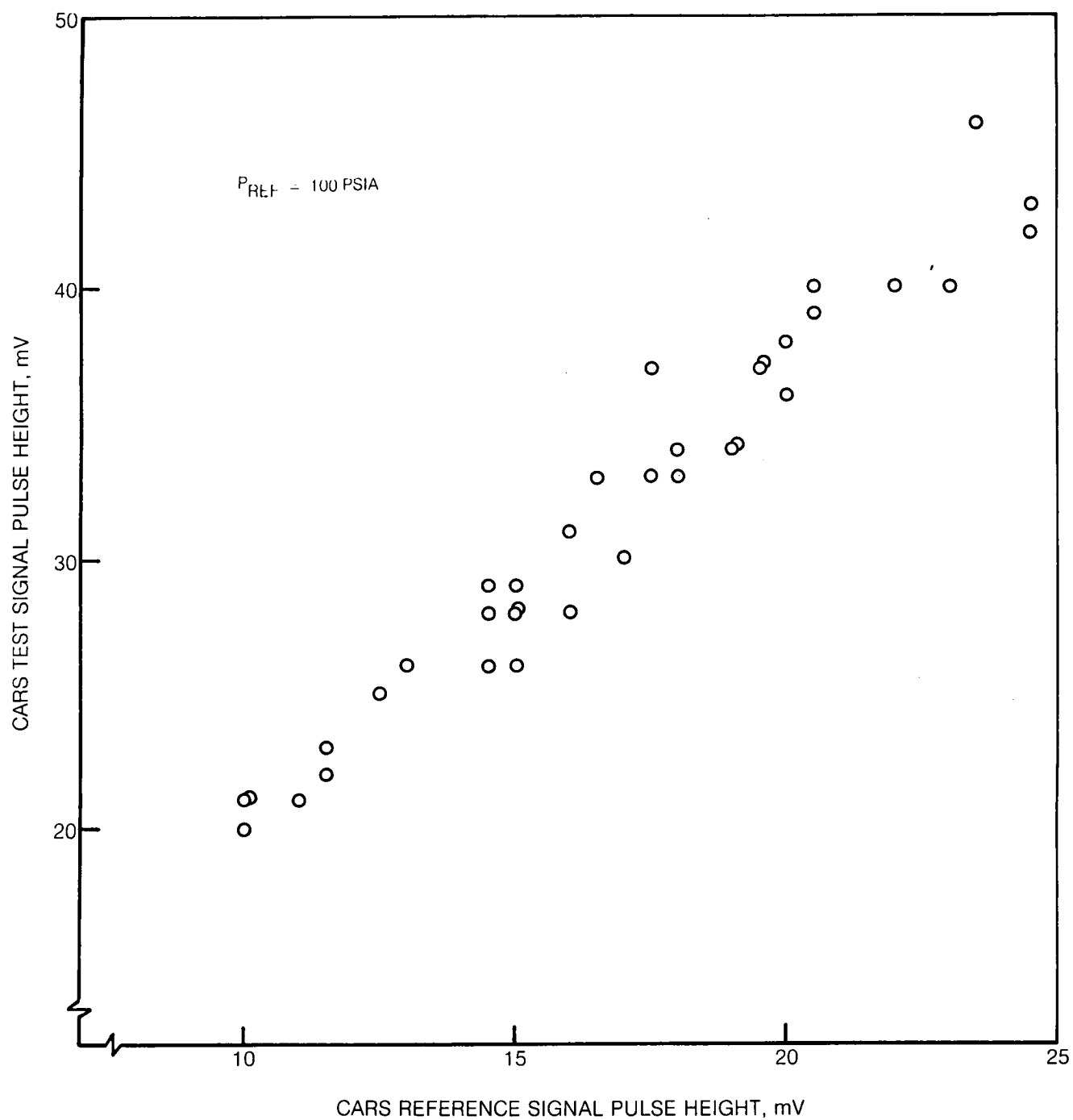
Measurements

Three types of measurements were undertaken using the reference cell. First the effect of angular displacement of one of the pump beams on CARS generation in the test leg and the reference leg was determined. The second test was to determine how well single shot signals generated in each leg agreed statistically. The third test was to use the reference cell in concentration measurements. For the latter tests, the concentrations determined by CARS were compared with the previous spontaneous Raman scattering results. In all these measurements, the pump and Stokes beams were focussed and crossed at 3° included angle with a 300 mm lens. The spatial resolution was 300 μm perpendicular to the focal axis and 11 mm along it.

A test of steering effects is critical for a reference leg in a parallel optical configuration. For these tests, the effect of deliberate misalignment of one of the pump beams was recorded for both legs. The pump beam primarily responsible for generating the BOXCARs signal is misaligned in the vertical direction, that is, the crossing angle was held constant. It was found that the angular range over which the mirror could be rotated and maintain the CARS signal above one half of the maximum signal was about a milliradian. With off-the-shelf glass windows on the reference cell, the signals generated in the test leg and the reference leg peaked at mirror angles separated by about a milliradian. When the entrance windows of the reference cell and the test cell were replaced by BK-7A $\lambda/10$ windows that are parallel to 5 sec (0.02 milliradian), the two legs tracked to better than 0.5 milliradian. Although it wasn't tried, it is felt that a thin, flat (1/10 wave) parallel (< 5 sec wedge) beam splitter would produce better results than the microscope slide. When a thick (~ 1 cm) flat was used, unsatisfactory results were obtained, because of the poor purity of the BOXCARs reference signal, perhaps caused by the reflection from the second surface of the thick splitter.

CARS signals generated in the test and reference cells by a single laser pulse were compared by displaying the signals together on an oscilloscope. The actual pulse from the PMT was too short to be displayed on a dual beam scope; therefore, the pulses were stretched with RC filters. The signals from both CARS legs were compared by measuring the peak voltages from oscilloscope photographs of the pulses. The peak pulse heights recorded for one series of tests are shown in Fig. A-3. The reference cell pressure was 100 psia. It is seen, overall, the signal magnitude varies by about ± 33 percent. It should be emphasized that the beams were not attenuated or steered during these tests. After adjusting the alignment of mirrors, the adjustments were not changed in order to avoid tracking problems described previously. The overall range of signals appears to result from laser power fluctuations and possibly the effect of vibration. If the two signals are compared, it is seen that 90 percent of the points fall within 7 percent of an average line through the points. At

STATISTICAL CORRELATION OF TEST AND REFERENCE SIGNALS



lower pressures in the reference, the statistical uncertainty with respect to the test signal was found to be commensurate with Poisson limited photo-statistics. At the high pressure level, however, the statistics are limited by the accuracy of reading the oscilloscope photographs. This error is estimated to be about 3 percent. Therefore, the observed statistical variation could be explained by the limited reading accuracy. This doesn't mean that this relatively large variation doesn't mask a smaller variation, however. This could be checked with more accurate (i.e., 8 bit) digital sample and hold circuits.

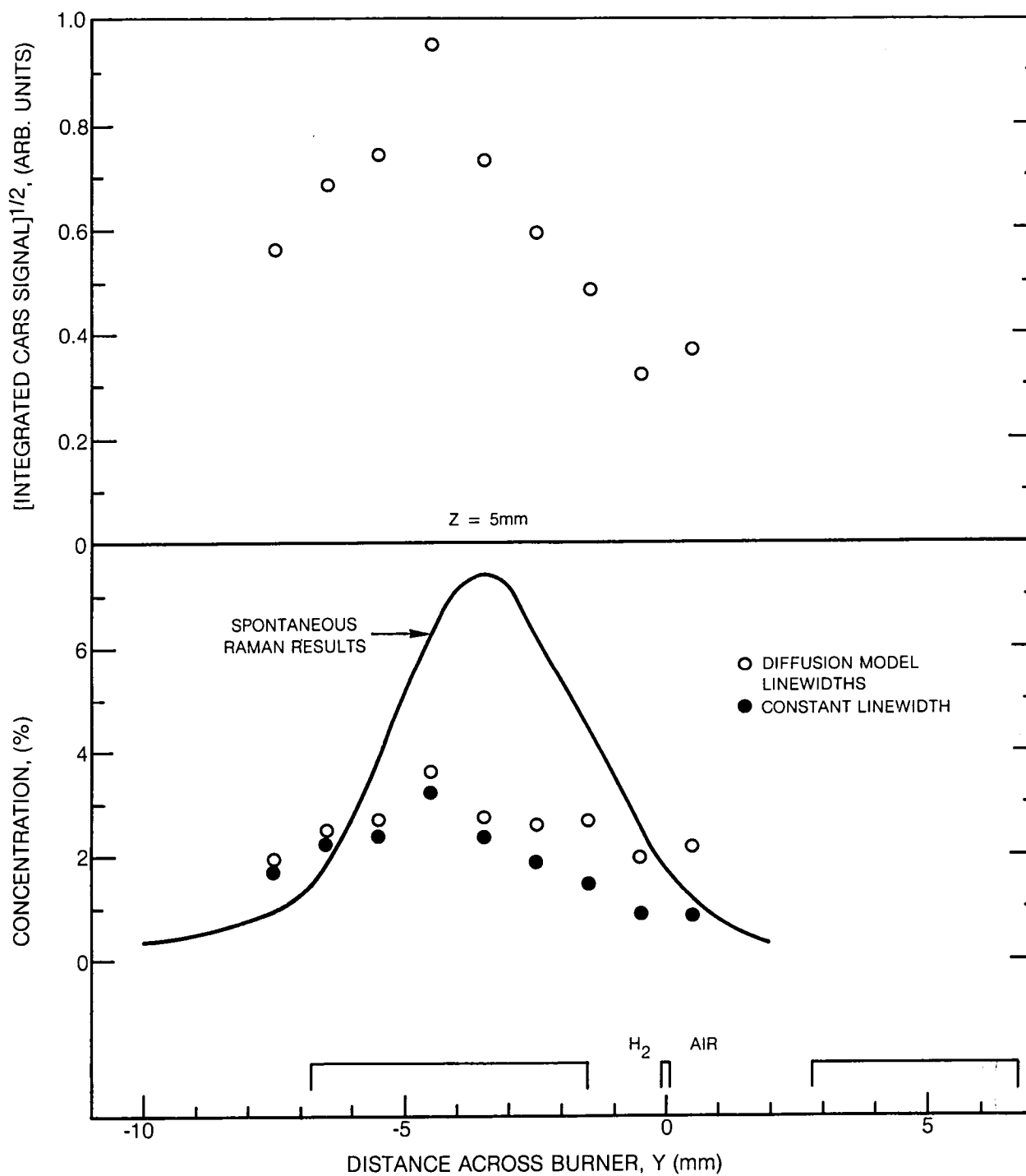
The last experiment undertaken in the reference cell tests was to check the CARS measurements of H_2 concentration in the diffusion flame against the spontaneous Raman results. Accordingly, the diffusion flame burner was set up and run at flowrates identical to the standard flowrates in the previous tests. The apparatus differed in only one respect from the previous configuration. Windows were used over the ends of the burner where the laser beams pass through the burner shroud (see Fig. 13). These windows were required to prevent convection currents from disturbing the flame. In the previous design, the end walls of the burner were kept fixed so that a small aperture to pass the beam could be used. In the second design, the windows were fixed to the burner requiring a larger aperture to accommodate full translation of the burner. The windows were found to produce spurious signals as discussed below.

Measurements of H_2 in the fuel side of the flame were made by translating the flame through the focal volume of the laser. Integrated CARS signals generated by flame H_2 were measured with a photomultiplier equipped with a narrow-band interference filter viewing the BOXCARS signal generated in the flame. The integrated CARS and reference PMT signals were detected with a boxcar integrator. The reference signal was used to normalize the flame generated signal using the A/B mode of the averager.

Figure A-4 shows the integrated CARS signal normalized to the reference signal as a function of position 5 mm above the burner. The integrated CARS signal is proportional to N^2/Γ ; accordingly, the square root of the CARS signal ratio, which is directly proportional to the H_2 number density in the constant linewidth limit, is shown plotted in the upper half of Fig. A-4. The CARS signal did not go to zero in the edges of the fuel zone as it should have. This is speculated to be a spurious effect arising from either CARS generation in the burner windows or forward scattering from the windows.

After profiling the flame, the burner was replaced with a cell filled with pure H_2 at 1 atmosphere pressure. The ratio of the integrated CARS test signal to the reference signal was recorded and used to normalize the flame data to determine the absolute concentration.

The analysis of the CARS data is hampered by the lack of knowledge of the Raman linewidth, in particular, the effect of foreign gas broadening which

INTEGRATED CARS CONCENTRATION MEASUREMENTS IN H_2 -AIR DIFFUSION FLAME

might be expected to be important in the flame where H_2 concentrations according to the Raman scattering measurements are less than 7 percent. However, Dicke narrowing, demonstrated before in the warm outer portion of the flame, may permit analysis of the data in the hot part of the flame without having to know the foreign gas broadening coefficient. The reason for this can be seen by referring to Fig. 11. The density scale can be divided into four regions according to the mechanism governing the linewidth. Starting from the low density end of the scale, there is the Doppler regime (1) where the linewidth is independent of density. This is bounded by a transition region (2) that leads to the diffusion region (3) in which the linewidth decreases inversely with increasing density. As the density increases still further, pressure broadening becomes important and the linewidth becomes directly proportional to the density. Fortunately, for data analysis, unless the foreign gas pressure broadening coefficient is very large compared to self-broadening, the data should fall in regions (1) through (3), and pressure broadening should not be important at these pressures (1 atm). The data of Roh and Schrieber (Ref. A-3) confirm the applicability of the diffusion model to the linewidth of H_2 in a large background of helium. Since the diffusion coefficient of H_2 in N_2 or air is known, all but region (4) can be calculated.* The magnitude of the broadening coefficient governs the location of the minimum in the curve, so that it should be possible to estimate the linewidth from the diffusion coefficient at lower densities (see Eqn. (19)). The linewidths were estimated based on this rationale. A $T^{1/2}$ temperature dependence was taken for the diffusion coefficient. The H_2 concentrations calculated from integrated CARS $\sim N^2/\Gamma$ are shown in the lower half of Fig. A-4.

The concentrations 5 mm above the burner measured by spontaneous Raman scattering are shown by a solid line for comparison. The spontaneous Raman sample extent was comparable to that for CARS perpendicular to the focal axis, but was 0.3 mm or about 1/3 smaller along the beam. The peak concentration, according to the CARS measurements, is about one-half the spontaneous Raman measured peak, and is located approximately one millimeter farther from the splitter plate. The CARS data are shown as two series of points in Fig. A-4, illustrating the effect of linewidth. The open circles represent the data reduced with the linewidth estimated from the diffusion model and the solid circles represent a constant linewidth. The difference between the two results is greatest in the hot side of the H_2 zone where the width is increasing as $T^{3/2}$.

Although the difference is large in the hot part of the flame, it is clear that the Raman width alone is not responsible for the discrepancy in the results. The widths would have to be increased by a factor of four to yield agreement at the peak, but this would exceed the Doppler width and would not be reasonable. It is more likely that the discrepancy in magnitude of the concentration involves

*Except for the exact dependence of linewidth in region (2), where the lineshape changes from Gaussian in the Doppler region to Lorentzian in the Dicke region.

the normalizing factor obtained from the 1 atmosphere pressure test cell. The CARS data also don't show as great a spatial variation as the spontaneous Raman results. It is possible that the data were not measured in identical parts of the flame, due either to flame shifts or to not repositioning the burner in exactly the same location with respect to the CARS focal volume. It is estimated that accuracy of repositioning the burner is ± 0.5 mm. The lower spatial resolution along the beam may in part also account for the lack of agreement between the CARS and spontaneous Raman results.

These data suggest that H_2 concentration measurements can be made from integrated CARS signals using a reference cell, although it is important to eliminate the effects of spurious signals. This should not be a problem in the geometry of the NASA LRC experiments because the windows are a greater distance from the center of the test section. The parallel approach adopted here for the location of the reference cell is thought to be preferable to the serial approach because it eliminates possible problems with lenses not being exactly identical. The serial approach, as pointed out before, can be useful for selecting data in certain situations. For example, if the test signal and post references signal agree but both are much lower than the pre-reference signal then refractive steering affects should be suspected. The beamsplitter should be optically flat on both surfaces and parallel and should be coated on one surface to provide sufficient reflection at 45° for the chosen polarization and anti-reflection coated on the other. The reflectivity should be chosen so that comparable signals are generated in the test and reference legs when the test leg is viewing the lowest concentration that is desired to be measured. This will maximize the measurement SNR. The chosen reflectivity will depend on the pressure used in the reference cell.

Finally, the importance of linewidth information has been pointed out, particularly the effect of foreign gas collision partners. The detailed factors which interplay and act to control linewidths and, hence CARS generation, under all conditions of varying concentrations are not well known at this time (Ref. A-4).

REFERENCES

- A-1. Marko, K. A. and L. Rimai: Space- and Time-Resolved Coherent Anti-Stokes Raman Spectroscopy for Combustion Diagnostics. Opt. Lett., Vol. 4, July 1979, pp. 211-213.
- A-2. Roh, W. B. and P. W. Schreiber: Pressure Dependence of Integrated CARS Power. Appl. Opt., Vol. 17, May 1978, pp. 1418-24.
- A-3. Levenson, M. D.: Feasibility of Measuring the Nonlinear Index of Refraction by Third-Order Frequency Mixing. IEEE J. Quant. Elec., Vol. QE-10, February 1974, pp. 110-115.
- A-4. St. Peters, R. L.: Augmented Coherent Anti-Stokes Raman Spectroscopy Linewidth Parameter from Laser-Mode Structure. Opt. Lett., Vol. 4, December 1979, pp. 401-2.

1. Report No. NASA CR-159280		2. Government Accession No.		3. Recipient's Catalog No.	
4. Title and Subtitle Investigation of the Feasibility of CARS Measurements in Scramjet Combustion				5. Report Date July 1980	
				6. Performing Organization Code	
7. Author(s) John A. Shirley, Robert J. Hall and Alan C. Eckbreth				8. Performing Organization Report No. R79-954390-13	
9. Performing Organization Name and Address United Technologies Research Center East Hartford, CT 06108				10. Work Unit No.	
				11. Contract or Grant No.	
12. Sponsoring Agency Name and Address National Aeronautics and Space Administration Washington, D. C. 20546				13. Type of Report and Period Covered Contractor Report	
				14. Sponsoring Agency Code	
15. Supplementary Notes Contract Monitor: G. Burton Northam, NASA Langley Research Center					
16. Abstract Results are presented of analytical and experimental investigations to determine the feasibility of using coherent anti-Stokes Raman Spectroscopy (CARS) to measure temperature and species concentration in supersonic combustion experiments. CARS spectra of H ₂ O, O ₂ and H ₂ have been measured in laboratory flames. Computer code calculated spectra agree very well with the measured spectra. Temperature, and O ₂ and H ₂ concentration profiles have been determined from CARS spectra in a laboratory H ₂ -air flat diffusion flame. Temperature measurements agree with radiation corrected, thermocouple measurements within 5 to 10%, depending on species concentration. The feasibility of measuring O ₂ concentrations up to 10%, from the spectral shape has been demonstrated. H ₂ concentrations determined from CARS intensities agree with spontaneous Raman measurements within a factor of two. Finally, a conceptual design has been formulated for diagnostics in the Langley Research Center scramjet combustion facility.					
17. Key Words (Suggested by Author(s)) CARS Scramjet Diagnostics Combustion Diagnostics			18. Distribution Statement Unclassified - Unlimited		
19. Security Classif. (of this report) Unclassified	20. Security Classif. (of this page) Unclassified		21. No. of Pages 91	22. Price*	

End of Document